Yu-Shiba-Rusinov Bound States in Quantum Dots

Master Thesis

Written by *Gorm O. Steffensen*

25. Juli 2017

Supervised by
Prof. Jens Paaske

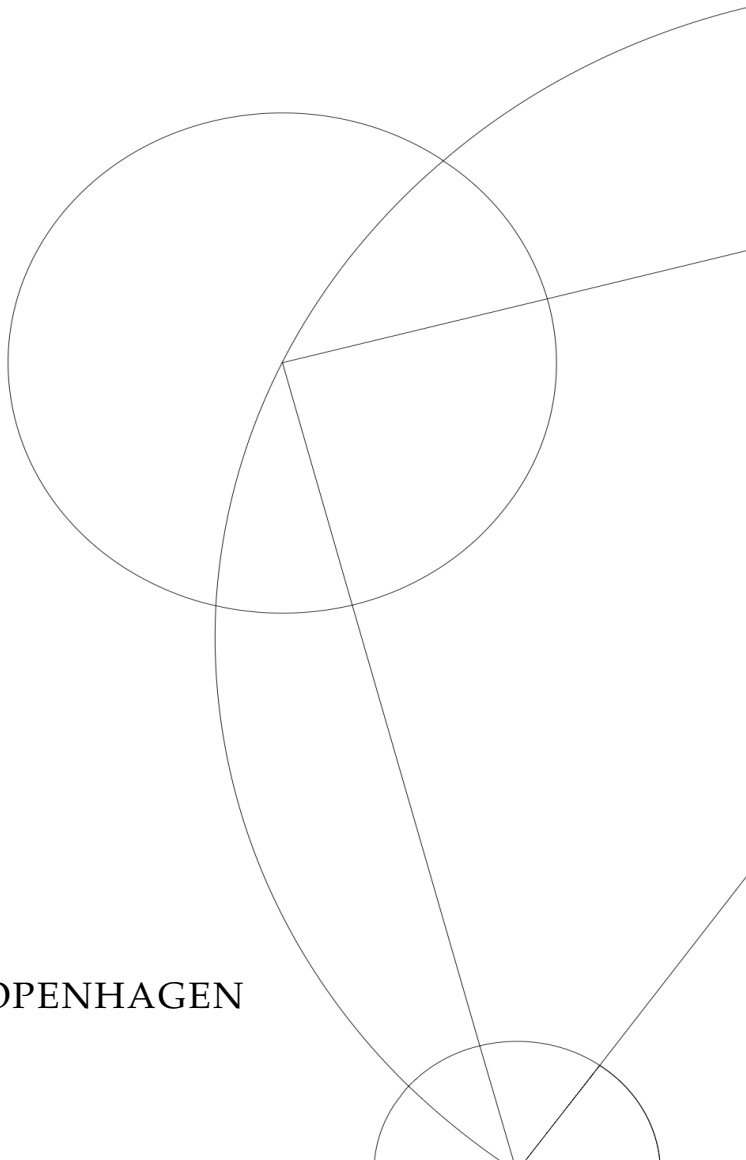

University of Copenhagen

UNIVERSITY OF
COPENHAGEN

FACULTY:	Science
INSTITUTE:	Niels Bohr Institute
AUTHOR(S):	Gorm O. Steffensen
EMAIL:	Gnimsen@gmail.com
TITLE AND SUBTITLE:	Yu-Shiba-Rusinov Bound States in Quantum Dots -
SUPERVISOR(S):	Prof. Jens Paaske
HANDED IN:	27.07.2017
DEFENDED:	21.08.2017

NAME _____

SIGNATURE _____

DATE _____

Abstract

In this thesis we present and derive the basic formalism of the magnetically induced Andreev Bound state, known as the Yu-Shiba-Rusinov (YSR) state, by use of a classical-spin approximation. We then show how YSR states are obtained in odd occupied quantum-dots, coupled to superconductors, using Schrieffer-Wolff transformations. Considering transport through superconductor-dot-metal structures we find that transport can either be meditated by Cooper-pairs or by relaxation of the YSR state. In this framework we find that Cooper-pair transport, even for a frequency asymmetric spectral function, always yields bias symmetric conductance, while relaxation transport shows the same asymmetries as the underlying spectral function. We then discuss specific superconductor-dot-dot-metal devices based on gate-controlled nanowires and consider the transport occurring in such setups. Using a Zero-Band-Width approximation we find a qualitative model able to describe all charge sectors for superconductor-dot-dot systems in the regime of large coupling to the superconductor. Within such systems we find that change of groundstate is signaled by zero-bias YSR crossings replacing the coulomb diamond structure expected for metallic leads. When exchange singlet formation competes with YSR triplet screening we obtain a new regime which we name partially screened.
By analyzing two specific bias-cuts of aforementioned device, in which the system behaves like a single impurity, we fit conduction using our classical-spin model and find it to conduct through relaxation processes. In these line-cuts, bias asymmetry is found even at the particle-hole symmetrical points which we explain using a modified Schrieffer-Wolff model.

Acknowledgements

I would very much like to give my gratitude to my supervisor Jens Paaske, who have been patient like a stone in regards to both my problems and bad humor. I can not count the hours i have sit at that small stool by the desk being schooled in physics, both when i needed it and when i had other things to do. That stool have learned me a great deal more physics than any course i have taken.

My gratitude must also be extended to Kasper Groove who have been kind enough to introduce me to the world experimental condensed matter and allowed me work on his data. I feel gifted by the opportunity to work with such a friendly and curios person. I must also send my regards to Marieke, Peter and Nesheim who have been so kind to read through big parts of this thesis correcting my grammar and enlightening me of my many mistakes.

And as is tradition, eternal praise must befall the holy lunchclub, whose food and social interactions have saved many students lost at the great sea of CMT.

Lastly, i would like to thank the dog breed Shiba Inu for being wonderful and providing light to an otherwise dark world.

Contents

1 Introduction

Superconductivity is an interesting phase appearing in many metals when cooled down below a critical temperature T_C. It was discovered experimentally by repeated measurements of its most characteristic macroscopic quality, namely dissipationless transport, measured as zero resistance currents. Following these discoveries theoreticians fought for years trying to develop a mechanism explaining the superconducting phase transition. A breakthrough appeared with the pioneering work of Barden-Cooper-Scrieffer (BCS) which provided a microscopic picture explaining the phase transition and related observations. A cool thing about living in the modern age is the recent development of nanostructures, such as nanowires and quantum-dots, allowing one to directly test, not only the macroscopic, but the microscopic parts of BCS theory such as manipulations of single Cooper-pairs and quasi-particles. This opens the door for exciting opportunities in exploration of novel electronics and quantum mechanics - an opportunity the old guard probably would have envied.

Next we will present a short review of BCS superconductivity explaining our primary building blocks in order to have a clear language for presenting Andreev Bound-states.

1.1 BCS Superconductors

The primary ingredient, in the theory of BCS superconductors, is the effective positive interactions between quasi-particles. The most famed being the interaction stemming from combined coulomb and phonon interactions which for electrons, with energy no-more then the Debye energy ω_D removed from the Fermi-surface, becomes positive. Writing down a simple Hamiltonian for such a system

$$H_{BCS} = \sum_{k\sigma} \xi_k c^\dagger_{k\sigma} c_{k\sigma} + \sum_{kk'} V_{kk'} c^\dagger_{k\uparrow} c^\dagger_{-k\downarrow} c_{-k'\downarrow} c_{k'\uparrow} \tag{1.1}$$

where ξ_k is the energy of the electron like excitations in the system and $c^{(\dagger)}$ is the usual fermionic annihilation(creation) operators. In the simplest derivations one typically choose's $V_{kk'}$ to be the forked function

$$V_{kk'} = \begin{cases} -V & \text{for } |\xi_k|, |\xi'_k| < \omega_D \\ 0 & \text{for } |\xi_k|, |\xi'_k| > \omega_D \end{cases} \tag{1.2}$$

For such a interaction one can do self-consistent mean-field to find that the anomalous correlation,

$$\Delta = -\sum_{k'} V_{kk'} \langle c_{-k'\downarrow} c_{k'\uparrow} \rangle \tag{1.3}$$

takes a non-zero value for temperatures lower then T_C. This result is often interpreted as the formation of a Cooper-pair liquid existing in parallel to the normal electrons gas, in which one can either remove or add two electrons in order to add or remove a Cooper-pair. Seeking as simple a model as possible which captures these anomalous effects one typically do mean-field for this correlation to obtain

$$H_{BCS} \approx H_{MF} = \sum_{k\sigma} \xi_k c^\dagger_{k\sigma} c_{k\sigma} + \sum_k \Delta c^\dagger_{k\uparrow} c^\dagger_{-k\downarrow} + \sum_k \Delta^* c_{-k\downarrow} c_{k\uparrow} \tag{1.4}$$

$$= \begin{pmatrix} c^\dagger_{k\uparrow} & c_{-k\downarrow} \end{pmatrix} \begin{pmatrix} \xi_k & \Delta \\ \Delta^* & -\xi_k \end{pmatrix} \begin{pmatrix} c_{k\uparrow} \\ c^\dagger_{-k\downarrow} \end{pmatrix} \tag{1.5}$$

which may seem weird at first glance as it looks particle none-conserving. But here it should be remembered that in mean-fielding we have effectively stopped counting how many Cooper-pairs their are and non-conserving interactions proportional to Δ involves Cooper-pairs. So in total the system is particle conserving as one could also guess as the original Hamiltonian eq.(1.1) is.

The BCS mean-field Hamiltonian can be diagonalized allowing one to describe it through the quasi-particles known as Bogoliubovs,

$$H_{MF} = \sum_k E_k \left(\gamma^\dagger_{k\uparrow}\gamma_{k\uparrow} + \gamma^\dagger_{k\downarrow}\gamma_{k\downarrow} \right) \tag{1.6}$$

with $\gamma_{k\sigma} = u_k c_{k\sigma} + \sigma v_k c^\dagger_{k\bar{\sigma}}$ and $E_k = \sqrt{\xi_k^2 + |\Delta|^2}$. Here $u_k(v_k)$ determines the electron(hole) weight of the excitation and is given by the equations,

$$|u_k|^2 = \frac{1}{2}\left(1 + \frac{\xi_k}{E_k}\right), \qquad |v_k|^2 = \frac{1}{2}\left(1 - \frac{\xi_k}{E_k}\right) \tag{1.7}$$

Here we see that for $\xi_k = 0$ the quasi-particles are fifty-fifty superpositions of electron and hole and as ξ_k becomes larger(smaller) it becomes more electron(hole) like. So how should one visualize such an excitation? Consider if one inserted an electron into a superconductor at energy $\xi_k > |\Delta|$ it could then form a Cooper-Pair with a electron at energy $-\xi_k$ leaving a hole at $-\xi_k$ with opposite pointing spin. Then a Cooper-pair could split up, one electron would fill the hole and the other becomes similar to the original electron inserted. If this process continues indefinitely the state evolves into being somewhat hole and somewhat electron with weights precisely given by u_k and v_k which is shown in Fig.1.1

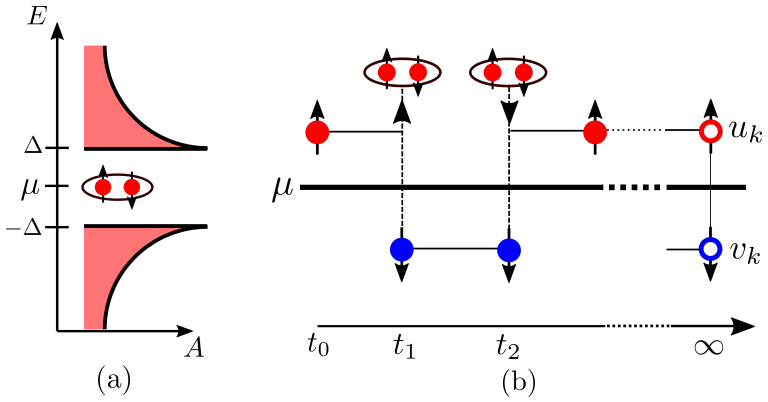

Figure 1.1: In (a) we show a representation of the superconducting spectral function, which have divergent peaks precisely at $\pm\Delta$ and Cooper-Pairs with energy μ. In (b) we show an example of how one can think about Bogoliubovs. If one starts with an electron it would, mediated by a Cooper-Pair flip into a hole, and then back and forth, until it becomes a superposition.

1.2 Andreev Bound States

In the current years dozens of experiments using superconducting junctions of different kinds are being done all over the world. A common feature in many such systems is the Andreev reflection

process where two electrons, with energies mirrored around the Fermi surface, tunnel into the superconductor to form a Cooper-pair. In a excitation sense this looks like a electron excitation is traded for a hole excitation, thereby explaining the name Andreev reflection. In small systems such effects are known to become resonant and lead to the formation of sub-gap states named Andreev Bound States (ABS). In this thesis we will be considering ABS formed on quantum-dot systems coupled to superconductors. Quantum dots are basically controllable artificial atoms, in the sense that they have well separated energy levels which occupancy can be controlled by capacitively coupled bottom gates. Coupling a single level to a superconductor strongly realizes sub-gap ABS. But in such setups ABS is a potentially confusing term, since it does not cover which process that leads to the formation of sub-gap resonances. We therefore separate them into two types:

1): The proximity induced state. This type of bound state is well described in the literature [1, 2] and arise in the regime $U << |\Delta|$ with U being the charging energy of the dot. The driving mechanism is the proximity effect, which drives the quantum dot superconducting, in the sense that a state composed of a superposition of dot state $|n = 0\rangle$ and $|n = 2\rangle$ becomes more energetically favored as coupling is increased. For large coupling this state becomes the ground-state in the middle of the $|n = 1\rangle$-coulomb diamond. In a exchange language one could say that for $|\Delta| \to \infty$ the quasi-particles are effectively removed from the picture and the dot hybridizes with Cooper-pairs. Meaning that a state allowing Cooper-pairs to tunnel in and out, and with mean occupancy $n = 1$, is favored, which is fulfilled by the superposition.

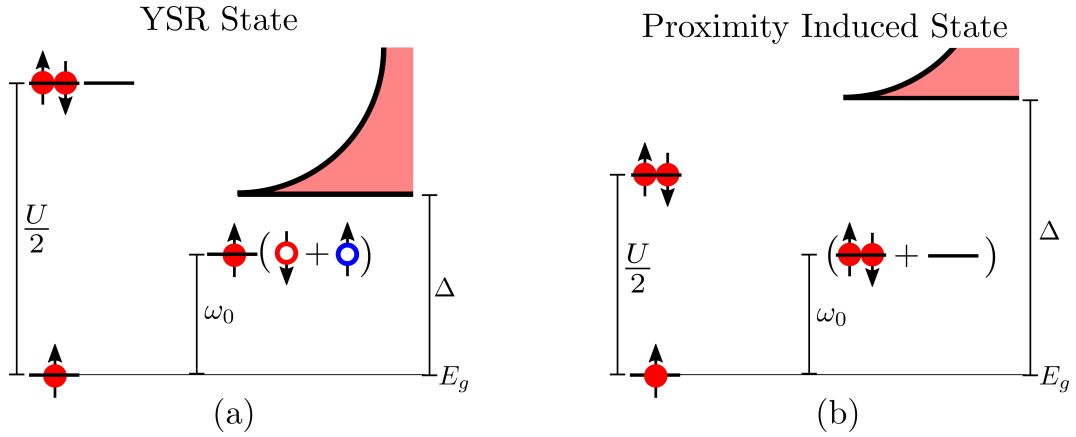

Figure 1.2: In (a) we show a representation of the dot-superconductor spectra in the YSR regime. Here we see dot states and Bogoliubov quasi-particles as well as the single YSR state. In (b) a similar spectra for the proximity induced state. Here the sub-gap state consist of a superposition of the empty and doubly occupied dot state in addition of a Cooper-Pair not shown.

2): The Yu-Shiba-Rusinov State. The Yu-Shiba-Rusinov state [3, 4, 5], or YSR state, arise in the opposite regime when $U >> |\Delta|$ and is mediated by magnetic exchange between quasi-particles in the superconductor and quantum dot states. This process have been described in [6, 7] and the basic explanation is that in this regime the quasi-particles are not far removed in energy, and they therefore hybridize with the $|n = 1\rangle$ dot state. In a exchange language one would say that quasi-particles with opposite pointing spin compared to the electron occupying the dot, are energetically favored as they can move in and out of the dot. This interaction forms a singlet state, composed of dot-electron and quasi-particles, which moves in from the gap as coupling is increased. For a critical coupling this state becomes the ground state when $|n = 1\rangle$. Using a language familiar to people working with magnetic impurities and Kondo effect one would call such a state screened, as the superconductor screens the spin of the nearby quantum-dot with a quasi-particles from its bulk.

These two states are shown visually at Fig.1.2. Is should be noted that the physics of these two states, in view of spectroscopy, are quite similar as for both one starts with a doublet for low coupling and then as coupling is increased a singlet moves down until it crosses and becomes the ground-state. Two noticeable differences: For the proximity induced state the two other occupancy states will still be visible inside of the gap which is not the case for YSR as shown in [6]. Also, as we will see later the formation of the YSR state leads to the disappearance of the gap peaks at $\pm\Delta$, which is not the case for proximity as seen in [8]. In the intermediate regime $U \approx \Delta$ the formed singlet is constituted of both quasi-particle and cooper-pair mixing attributes of both states [9, 10]. In experiments the intermediate regime and the YSR regime is the most common as the charging energy U is typically larger then Δ.

In this thesis we will work specifically on YSR states in quantum dots, their transport properties and how they behave in different regimes. The YSR state is interesting because it is an easy probeable many-body state with close connections to the rich fields of STM physics [11, 12, 13] and Kondo physics [14, 15] from which its theory originated. But as explained above, it is not a unusual visitor in the world of quantum dots [16], which are receiving a high amount of activity in the recent years related to the development of quantum computers. It also serves as a probeable sub-gap state for the development of transport theory in superconducting structures, which maybe helpful in understanding another famous sub-gap state: the Majorana fermion. Lastly, chains of YSR states have been shown to be able to yield a magnetic helix order which can be driven to an topological none-trivial regime yielding Majorana's at the end of the chain [17, 18]. With this motivation we will continue into a summary of the thesis to come.

In the next section we will derive the basic Greens function and Nambu framework needed to do calculations on coupled systems, including superconductivity and magnetic interactions. With this structure in place we will move on to derive the YSR state's Green function and spectral properties using a classical spin approximation which is done in Section.3. Then in Section.4 and Section.5 we will consider superconductor-dot-metal as a platform for YSR physics and consider transport from metal to superconductor too see how it probes the sub-gap spectra. In Section.6 and Section.7 we will present a description of double-dot systems and develop a Zero-Band-Width method of obtaining these structures spectra. We will then utilize these methods too understand data from two devices and discuss the relevant dynamics. Lastly, before moving into conclusions, we will try to apply our classical-spin approximation to certain line-cuts of the double-dot experiment in Section.8. Here we se, that certain regions of a double-dot systems behaves almost as a single-dot, allowing us to extract parameters and analyze the given transport patterns.

2 Framework

In this section we will do a brief derivation of Green function structure necessary for future calculations. These derivations will in essence follow the same lines as [19] and constitutes the basic formalism used throughout this thesis. Also we will show that, with some constraints on the Hamiltonian, the matrix structure existing in Greens functions can be expanded to also include 4×4 Nambu space greatly simplifying calculations containing both superconductors and spin-interactions.

2.1 Greens functions

We start by considering a generic Hamiltonian

$$H = H_0 + H_I \tag{2.1}$$

where H_0 is quadratic in operators Ψ_a which create state $|\Psi_a\rangle$ from the vacuum state and where a runs over all states present. H_I is some more complicated interaction and we consider both H terms to be time-independent. This means that we can generally write $H_0 = \sum_{ab} \Psi_a^\dagger h_0(a,b)\Psi_b$. From here we define the imaginary-time Greens functions

$$\mathcal{G}(\tau,\tau',a,b) = -\langle T_\tau(\Psi_a(\tau)\Psi_b^\dagger(\tau')\rangle = -\frac{1}{Z}\mathrm{Tr}\left[e^{-\beta H}T_\tau(\Psi_a(\tau)\Psi_b^\dagger(\tau'))\right] \tag{2.2}$$

where $\Psi_a(\tau)\Psi_b^\dagger(\tau')$ are operators from the Hamiltonian. Here τ is imaginary time, Z the partition function, brackets refer to the normal thermodynamical average and T_τ is the imaginary time-ordering which for fermions adds a sign when two field operators are interchanged.

Looking at equation eq.(2.2) one clearly sees that the thermodynamical term Exp$[-\beta H]$ is on the same form as time evolution Exp$[H\tau]$ and as the trace forces equality of index on the left and right side we end up with a cyclic constraint on imaginary time,

$$\mathcal{G}(\tau,\tau',a,b) = \mathcal{G}(\tau-\tau',a,b) = \pm\mathcal{G}(\tau-\tau'+\beta,a,b) \tag{2.3}$$

where $+$ is for bosonic operators and $-$ is for fermionic. From here one obtains the standard Matsubara Greens function by fourier transforming over the imaginary-time separation $\tau - \tau'$ yielding

$$\mathcal{G}(i\omega_n,a,b) = \int_0^\beta d\tau \mathcal{G}(\tau-\tau',a,b)e^{i\omega_n\tau} \tag{2.4}$$

where the cyclic property confines $\omega_n = (2n+1)\pi/\beta$ with n being a integer and thereby reduces the Fourier transform to a fourier series over the interval β. Next one determines the Greens function by use of equations of motion

$$\begin{aligned}
-\partial_\tau\mathcal{G}(\tau-\tau',a,b) &= \partial_\tau\left[\theta(\tau-\tau')\langle\Psi_a(\tau)\Psi_b^\dagger(\tau')\rangle \pm \theta(\tau'-\tau)\langle\Psi_b^\dagger(\tau')\Psi_a(\tau)\rangle\right] \\
&= \delta(\tau-\tau')\langle\Psi_a(\tau)\Psi_b^\dagger(\tau') \mp \Psi_b^\dagger(\tau')\Psi_a(\tau)\rangle + \langle T_\tau([H_0+H_I,\Psi_a(\tau)]\Psi_b^\dagger(\tau'))\rangle \\
&= \delta(\tau-\tau')\delta_{ab} - \sum_c h_{0ac}\langle T_\tau(\Psi_c(\tau)\Psi_b^\dagger(\tau'))\rangle + \langle T_\tau([H_I,\Psi_a(\tau)]\Psi_b^\dagger(\tau'))\rangle
\end{aligned} \tag{2.5}$$

$$-\partial_{\tau'}\mathcal{G}(\tau-\tau',a,b) = -\delta(\tau-\tau')\delta_{ab} + \sum_c\langle T_\tau(\Psi_a(\tau)\Psi_c^\dagger(\tau'))\rangle h_{0cb} + \langle T_\tau(\Psi_a(\tau)[H_I,\Psi_b^\dagger(\tau')])\rangle \tag{2.6}$$

Which is the general form of equations of motion. Next we will consider the special case $H_I = 0$ which is the most relevant for this thesis and use the so called matrix notation referring to the variable structure $AB(a,b) = \sum_c A(a,c)B(c,b)$ which follows the rules of matrix multiplication. It should be stated that in this notation c could be any state, including momentum k and spin, but also different types of fermions. Using this structure and removing the index $h_0 = h$ the previous equations can be rewritten into the simple form

$$-\partial_\tau \mathcal{G} = I + h\mathcal{G} \quad \Rightarrow \quad i\omega_n \mathcal{G} = I + h\mathcal{G} \tag{2.7}$$

$$\partial_{\tau'} \mathcal{G} = -\partial_\tau \mathcal{G} = I + \mathcal{G}h \quad \Rightarrow \quad i\omega_n \mathcal{G} = I + \mathcal{G}h \tag{2.8}$$

with $I = \delta_{ab}$ and all greens functions having suppressed a common frequency $\mathcal{G} = \mathcal{G}(i\omega_n)$. Next we sort Greens functions, separating internal degrees of freedom as momentum and spin from different states living in different sub-spaces. Therefore we rewrite the previous equation but with Latin index a only denoting the sub-space and Greek to internal degrees of freedom,

$$i\omega_n \mathcal{G}_{aa\gamma\mu} = \delta_{aa}\delta_{\gamma\mu} + \sum_b \sum_\rho h_{ab\gamma\rho}\mathcal{G}_{ba\rho\mu} \tag{2.9}$$

$$\Rightarrow \sum_\gamma \left(i\omega_n \delta_{\rho\gamma} - h_{aa\rho\gamma}\right) \mathcal{G}_{aa\gamma\mu} = \delta_{aa}\delta_{\rho\mu} + \sum_{b\neq a\gamma} h_{ab\rho\gamma}\mathcal{G}_{ba\gamma\mu} \tag{2.10}$$

where we have summed and renamed indices. Next we define the bare Greens function $\mathcal{G}_{0a\rho\gamma} = \left(i\omega_n\delta_{\rho\gamma} - h_{aa\rho\gamma}\right)^{-1}$ which is the Greens function if their is no interactions with other fermions, $h_{ab} = 0$ for $b \neq a$ as the right-hand side of the above equation will then be an identity. Next we reinstate the matrix notation for the internal degrees of freedom,

$$\mathcal{G}_{0a}^{-1}\mathcal{G}_{aa} = I + \sum_{b\neq a} h_{ab}\mathcal{G}_{ba} \tag{2.11}$$

$$\Rightarrow \mathcal{G}_{aa} = \mathcal{G}_{0a} + \mathcal{G}_{0a}\sum_{b\neq a} h_{ab}\mathcal{G}_{ba} \tag{2.12}$$

$$\Rightarrow \mathcal{G}_{aa} = \mathcal{G}_{0a} + \sum_{b\neq a} \mathcal{G}_{ab}h_{ba}\mathcal{G}_{0a} \tag{2.13}$$

where the last result is what is obtained if one started from Eq.(2.8) instead of (2.7). Next in order to fully determine such systems, one also needs equations for the coupled Greens functions using the above equation one obtains a similar result except that the identity terms cancels out,

$$\mathcal{G}_{ba} = \sum_{c\neq b} \mathcal{G}_{0b}h_{bc}\mathcal{G}_{ca} \quad \text{and} \quad \mathcal{G}_{ba} = \sum_{c\neq a} \mathcal{G}_{bc}h_{ca}\mathcal{G}_{0a} \tag{2.14}$$

which is the full set of equations necessary for solving systems of time-independent quadratic Hamiltonians including coupling between different fermion systems. Next we will introduce the concept of Nambu-space to construct quadratic Hamiltonians which includes magnetic and superconducting interactions.

2.2 Nambu space

In this thesis we will often be working with both superconducting and magnetic interactions so this section is dedicated to definitions and usage of Nambu space. Consider a Superconducting Hamiltonian with some spin scattering interaction J

$$H = \sum_k \left[\sum_\sigma \xi_k c^\dagger_{k\sigma} c_{k\sigma} + \Delta c^\dagger_{k\uparrow} c^\dagger_{-k\downarrow} + \Delta c_{-k\downarrow} c_{k\uparrow} + J \sum_{k'} (c^\dagger_{k\uparrow} c_{k'\uparrow} - c^\dagger_{k\downarrow} c_{k'\downarrow}) \right] \tag{2.15}$$

which contains multiple interactions. In derivations, and especially in perturbation theory, it will be annoying always having to expand in all interactions, so we desire a way to automatically include some of the interactions in a quadratic form. This can be done by choosing a new basis,

$$\Psi^\dagger_k = \begin{pmatrix} c^\dagger_{k\uparrow}, & c_{-k\downarrow}, & c^\dagger_{k\downarrow}, & -c_{-k\uparrow} \end{pmatrix} \tag{2.16}$$

here the sign on the last term is chosen for convenience. Remembering that the whole 2×2 Hilbert space is spanned by Pauli matrices one can write out the full 4×4 space as tensor products of Pauli matrices. Defining the tensor product structure such that τ operates in particle-hole space corresponding to entrance $1, 2$ and $3, 4$ of $\Psi^\dagger_k$ while σ operates in spin space corresponding to $1, 3$ and $2, 4$. Also we use the shorthand notation $\sigma_i \tau_j = \sigma_i \otimes \tau_j$ and we suppress identities $\tau_i = \sigma_0 \otimes \tau_i$ which allows us to write matrices in the following way,

$$\tau_x = \begin{pmatrix} 0 & 1 & 0 & 0 \\ 1 & 0 & 0 & 0 \\ 0 & 0 & 0 & 1 \\ 0 & 0 & 1 & 0 \end{pmatrix}, \qquad \sigma_y \tau_y = \begin{pmatrix} 0 & 0 & 0 & -1 \\ 0 & 0 & 1 & 0 \\ 0 & 1 & 0 & 0 \\ -1 & 0 & 0 & 0 \end{pmatrix} \tag{2.17}$$

Using this notation we can rewrite out Hamiltonian as

$$H = \frac{1}{2} \sum_{kk'} \Psi^\dagger_k \left[(\xi_k \tau_z + \Delta \tau_x) \delta_{kk'} + J \sigma_z \right] \Psi_{k'} = \frac{1}{2} \sum_{kk'} \Psi^\dagger_k h_{k,k'} \Psi_{k'} \tag{2.18}$$

in obtaining this expression from eq.(2.15) we used $\xi_k \to \xi_{-k}$, neglected constant terms and introduced a factor $1/2$ to fix overcounting. A subtlety in using the 4×4 Nambu space is that regular anti-commutators take a slightly different form

$$\left\{ \Psi^\dagger_{k\mu}, \Psi_{k'\mu'} \right\} = \delta_{kk'} \delta_{\mu\mu'}, \qquad \left\{ \Psi^\dagger_{k\mu}, \Psi^\dagger_{k'\mu'} \right\} = \delta_{-kk'} (\sigma_y \tau_y)_{\mu\mu'} \tag{2.19}$$

which will turn out to be a little problematic in regards to Green function structure, but first let us define the Green-functions in Nambu space. The Nambu Greens function is defined as the outer product of the Nambu spinors

$$\mathcal{G}_{\mu\nu}(\tau, \tau', a, b) = -\langle T_\tau (\Psi_{a\mu}(\tau) \Psi^\dagger_{b\nu}(\tau') \rangle \tag{2.20}$$

which forms a matrix written here in index $\mu\nu$. Next we would like to incorporate Nambu space into the existing Greens-function framework, in order for this to work the equations of motion in eq.(2.5)

must yield a similar structure in Nambu space as to normal space. This equation consist of two parts an identity and the commutator with H. First notice that the identity term also forms if the states where in Nambu space as the new spinors anti-commutator also yields an identity as seen in Eq.(2.19)

The problems is terms like $[H, \Psi_a]\,\Psi_b^\dagger = -h_{ac}\Psi_c\Psi_b^\dagger$ with normal states, where we need to check that operators in Nambu space behaves similarly. We here consider the case of operators belonging to the same fermionic space too avoid to many indexes, but the result generalizes to different spaces as well, and as spin now is incorporated in Nambu structure the only internal degree of freedom is k so we write,

$$\begin{aligned}
[H, \Psi_{k\mu}]\,\Psi_{k'\mu'}^\dagger &= \frac{1}{2}\sum_{k''k'\eta''\eta'}\left(\Psi_{k'\eta'}^\dagger h_{k'\eta'k''\eta''}\Psi_{k''\eta''}\Psi_{k\mu} - \Psi_{k\mu}\Psi_{k'\eta'}^\dagger h_{k'\eta'k''\eta''}\Psi_{k''\eta''}\right)\Psi_{k'\mu'}^\dagger \\
&= -\frac{1}{2}\sum_{k''\eta''} h_{k\mu k''\eta''}\Psi_{k''\eta''}\Psi_{k'\mu'}^\dagger + \frac{1}{2}\sum_{k'\eta'\eta''}\Psi_{k'\eta'}^\dagger h_{k'\eta'-k\eta''}(\sigma_y\tau_y)_{\eta''\mu}\Psi_{k'\mu'}^\dagger \\
&= -\frac{1}{2}\sum_{k''\eta''} h_{k\mu k''\eta''}\Psi_{k''\eta''}\Psi_{k'\mu'}^\dagger - \frac{1}{2}\sum_{k'\eta'\eta''}\Psi_{k'\eta'}^\dagger(\sigma_y\tau_y)_{\eta'\eta''}h_{k'\eta''-k\mu}\Psi_{k'\mu'}^\dagger \qquad (2.21)\\
&= -\frac{1}{2}\sum_{k''\eta''} h_{k\mu k''\eta''}\Psi_{k''\eta''}\Psi_{k'\mu'}^\dagger - \frac{1}{2}\sum_{k'\eta''} h_{k'\eta''-k\mu}\Psi_{k'\eta''}\Psi_{k\mu'}^\dagger \\
&= -\sum_{k''\eta''} h_{kk''\mu\eta''}\Psi_{k''\eta''}\Psi_{k'\mu'}^\dagger
\end{aligned}$$

from the second to third line we used anti-commutators, from third to fourth line we used $\{h_k, \sigma_y\tau_y\} = 0$ and lastly we used that $\Psi_k^\dagger(\sigma_y\tau_y) = \Psi_{-k}$, $h_k = h_k^T$ and $h_{k,-k'} = h_{k,k'} = h_{k',k}$. So we see here that in order for these relations to be true, a number of restrictions need to be put on h. The Hamiltonians we are working with, as the one presented in this section, always fulfills these properties.

Lastly a quick trick yields a useful result, consider

$$\begin{aligned}
&\left([H, \Psi_{k\mu}]\,\Psi_{k'\mu'}^\dagger\right)^\dagger = -\Psi_{k'\mu'}\left[H, \Psi_{k\mu}^\dagger\right] = \left(-\sum_{k''\eta''} h_{kk''\mu\eta''}\Psi_{k''\eta''}\Psi_{k'\mu'}^\dagger\right)^\dagger = -\sum_{k''\eta''}\Psi_{k'\mu'}\Psi_{k''\eta''}^\dagger h_{k''k\eta''\mu} \\
&\Rightarrow \Psi_{k'\mu'}\left[H, \Psi_{k\mu}^\dagger\right] = \sum_{k''\eta''}\Psi_{k'\mu'}\Psi_{k''\eta''}^\dagger h_{k''k\eta''\mu} \qquad (2.22)
\end{aligned}$$

These two equations precisely mimic the matrix structure, except the inclusion of Nambu space, which we used in the calculation of Eq.(2.12) and related quantities, therefore we are allowed to include Nambu space freely into the matrix structure in Eq.(2.12), Eq.(2.13) and Eq.(2.14) which constitutes a powerful set of equations which we will use for solving coupled systems with both magnetic and superconducting interactions in Section.5.

3 Magnectic Interactions - YSR state

The basic concept of the Yu-Shiba-Rusinov state comes from a local magnetic exchange term applied to a superconductor. This system was first investigated by Yu-Shiba-Rusinov [3, 4, 5] where they, in order to solve the complicated spin-spin correlations, approximated the spin to be classical instead of quantum mechanical. What they found is that such interactions leads to the formation of a bound state.

In this section, starting from the addition of an potential and magnetic scattering term, we will show that one obtains a sup-gap resonance which will turn out to be the YSR state. From there we will consider the spectral properties of the YSR state focusing of the symmetry breaking properties of the potential scattering term. In the end we will derive a more simple formalism for the YSR state consisting of only two particles but with the loss of information about out of gap behavior. The Hamiltonian for a local spin-spin interaction is

$$H_K = \int dr \sum_{\sigma\sigma'} J\delta(r) c^\dagger_\sigma(r) \boldsymbol{S} \cdot \boldsymbol{\sigma}_{\sigma\sigma'} c_{\sigma'}(r) \tag{3.1}$$

where J is the strength of the magnetic interaction, $\boldsymbol{S}$ is the local spin operator and $\boldsymbol{\sigma} = (\sigma_x, \sigma_y, \sigma_z)$ is a vector of Pauli-matrices. Making this spin classical is done by letting $\boldsymbol{S} \to \infty$ and fixing the direction while letting $J \to 0$ such that $J|S| = \text{const}$. For simplicity one commonly chooses $\boldsymbol{S}$ to point in the z-direction.

Now we will cast everything in Nambu spinor form as discussed in the previous section. Inserting H_K into a standard BCS superconductor and adding a local potential scattering term W yields,

$$H = \frac{1}{2} \int dr dr' \Psi^\dagger_r \left[\xi(r - r')\tau_z + \Delta\tau_x + (J\sigma_z + W\tau_z)\delta(r)\delta(r') \right] \Psi_{r'} \tag{3.2}$$

written with the spinor defined in Section.2.2 fourier transformed into r space. We include the potential scattering term since most models derived from real systems, either impurities on a substrate or quantum dots, yields both magnetic and non-magnetic scattering. This will be our full Hamiltonian and next we derive the corresponding Greens function starting from equation of motion,

$$\mathcal{G}(i\omega_n, r = 0) = \left[i\omega_n - h(r = 0) \right]^{-1} = \left[\mathcal{G}_0^{-1}(r = 0) - V \right]^{-1} \tag{3.3}$$

here we defined the bare Greens-function of the Superconductor, which we calculate in the next subsection, treating it separately from the local interactions $V = J\sigma_z + W\tau_z$ as it is not diagonal in r.

3.1 Bare Greens Function

Here we calculate the bare Greens-function for a BCS superconductor in r space. Since $\mathcal{G}_0$ is diagonal in k we start from there and perform a fourier transform,

$$\mathcal{G}_0(r, i\omega_n) = \int d^3k \frac{e^{i\boldsymbol{k}\cdot\boldsymbol{r}}}{i\omega_n - \xi_k\tau_z - \Delta\tau_x} = 2\pi \int dk \int_{-1}^{1} d\cos(\theta) \frac{k^2 e^{ikr\cos(\theta)}}{i\omega_n - \xi_k\tau_z - \Delta\tau_x} \tag{3.4}$$

as we consider local interactions only in this thesis we set $r = 0$ and suppress the r index,

$$G(i\omega_n) = 4\pi \int dk \frac{k^2}{i\omega_n - \xi_k\tau_z - \Delta\tau_x} \tag{3.5}$$

next we will change integration variable to ξ_k by use of the density of states

$$\frac{dk}{d\xi_k} = \frac{dk}{dN}\frac{dN}{d\xi_k} = \frac{1}{4\pi k^2}\nu_0(\xi_k) \tag{3.6}$$

where the denominator is simply the surface of a sphere as we consider the Fermi surface to be a sphere in momentum.

Using this to change integration and setting the density of states constant around the fermi-surface $\nu_0(\xi_k) = \nu_F$ yields

$$\mathcal{G}(i\omega_n) = \nu_F \int d\xi_k \frac{1}{i\omega_n - \xi_k\tau_z - \Delta\tau_x} = \nu_F \int d\xi_k \frac{i\omega_n + \Delta\tau_x + \xi_k\tau_z}{(i\omega_n)^2 - \xi_k^2 - \Delta^2} \tag{3.7}$$

here we quickly recognize that the $\xi_k\tau_z$ drops out as it is a asymmetric function

$$\mathcal{G}_0(i\omega_n) = -\nu_F \int d\xi_k \frac{i\omega_n + \Delta\tau_x}{(\xi_k + \sqrt{(i\omega_n)^2 - \Delta^2})(\xi_k - \sqrt{(i\omega_n)^2 - \Delta^2})} \tag{3.8}$$

now in order so solve this by complex integration we perform analytical continuation substituting $i\omega_n \to \omega + i\eta$ which gives us the retarded Greens function.

First lets consider how the denominator changes under this substitution

$$\sqrt{\omega^2 + i\omega\eta - \Delta^2} \approx \sqrt{\omega^2 - \Delta^2} + i\text{sgn}(\omega)\eta \tag{3.9}$$

where we have ignored terms of higher order in η, taylor expanded and rescaled η as it is infinitesimal small anyway, only keeping track of signs

Then the Greens function becomes

$$\mathcal{G}_0(i\omega_n) = -\nu_F \lim_{\eta\to 0} \int d\xi_k \frac{i\omega_n + \Delta\tau_x}{(\xi_k + i\text{sgn}(\omega)\eta + \sqrt{\omega^2 - \Delta^2})(\xi_k - i\text{sgn}(\omega)\eta - \sqrt{\omega^2 - \Delta^2})} \tag{3.10}$$

we will now solve this by integrating over the positive half plane, but we need to consider the expression in two cases:

1) If $\Delta > \omega$ then the square roots gives an i and the $\eta \to 0$ limit can be taken before integration and the pole becomes $\xi_k = i\sqrt{\Delta^2 - \omega^2}$

2) If $\Delta < \omega$ then the η term decides which of the poles is on the positive half plane and so the pole becomes $\xi_k = i\eta + \text{sgn}(\omega)\sqrt{\omega^2 - \Delta^2}$ and $\eta \to 0$ is taken at the end.

All in all we obtain the forked function

$$\mathcal{G}_0^R(\omega) = -\theta(\Delta - |\omega|)\pi\nu_F \frac{\omega + \Delta\tau_x}{\sqrt{\Delta^2 - \omega^2}} - i\theta(|\omega| - \Delta)\text{sgn}(\omega)\pi\nu_F \frac{\omega + \Delta\tau_x}{\sqrt{\omega^2 - \Delta^2}} \tag{3.11}$$

which is the common building block of the superconductor.

Throughout this thesis we will often write this Greens function as

$$\mathcal{G}_0^R(\omega) = -\pi\nu_F \frac{\omega + \Delta\tau_x}{\sqrt{\Delta^2 - \omega^2}} \tag{3.12}$$

but when doing computations one needs to be careful using eq.(3.11) to properly determine signs.

Notice that for spectral properties only the imaginary values matter and so for $|\omega| < \Delta$ the spectral function is zero as expected from a superconductor as this is within the gap where no quasi-particles are present.

3.2 YSR state

Now with the bare Greens function calculated we return to the full retarded Greens function with local interactions included. The calculations done here follows the conventions used in [20, 13] but with some slight changes of signs in order to keep consistence with the rest of the thesis. Considering the full Greens function

$$\mathcal{G}^R(\omega) = \left[(\mathcal{G}_0^R(\omega))^{-1} - V\right]^{-1} = \pi\nu_F \left[\frac{\omega - \Delta\tau_x}{\sqrt{\Delta^2 - \omega^2}} - \pi\nu_F(J\sigma_z + W\tau_z)\right]^{-1} \tag{3.13}$$

Here we clearly see that the natural unitless scales are $\alpha = \pi\nu_F J$ and $\beta = \pi\nu_F W$.

A great advantage of choosing z as spin direction is that we can block separate this equation into two spin-blocks by setting $\sigma_z = \sigma = \pm$ yielding

$$\mathcal{G}_\sigma^R(\omega) = \pi\nu_F\sqrt{\Delta^2 - \omega^2}\left[(\omega - \sigma\alpha\sqrt{\Delta^2 - \omega^2}) - \Delta\tau_x - \beta\sqrt{\Delta^2 - \omega^2}\tau_z\right]^{-1} \tag{3.14}$$

where σ is determined by which spin block you are considering. These are written in the reduced Nambu space,

$$\psi_\uparrow = \begin{pmatrix} c_{k\uparrow} \\ c_{-k\downarrow}^\dagger \end{pmatrix} \qquad \psi_\downarrow = \begin{pmatrix} c_{k\downarrow} \\ -c_{-k\uparrow}^\dagger \end{pmatrix} \tag{3.15}$$

inversion of a 2×2 matrix is a simple operation yielding

$$\begin{aligned} \mathcal{G}_\sigma^R(\omega) =& \frac{\pi\nu_F\sqrt{\Delta^2 - \omega^2}}{((\omega - \sigma\alpha\sqrt{\Delta^2 - \omega^2})^2 - \beta^2(\Delta^2 - \omega^2) - \Delta^2}\left[(\omega - \sigma\alpha\sqrt{\Delta^2 - \omega^2}) + \Delta\tau_x + \beta\sqrt{\Delta^2 - \omega^2}\tau_z\right] \\ =& \frac{-\pi\nu_F}{\sqrt{\Delta^2 - \omega^2}(1 - \alpha^2 + \beta^2) + 2\alpha\sigma\omega}\begin{pmatrix} \omega - (\sigma\alpha - \beta)\sqrt{\Delta^2 - \omega} & \Delta \\ \Delta & \omega - (\sigma\alpha + \beta)\sqrt{\Delta^2 - \omega^2} \end{pmatrix} \end{aligned} \tag{3.16}$$

bound states are obtained by considering resonances that is when the Greens functions denominator is zero,

$$0 = \sqrt{\Delta^2 - \omega^2}(1 - \alpha^2 + \beta^2) - 2\alpha\sigma\omega \tag{3.17}$$

$$\Rightarrow 4\alpha^2\omega^2 = (\Delta^2 - \omega^2)(1 - \alpha^2 + \beta^2)^2 \tag{3.18}$$

$$\Rightarrow \omega_0 = \pm\Delta\frac{1 - \alpha^2 + \beta^2}{\sqrt{(1 - \alpha^2 + \beta^2)^2 + 4\alpha^2}} \tag{3.19}$$

which is a very important result. This is the energy of a YSR bound state for a classical spin and a potential scattering term. One quicly notices that $|\omega_0| < \Delta$ so this state is truly a sub-gap state for all range of parameters. When no potential scattering is present it takes the more simple form

$$\omega_0(\beta = 0) = \pm\Delta \frac{1 - \pi^2 \nu_F^2 J^2}{1 + \pi^2 \nu_F^2 J^2} \tag{3.20}$$

which is the familiar expression found by [4]. For $\alpha = 0$ the bound states exist precisely at the gap and as one increases α the bound states moves down the gap and will eventually cross zero as shown on Fig.3.1. For Spin-half as we later treat in this paper this crossing marks the transition from a spin-$1/2$

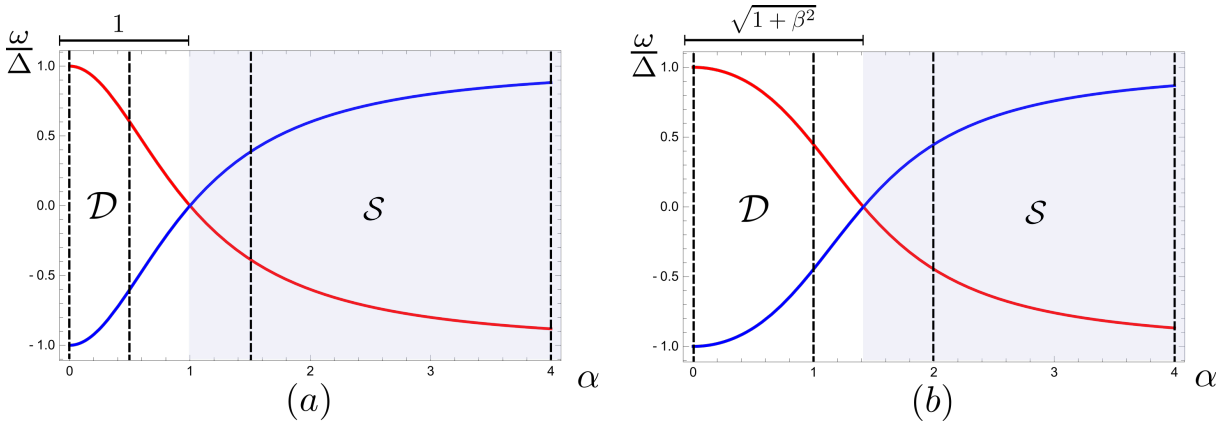

Figure 3.1: Here we plot $\pm\omega_0$ as a function of α using Eq.(3.19). For (a) $\beta = 0$ and for (b) $\beta = 1$. For a real spin, here considering $S = 1/2$, the crossing marks a change of groundstate which is why $\mathcal{D}$ is on the left side for Doublet and $\mathcal{S}$ is on the right side for Singlet. The horizontal dotted lines along both (a) and (b) refers to spectral cuts made in Fig.3.3

doublet to a screened singlet groundstate, and the singlet is when the spin is screened by a quasi-particle with opposite pointing spin from the superconductor.

Since the classical-spin does not have a spin space as a spin-$1/2$ would, this change of groundstate is not visible in the math, but is a phenomenological fact and will become apparent when we consider the Zero-Band-Width model in Section.7.

Next we will consider spectral representations of the YSR state to show how truly different this state is from the normal superconducting state. Our full Greens function for the system takes the shape

$$\mathcal{G}^R(\omega) = \begin{pmatrix} \mathcal{G}^R_\uparrow(\omega) & 0 \\ 0 & \mathcal{G}^R_\downarrow(\omega) \end{pmatrix} \tag{3.21}$$

in the full 4×4 Nambu space. In Nambu representation the spectral function is given by

$$A(\omega) = \mathcal{G}^A(\omega) - (\mathcal{G}^A(\omega))^\dagger \tag{3.22}$$

but as the full Greens function is block diagonal we can consider the blocks separately and as off-

diagonal components in each block are identical, it reduces to the imaginary part so we obtain,

$$A(\omega) = \begin{pmatrix} A_\uparrow(\omega) & 0 \\ 0 & A_\downarrow(\omega) \end{pmatrix} \qquad \text{with} \qquad A_\sigma = -\text{Im}\left[\mathcal{G}^R_\sigma(\omega)\right] \tag{3.23}$$

which components for $\sigma = \uparrow$ are plotted in Fig.3.2 for visualization.

$$\begin{pmatrix} -\text{Im}\left[\mathcal{G}^R_{\uparrow,11}(\omega)\right] & -\text{Im}\left[\mathcal{G}^R_{\uparrow,12}(\omega)\right] \\ -\text{Im}\left[\mathcal{G}^R_{\uparrow,21}(\omega)\right] & -\text{Im}\left[\mathcal{G}^R_{\uparrow,22}(\omega)\right] \end{pmatrix} \longrightarrow$$

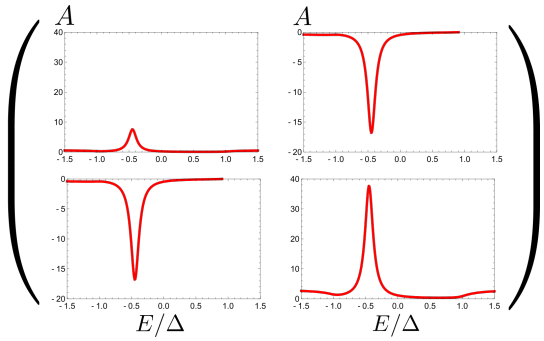

Figure 3.2: Plot of $A_{m\uparrow}(\omega)$ for $\alpha = 1$ and $\beta = 1$ in order to show how different Nambu components look. For resonances to be visible an artificial broadening of $\eta = 0.075$ have been added by $\omega \to \omega + i\eta$ The diagonal components are commonly denoted the spectral function of the electron (11) and hole sector (22).

The most common thing to consider is the diagonal components of the spectral function as it enters directly into transport calculations and as we will later see in section 5 that holes feel change of bias opposite to electrons, as the Fermi level is displaced in the negative direction under application of bias. Therefor we define a spectral representation more closely related to transport,

$$B_\uparrow(\omega) = \text{Im}\left[\mathcal{G}^R_{\uparrow,11}(\omega)\right] + \text{Im}\left[\mathcal{G}^R_{\uparrow,22}(-\omega)\right] \tag{3.24}$$

which is the spectral function probed by direct tunneling. With this definition we also find $B_\uparrow(\omega) = B_\downarrow(\omega)$ which is expected from the symmetry of the problem.

With this definition we create plots of B for different interactions strengths α drawn as lines on Fig.3.1 at Fig.3.3. A number of important features of the YSR state become visible in these plots. First notice that as α increases the peaks moves away from the band gap and at the same time the band gap weakens. This is also clear from comparing the bare superconductors Green function with the new effective eq.(3.16) where the divergence at Δ is not present, and it instead goes to zero, but a divergence at ω_0 have appeared. So YSR interaction seems more as a inward shift of gap divergences than the appearance of a new feature.

Secondly, notice that the inclusion of a potential scattering terms lifts the particle-hole symmetry and leaves the spectral function asymmetric around ω. This is due to the symmetry breaking role of the W term which can already be seen in the Greens function Eq.(3.16) where β terms have signs dependent on the particle-hole sector. A larger discussion can be found in [20] but it is worth remembering as this symmetry breaking will be a focus in future transport calculations, since it turns out that the related asymmetry in conductance is highly non-trivial to obtain.

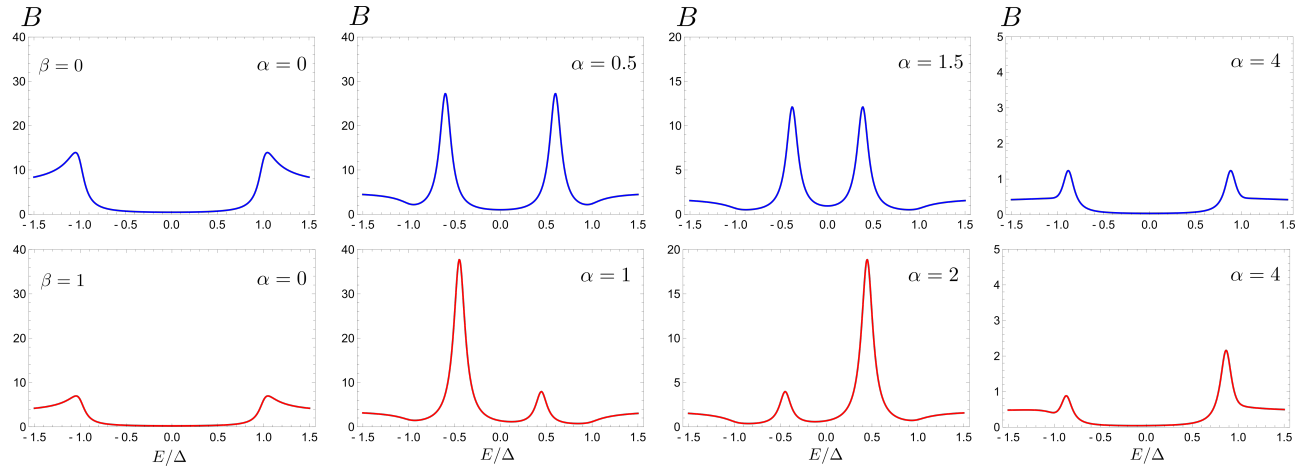

Figure 3.3: Here one sees how the function $B(\omega)$ evolve as α vary's. The blue lines are for $\beta = 0$ and the red lines for $\beta = 1$. From the left each plot relates to a line-cut on Fig.3.1. For resonances to be visible an artificial broadening of $\eta = 0.075$ have been added by $\omega \to \omega + i\eta$. Be aware that the scales change as α increases since the spectral function drops off rapidly for large α.

3.3 Simplified YSR

The preceding description of the YSR state is the most general classical evaluation, but its complexity complicates understanding in regards to calculations of transport and other properties. Therefore we will here, largely inspired by [13], develop a simplified model where we lose information about quantities out side of the gap but win more intuitive equations.

We start from the YSR Greens function

$$\mathcal{G}^R_{\uparrow}(\omega) = \frac{-\pi\nu_F}{\sqrt{\Delta^2-\omega^2}(1-\alpha^2+\beta^2)+2\alpha\sigma\omega}\begin{pmatrix}\omega-(\sigma\alpha-\beta)\sqrt{\Delta^2-\omega^2} & \Delta \\ \Delta & \omega-(\sigma\alpha+\beta)\sqrt{\Delta^2-\omega^2}\end{pmatrix} \tag{3.25}$$

which we then expand around the YSR energy ω_0 in the denominator. Substituting $\omega = -\sigma\omega_0 + \delta\omega$ into the denominator and expanding the square root yields

$$\sqrt{\Delta^2-\omega^2}(1-\alpha^2+\beta^2)+2\alpha\sigma\omega \approx \frac{\sigma\delta\omega}{2\alpha}((1-\alpha^2+\beta^2)^2+4\alpha^2) \tag{3.26}$$

and in the numerator we simply set $\omega = -\sigma\omega_0$ and obtain

$$\omega_0-(\sigma\alpha\mp\beta)\sqrt{\Delta^2-\omega_0^2} = \frac{-\sigma\Delta}{\sqrt{(1-\alpha^2+\beta^2)^2+4\alpha^2}}(1+(\alpha\mp\sigma\beta)^2) \tag{3.27}$$

resetting $\delta\omega = \omega + \sigma\omega_0$ and putting all the pieces together yields

$$\mathcal{G}^R_{a\uparrow}(\omega) = \frac{1}{\omega+\omega_0}\begin{pmatrix}v^2 & uv \\ uv & u^2\end{pmatrix}, \qquad \mathcal{G}^R_{a\downarrow}(\omega) = \frac{1}{\omega-\omega_0}\begin{pmatrix}u^2 & -uv \\ -uv & v^2\end{pmatrix} \tag{3.28}$$

with the new definitions

$$u^2 = 2\pi\nu_F\Delta\alpha\frac{1+(\alpha+\beta)^2}{((1-\alpha^2+\beta^2)^2+4\alpha^2)^{\frac{3}{2}}}, \qquad v^2 = 2\pi\nu_F\Delta\alpha\frac{1+(\alpha-\beta)^2}{((1-\alpha^2+\beta^2)^2+4\alpha^2)^{\frac{3}{2}}} \tag{3.29}$$

from which it becomes clear that the case $\beta = 0$ yields symmetric spectral heights. To make these effects even more apparent we can rewrite this as,

$$u^2 = z + \delta z, \quad v^2 = z - \delta z \tag{3.30}$$

$$z = 2\pi\nu_F\Delta\alpha\frac{1+\alpha^2+\beta^2}{((1-\alpha^2+\beta^2)^2+4\alpha^2)^{\frac{3}{2}}}, \qquad \delta z = 4\pi\nu_F\Delta\alpha\frac{\alpha\beta}{((1-\alpha^2+\beta^2)^2+4\alpha^2)^{\frac{3}{2}}} \tag{3.31}$$

defining an similar Spectral function to eq.(3.24) where we perform analytical continuation yields

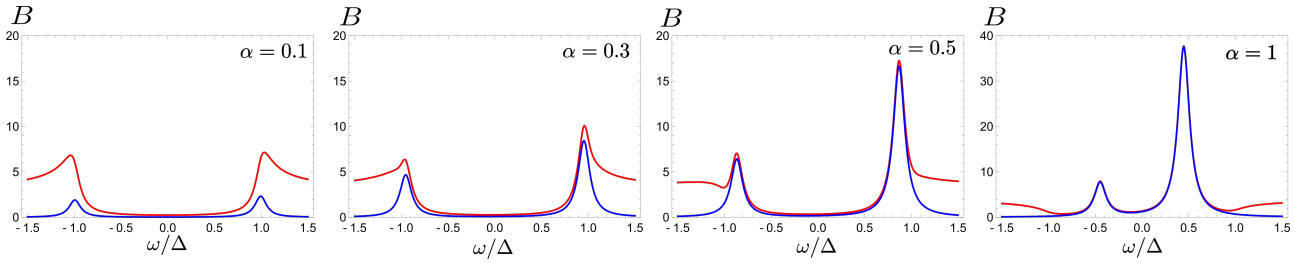

Figure 3.4: Here we see a comparison between the spectral function from the exact Greens-function (Red) and the approximate one (Blue) expanded around the resonance ω_0. Parameters are $\beta = 1$, varying α and $\eta = 0.075$

$$B_\uparrow(\omega) = \text{Im}\left[\mathcal{G}^R_{a\uparrow,11}(\omega)\right] + \text{Im}\left[\mathcal{G}^R_{a\uparrow,22}(-\omega)\right] = \frac{\eta(z-\delta z)}{(\omega+\omega_0)^2+\eta^2} + \frac{\eta(z+\delta z)}{(\omega-\omega_0)^2+\eta^2} \tag{3.32}$$

from which the YSR appears as a simple Lorentzian around the resonance. in Fig.3.4 a comparison is made between our two models and we see that the Lorentzian form fails to capture all out of gap features, so if one only wants to describe the sub-gap YSR features this approximate model provides a acceptable picture. The model also fails when the YSR state approaches the gap and weakens for very large and small α.

A great advantage of this approximate form is that it allows to work with a reduced Hamiltonian. Considering the Greens function eq.(3.28) one can express it in the basis

$$\mathcal{G}^R_{a\uparrow}(\omega) = |\phi_\uparrow\rangle\frac{1}{\omega+\omega_0}\langle\phi_\uparrow|, \qquad \mathcal{G}^R_{a\downarrow}(\omega) = |\phi_\downarrow\rangle\frac{1}{\omega-\omega_0}\langle\phi_\downarrow| \tag{3.33}$$

with $|\phi_\uparrow\rangle = (v,u)$ and $|\phi_\downarrow\rangle = (-u,v)$ which spans a diagonal basis $\langle\phi_\uparrow|\phi_\downarrow\rangle = 0$ but is not normalized $\langle\phi_\sigma|\phi_\sigma\rangle = u^2+v^2 \neq 1$. Now we define a new effective Hamiltonian for the superconductor-impurity system demanding that it generates the Greens functions. One can choose the simple form,

$$H_{eff} = \psi^\dagger_\uparrow|\phi_\uparrow\rangle\omega_0(u^2+v^2)^{-1}\langle\phi_\uparrow|\psi_\uparrow + \psi^\dagger_\downarrow|\phi_\downarrow\rangle\omega_0(u^2+v^2)^{-1}\langle\phi_\downarrow|\psi_\downarrow \tag{3.34}$$

$$= \psi^\dagger_\uparrow|\hat{\phi}_\uparrow\rangle\omega_0\langle\hat{\phi}_\uparrow|\psi_\uparrow + \psi^\dagger_\downarrow|\hat{\phi}_\downarrow\rangle\omega_0\langle\hat{\phi}_\downarrow|\psi_\downarrow \tag{3.35}$$

where the factor $(u^2+v^2)^{-1}$ is simply there as a normalization factor from the inversion of the matrix, and since it is span-1, it is its own inverse. Thereby $|\phi_\sigma\rangle\langle\phi_\sigma|\phi_\sigma\rangle\langle\phi_\sigma| = |\phi_\sigma\rangle(u^2+v^2)\langle\phi_\sigma|$ from which the normalization is necessary. In the last line we define the hat to mean $\hat{A} = A/\sqrt{u^2+v^2}$. Also ψ_σ just refers to the Nambu spinor in the σ block as defined earlier. We can rewrite our Hamiltonian in a more canonical form

$$H_{eff} = -\gamma_\uparrow^\dagger \omega_0 \gamma_\uparrow + \gamma_\downarrow^\dagger \omega_0 \gamma_\downarrow \tag{3.36}$$

where we define $\gamma_\sigma^\dagger = (\hat{v}c_\sigma^\dagger + \sigma\hat{u}c_{\bar{\sigma}})$ from which we see that they are just local Bogoliubovs with a normalization. This new Hamiltonian allows us to easily do calculations on YSR states so long one can disregard the gap.

With all this formalism in check we are ready to consider systems where YSR states are obtainable in a physical relevant model. In the next section we will consider the case of a single quantum-dot coupled to a superconductor. Since a quantum-dot behaves as a magnetic moment whenever an odd number of electrons are placed on the dot YSR physics can be obtained.

4 Single-dot system

In this section we will discuss the formation and effect of YSR states on single quantum dot systems. The general idea is that when a single electron is placed on the utmost dot orbital it must contain a free $1/2$-spin. A superconductor then interacts with this spin through tunnel interactions yielding an effective magnetic coupling from which a sub-gap YSR state forms.

For dot systems the common starting point is the Anderson model,

$$H = H_d + H_L + H_t \tag{4.1}$$

$$H_d = \sum_\sigma \epsilon_d n_\sigma + U n_\uparrow n_\downarrow$$

$$H_L = \sum_{\alpha k} \left[\sum_\sigma \xi_{\alpha k} c^\dagger_{\alpha k\sigma} c_{\alpha k\sigma} + \Delta_\alpha (c^\dagger_{\alpha k\uparrow} c^\dagger_{\alpha -k\downarrow} + c_{\alpha -k\downarrow} c_{\alpha k\uparrow}) \right], \tag{4.2}$$

$$H_t = t_\alpha \sum_{k\sigma\alpha} c^\dagger_{\alpha k\sigma} d_\sigma + \text{h.c}$$

where H_L is the Hamiltonian for the leads in generic form, H_d is the Hamiltonian for a single level with local Coulomb interaction U, where n_σ is the number operator on the dot and H_t is the tunnel Hamiltonian connecting these components.

4.1 Excitations - Coulomb diamonds

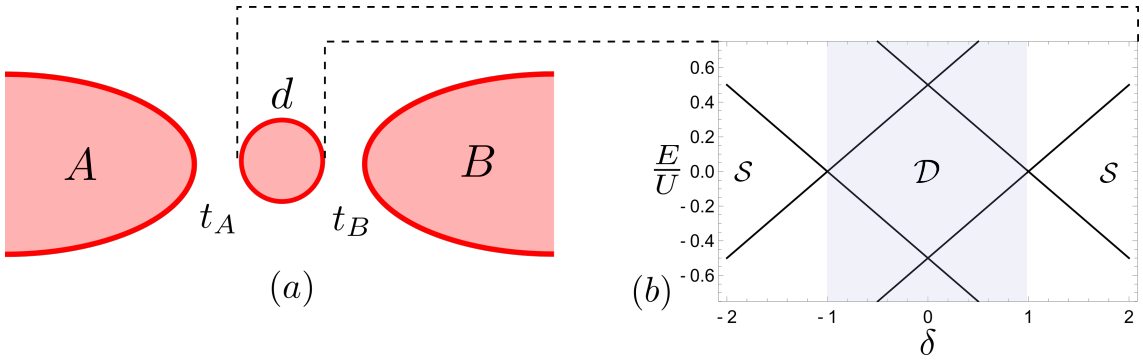

Figure 4.1: In (a) one sees a schematic of a single dot d connected to two leads A and B through tunnel couplings t_A and t_B. In (b) one sees the excitation spectrum and a mirrored spectrum of a single quantum-dot with local coulomb interaction U. These patterns are called Coulomb diamonds and a single diamond have width and height U. The color change mark different ground-states. To the left: Empty dot singlet. Middle: Single occupied doublet. Right: Double occupied singlet

For clarity we will quickly discuss the dot Hamiltonian H_d and the related Coulomb diamond picture. First of all, a single quantum-dot has 4 possible states,

$$\langle m| \in \langle 0|, \langle \sigma|, \langle \uparrow\downarrow| \tag{4.3}$$

where $\langle\sigma|$ is two states as it is a spin doublet. These states have the related energies from H_d

$$E_m \in [0,\ \ \epsilon_d,\ \ 2\epsilon_d + U] \tag{4.4}$$

since we are most interested in the single-occupied regime we will change variables to $\epsilon_d = -U/2(1+\delta)$ where δ now describes the displacement away from the particle-hole symmetric point which is the point where it is as easy to excite the filled $\langle\uparrow\downarrow|$ state as the empty state $\langle 0|$.

Since we only probe excitations, constant shifts of energy does not matter, and we can rewrite the energies as

$$E_m \in \left[\frac{U}{2}(1+\delta),\ \ 0,\ \ \frac{U}{2}(1-\delta)\right] \tag{4.5}$$

being a function of δ. The corresponding excitation spectrum is the familiar Coulomb diamond, where $\delta \pm 1$ are the degeneracy points between different ground states and $\delta = 0$ the center of the odd occupancy diamond. In simple transport experiments one would probe this diamond feature by use of two metallic probes. This yields two different regimes of transport:

1) If the bias between the two leads is smaller than any excitation in the dot, the dot is considered to be Coulomb-blockaded and any transport from lead A to B must happen through cotunneling, which is tunneling through higher energy excitations.

2) If the bias is higher than a given excitation, then current can run by constantly loading and removing electrons on the excited state, therefore one will see a dramatic rise in current when this occurs. This is denoted sequential-tunneling.

Therefore, as done in multiple experiments, one can control dot occupancy by a capacitively coupled bottom gate and then measure differential conductance $\frac{dI}{dV}$ as a function of bottom gate and bias voltage. This would yield the coulomb diamond pattern as plotted in Fig.4.1 with a constant background from cotunneling and dramatic conductance increase at bias matching the excitations as this would increase sequential tunneling.

4.2 Superconducting lead

As we are interested in the interaction between superconductors and quantum spin we will consider one of the leads to be superconducting. In order to obtain an effective YSR model we need to reduce the Anderson model to a Kondo like model. This can be done when the dots are placed deep within the cotunneling regime in which dot occupancy is locked.

Next one uses a Schrieffer-Wolff transform, following [10, 21], to derive an effective model. In Appendix.B the Schrieffer-Wolff transformation is derived and explained in detail, here we will just apply it.

First we will consider second-order Schrieffer-Wolff around $\delta = 0$ to derive the superconductors self-interaction through the quantum dot. In this derivation we consider the two single occupied states to be m-states and the two singlet states $\langle\uparrow\downarrow|$ and $\langle 0|$ to far-away in energy l-states which will be removed in the perturbation,

$$\langle m| \in \langle\lambda,\sigma| \qquad \langle l| \in \langle\lambda,0|\,,\ \langle\lambda,\uparrow\downarrow| \tag{4.6}$$

where λ is any eigenstate of the superconductor.

4.3 Second order perturbation - Self-interactions

Here we will calculate the effective interaction between a superconductor and itself, up to second order as to obtain an effective Kondo model. It should be stated that these results easily translate into superconductor-metal interaction by letting Δ for one of the leads go to zero. To use Schrieffer-Wolff most effectively we follow this recipe:

1): Write down all possible paths connecting m states.
2): For all paths manipulate operators into a normal ordered fashion
3): Calculate the energy-denominators from the transformation.

Here we will be calculating in the superconducting diagonal basis by using Bogoliubov quasi-particles which will in effect dramatically increase the number of paths one can go through a single dot, as one can both remove or add a quasi-particle when adding an electron on the dot. Therefore we will consider the paths in normal electron formalism and later change into Bogoliubov basis where one have to give each path its corresponding energy denominator. The two paths are defined as

$$1) \quad \langle \lambda, \sigma| \rightarrow \langle \lambda \pm qp, \uparrow\downarrow| \rightarrow \langle \lambda', \sigma| \tag{4.7}$$

$$2) \quad \langle \lambda, \sigma| \rightarrow \langle \lambda \pm qp, 0| \rightarrow \langle \lambda', \sigma| \tag{4.8}$$

where the number of particles in the superconductor λ' varies from λ by 0 or ± 2 quasi-particles dependent of path. These paths can also be regarded as two permutations of the tunnel Hamiltonians necessary for the transition as shown in Fig.4.2 The Hamiltonian connecting these different states is

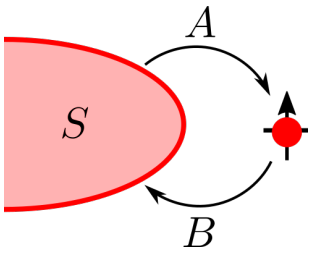

Figure 4.2: A graphical interpretation of the paths considered in Schrieffer-Wolff transformation. The two paths correspond to: $1)$ $H_B H_A$ and $2)$ $H_A H_B$. Which is to be read from the right. H is the relevant tunnel Hamiltonian for the shown path.

the tunneling Hamiltonian Eq.(4.2) so what we are doing is effectively perturbations in tunnel couplings over energy of the l states which close to $\delta = 0$ is approximately $U_\alpha/2$. Next, following the recipe, we will consider operator order for these two paths, where we will change into the diagonal basis of the superconductor described by Bogoliubov quasi-particles $c_{k\sigma} = u_k \gamma_{k\sigma} - \sigma v_k \gamma^\dagger_{-k\bar{\sigma}}$ and expand into

more paths,

$$\begin{aligned}
&1) \quad H_B H_A \Rightarrow t_S^2 \sum_{kk'\sigma\sigma'} c_{k\sigma}^\dagger d_\sigma d_{\sigma'}^\dagger c_{k'\sigma'} = t_S^2 \sum_{kk'\sigma\sigma'} (u_k \gamma_{k\sigma}^\dagger - \sigma v_k \gamma_{-k\bar{\sigma}}) d_\sigma d_{\sigma'}^\dagger (u_{k'} \gamma_{k'\sigma'} - \sigma' v_{k'} \gamma_{-k'\bar{\sigma}'}^\dagger) \\
&\Rightarrow H_{1eff} = \sum_{kk'\sigma\sigma'} t_S^2 \left(\delta_{\sigma\sigma'} - d_{\sigma'}^\dagger d_\sigma \right) \\
&\left(A_+^{(1)} u_k u_{k'} \gamma_{k\sigma}^\dagger \gamma_{k'\sigma'} - A_-^{(1)} \sigma\sigma' v_k v_{k'} \gamma_{k\bar{\sigma}'}^\dagger \gamma_{k\bar{\sigma}} - B^{(1)} \sigma v_k u_{k'} \gamma_{-k\bar{\sigma}} \gamma_{k'\sigma'} - B^{(1)} \sigma' u_k v_{k'} \gamma_{k\sigma}^\dagger \gamma_{-k'\bar{\sigma}'}^\dagger \right)
\end{aligned} \tag{4.9}$$

$$\begin{aligned}
&2) \quad H_A H_B \Rightarrow t_S^2 \sum_{kk'\sigma\sigma'} d_\sigma^\dagger c_{k\sigma} c_{k'\sigma'}^\dagger d_{\sigma'} = t_S^2 \sum_{kk'\sigma\sigma'} d_\sigma^\dagger (u_k \gamma_{k\sigma} - \sigma v_k \gamma_{-k\bar{\sigma}}^\dagger)(u_{k'} \gamma_{k'\sigma'}^\dagger - \sigma' v_{k'} \gamma_{-k'\bar{\sigma}'}) d_{\sigma'} \\
&\Rightarrow H_{2eff} = - \sum_{kk'\sigma\sigma'} t_S^2 d_{\sigma'}^\dagger d_\sigma \\
&\left(A_+^{(2)} u_k u_{k'} \gamma_{k\sigma}^\dagger \gamma_{k'\sigma'} - A_-^{(2)} \sigma\sigma' v_k v_{k'} \gamma_{k\bar{\sigma}'}^\dagger \gamma_{k\bar{\sigma}} - B^{(2)} \sigma v_k u_{k'} \gamma_{-k\bar{\sigma}} \gamma_{k'\sigma'} - B^{(2)} \sigma' u_k v_{k'} \gamma_{k\sigma}^\dagger \gamma_{-k'\bar{\sigma}'}^\dagger \right)
\end{aligned} \tag{4.10}$$

where we have used $u_k = u_{-k}$ and $v_k = v_{-k}$, interchanged dummy indeces and discarded terms not dependent on γ. Importantly, in the last step in each calculation we inserted the energy denominator corresponding to that specific path.

Next we consider the energy denominator from eq.(B.14) where we neglect the k dependence of the quasi particles since we attribute processes closest to the gap to be dominant, thereby setting $E_{Sk} \approx |\Delta|$ and use $\epsilon_S \approx -\frac{U}{2}(1+\delta)$ yielding

$$\begin{aligned}
A_\pm^{(1)} &= \frac{1}{2}\left(\frac{1}{E_\sigma - E_{2\mp qp}} + \frac{1}{E_{\sigma'} - E_{2\mp qp}} \right) = \frac{1}{E_\sigma - E_{2\mp qp}} = \frac{1}{\epsilon_d - 2\epsilon_d - U \pm \Delta} \\
&= \frac{2}{U} \frac{-1}{1-\delta} \sum_{n=0}^{\infty} \left(\frac{2\Delta}{U} \frac{\mp 1}{1-\delta} \right)^n
\end{aligned} \tag{4.11}$$

$$\begin{aligned}
A_\pm^{(2)} &= \frac{1}{2}\left(\frac{1}{E_\sigma - E_{0\pm qp}} + \frac{1}{E_{\sigma'} - E_{0\pm qp}} \right) = \frac{1}{E_\sigma - E_{0\pm qp}} = \frac{1}{\epsilon_d \mp \Delta} \\
&= \frac{2}{U} \frac{-1}{1+\delta} \sum_{n=0}^{\infty} \left(\frac{2\Delta}{U} \frac{\pm 1}{1+\delta} \right)^n
\end{aligned} \tag{4.12}$$

$$\begin{aligned}
B^{(1)} &= \frac{1}{2}\left(\frac{1}{E_\sigma - E_{2\mp qp}} + \frac{1}{E_{\sigma\pm 2qp} - E_{2\mp qp}} \right) = \frac{1}{2}\frac{1}{-\epsilon_d - U + \Delta} + \frac{1}{2}\frac{1}{-\epsilon_d - U - \Delta} \\
&= \frac{2}{U} \frac{-1}{1-\delta} \sum_{n=0}^{\infty} \left(\frac{2\Delta}{U} \frac{1}{1-\delta} \right)^{2n}
\end{aligned} \tag{4.13}$$

$$\begin{aligned}
B^{(2)} &= \frac{1}{2}\left(\frac{1}{E_\sigma - E_{0\pm qp}} + \frac{1}{E_{\sigma\mp 2qp} - E_{0\pm qp}} \right) = \frac{1}{2}\frac{1}{\epsilon_d + \Delta} + \frac{1}{2}\frac{1}{\epsilon_d - \Delta} \\
&= \frac{2}{U} \frac{-1}{1+\delta} \sum_{n=0}^{\infty} \left(\frac{2\Delta}{U} \frac{1}{1+\delta} \right)^{2n}
\end{aligned} \tag{4.14}$$

here the $\pm qp$ indicates if quasi-particles are removed or added to the superconductor for a given path, yielding a contribution of Δ, the 0 or 2 index are particles on the dot and σ index is the spin of a

single particle on the dot. At this stage it also becomes clear that in order for us to have a controlled expansion then $\Delta << |\epsilon_d|, |\epsilon_d + U|$ or else the denominators would diverge. This yields

$$\Delta << \frac{U}{2}|1 \pm \delta| \tag{4.15}$$

As we would like an effective spin model in the end we rewrite the S-dot operators in term of spin operators using the following relations,

$$\begin{aligned} d_\uparrow^\dagger d_\uparrow &= \frac{1}{2} + S_z \\ d_\downarrow^\dagger d_\downarrow &= \frac{1}{2} - S_z \\ d_\uparrow^\dagger d_\downarrow &= S_x + iS_y \\ d_\downarrow^\dagger d_\uparrow &= S_x - iS_y \end{aligned} \tag{4.16}$$

Inserting these into eq.(4.10) we notice a important distinction between the spin dependent part and the spin independent part, namely that the $\delta_{\sigma\sigma'}$ term enters into the non-spin dependent part and changes the sign. So to obtain the new effective terms one should add the contribution from path $1)$ to $2)$ for spin dependent terms and subtract them for non-spin dependent terms proportional to the identity. Even though this recipe is simple, the math gets tedious when including all orders of Δ as the sorting of different terms and signs is not trivial. We will therefor here present the main result which depends on the following couplings found from the denominators,

$$\begin{aligned} J_S &= \frac{2t_S^2}{U}\sum_{n=0}^{\infty}\left(\frac{2\Delta}{U}\right)^{2n}\left(\frac{1}{(1+\delta)^{2n+1}} + \frac{1}{(1-\delta)^{2n+1}}\right) \\ &= \frac{t_S^2}{U}\frac{2}{1-\delta^2}\left[\mathbf{2} + \sum_{n=1}^{\infty}\left(\frac{2\Delta}{U}\right)^{2n}\frac{(1-\delta)^{2n+1} + (1+\delta)^{2n+1}}{(1-\delta^2)^{2n}}\right] \end{aligned} \tag{4.17}$$

$$\begin{aligned} W_S &= \frac{1}{2}\frac{2t_S^2}{U}\sum_{n=0}^{\infty}\left(\frac{2\Delta}{U}\right)^{2n}\left(\frac{1}{(1+\delta)^{2n+1}} - \frac{1}{(1-\delta)^{2n+1}}\right) \\ &= \frac{t_S^2}{U}\frac{1}{1-\delta^2}\left[\boldsymbol{-2\delta} + \sum_{n=1}^{\infty}\left(\frac{2\Delta}{U}\right)^{2n}\frac{(1-\delta)^{2n+1} - (1+\delta)^{2n+1}}{(1-\delta^2)^{2n}}\right] \end{aligned} \tag{4.18}$$

$$\begin{aligned} J_{S\Delta} &= \frac{2t_S^2}{U}\sum_{n=1}^{\infty}\left(\frac{2\Delta}{U}\right)^{2n-1}\left(\frac{1}{(1+\delta)^{2n}} - \frac{1}{(1-\delta)^{2n}}\right) \\ &= \frac{4t_S^2\Delta}{U^2}\sum_{n=1}^{\infty}\frac{(1-\delta)^{2n} - (1+\delta)^{2n}}{(1-\delta^2)^{2n}} \end{aligned} \tag{4.19}$$

$$\begin{aligned} W_{S\Delta} &= \frac{1}{2}\frac{2t_S^2}{U}\sum_{n=1}^{\infty}\left(\frac{2\Delta}{U}\right)^{2n-1}\left(\frac{1}{(1+\delta)^{2n}} + \frac{1}{(1-\delta)^{2n}}\right) \\ &= \frac{2t_S^2\Delta}{U^2}\sum_{n=1}^{\infty}\frac{(1-\delta)^{2n} + (1+\delta)^{2n}}{(1-\delta^2)^{2n}} \end{aligned} \tag{4.20}$$

where in general the sums have been split into even and odd parts as to accommodate the sign differences. The terms shown in bold text are the two terms yielding the standard Schrieffer-Wolff terms for a metal, all other terms are of higher order in Δ/U.

With all this in check, we write out the full second order perturbation, being careful about signs from different combinations of u_k and v_k terms and get,

$$\hat{H}^{(2)} = H_{1eff} + H_{2eff} = H_J + H_W + H_{J\Delta} + H_{W\Delta} \tag{4.21}$$

$$\begin{aligned} H_J = {} & J_S S_z \left[K_{kk'}(\gamma^\dagger_{k\uparrow}\gamma_{k'\uparrow} - \gamma^\dagger_{k\downarrow}\gamma_{k'\downarrow}) - (L_{kk'} - L_{k'k})\gamma_{-k\downarrow}\gamma_{k'\uparrow} - (L_{k'k} - L_{kk'})\gamma^\dagger_{k\uparrow}\gamma^\dagger_{-k'\downarrow} \right] \\ & + J_S S_+ \left[K_{kk'}\gamma^\dagger_{k\downarrow}\gamma_{k'\uparrow} + L_{k'k}\gamma_{-k\uparrow}\gamma_{k\uparrow} + L_{k'k}\gamma^\dagger_{k\downarrow}\gamma^\dagger_{-k'\downarrow} \right] \\ & + J_S S_- \left[K_{kk'}\gamma^\dagger_{k\uparrow}\gamma_{k'\downarrow} + L_{kk'}\gamma_{-k\downarrow}\gamma_{k\downarrow} + L_{kk'}\gamma^\dagger_{k\uparrow}\gamma^\dagger_{-k'\uparrow} \right] \end{aligned} \tag{4.22}$$

$$H_W = W_S \left[M_{kk'}(\gamma^\dagger_{k\uparrow}\gamma_{k'\uparrow} + \gamma^\dagger_{k\downarrow}\gamma_{k'\downarrow}) - (L_{kk'} + L_{k'k})\gamma_{-k\downarrow}\gamma_{k'\uparrow} - (L_{k'k} + L_{kk'})\gamma^\dagger_{k\uparrow}\gamma^\dagger_{-k'\downarrow} \right] \tag{4.23}$$

$$H_{J\Delta} = J_{S\Delta} M_{kk'} \left[S_z(\gamma^\dagger_{k\uparrow}\gamma_{k'\uparrow} - \gamma^\dagger_{k\downarrow}\gamma_{k'\downarrow}) + S_+\gamma^\dagger_{k\downarrow}\gamma_{k'\uparrow} + S_-\gamma^\dagger_{k\uparrow}\gamma_{k'\downarrow} \right] \tag{4.24}$$

$$H_{W\Delta} = W_{S\Delta} K_{kk'} \left[\gamma^\dagger_{k\uparrow}\gamma_{k'\uparrow} + \gamma^\dagger_{k\downarrow}\gamma_{k'\downarrow} \right] \tag{4.25}$$

with the following definitions

$$K_{kk'} = u_k u_{k'} + v_k v_{k'}, \quad M_{kk'} = u_k u_{k'} - v_k v_{k'}, \quad L_{kk'} = u_k v_{k'} \tag{4.26}$$

notice that in $H_{W\Delta}$ and $H_{J\Delta}$ no L dependent terms arise as the energy denominator B contains no odd terms. Which is the same Hamiltonian as found by [10]. Now for clarity we will shift back to $c^\dagger$, c space yielding for the normal terms

$$H_J = J_S \sum_{kk'\sigma\sigma'} c^\dagger_{k\sigma S} S \cdot \sigma_{\sigma\sigma'} c_{k'\sigma' S}, \quad H_W = W_S \sum_{kk'\sigma} c^\dagger_{\sigma k S} c_{\sigma k' S} \tag{4.27}$$

Which is the expected form from a Schrieffer-Wolff transformation in a normal metal and for the new terms,

$$H_{W\Delta} = W_{S\Delta} \sum_{\sigma k k'} \left[\left(u_k^2 u_{k'}^2 - v_k^2 v_{k'}^2\right) c^\dagger_{k\sigma S} c_{k'\sigma S} + (u_k^2 v_{k'} u_{k'} + v_{k'}^2 u_k v_k) c^\dagger_{k\sigma S} c^\dagger_{-k'\bar{\sigma} S} + \text{h.c} \right] \tag{4.28}$$

$$H_{J\Delta} = J_{S\Delta} \sum_{\sigma\sigma' k k'} S \cdot \sigma_{\sigma\sigma'} \left[\left(u_k^2 u_{k'}^2 - v_k^2 v_{k'}^2\right) c^\dagger_{k\sigma S} c_{k'\sigma' S} + \sigma(u_k^2 v_{k'} u_{k'} + v_{k'}^2 u_k v_k) c^\dagger_{k\sigma S} c^\dagger_{-k'\bar{\sigma}' S} + \text{h.c} \right] \tag{4.29}$$

Notice that these last terms consist of a modification of pairing in the superconductor and a modification of eq.(4.27) proportional to $u_k u_{k'} - v_k v_{k'}$. If one sets the dot to be particle-hole symmetric $\delta = 0$ one would expect the whole system to be particle-hole symmetric as a BCS superconductor is particle-hole symmetric by itself.

In order to verify this, one does the following substitutions $c^\dagger \to c$, $u_k \to v_k$ and $v_k \to u_k$ and verify that $H_J, H_{W\Delta} \to H_J, H_{W\Delta}$ and $H_W, H_{J\Delta} \to -H_W, -H_{W\Delta}$.

Then for $\delta = 0$ we get $H_W, H_{J\Delta} = 0$ and symmetry is indeed held. If $\delta \neq 0$ then there is no guarantee of symmetry. The two terms J_S and W_S correspond to the potential and magnetic scattering terms

analyzed in Section.3 where we found that the breaking of particle-hole symmetry left the YSR state with an asymmetric spectral function. The new terms $J_{S\Delta}$ and $W_{S\Delta}$ correspond to higher order effects, including terms inducing spin-dependent superconductivity as seen from Eq.(4.29). From here on we will only consider lowest order in Δ/U therefore we can disregard the terms $J_{S\Delta}$ and $W_{S\Delta}$, but this analysis verifies that to all orders of Δ/U the system by itself conserves particle-hole symmetry at $\delta = 0$.

4.4 SDN junction

We will now consider a system composed of a single superconductor coupled to a dot which is also weakly coupled to a metal, written as SDN (Superconductor-Dot-Normal-metal). The weak coupling is to assure us that we can disregard Kondo physics, where the metalic lead tries to screen the quantum dot which becomes relevant at large metallic coupling and low temperature [22]. This will let us use the metal as a probe of the Superconductor-Dot system, We will now consider our system to be placed

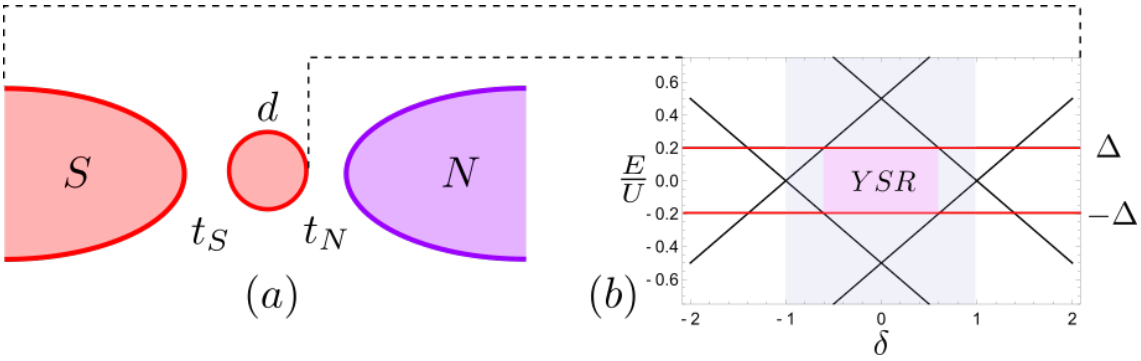

Figure 4.3: In (a) one sees a schematic of a single dot d connected to a Superconducting lead and a metallic lead, the dot is painted red to illustrate its strong coupling to the superconductor compared to the metal. In (b) one sees the coulomb diamond with a gap on top, illustrating the physics of a dot and superconductor together. The pink box illustrates where our Schrieffer Wolff approximation is working determined by $\Delta << |U/2(1 \pm \delta)|$. Here $\Delta = U/5$

in the regime $\Delta << U/2$ as to obtain YSR physics and we will only consider the regime deep within the coulomb diamond further restricting $\Delta << U/2|1 \pm \delta|$. In this regime we ignore interaction of

higher order in $2\Delta/U$ and can therefore write up a effective Hamiltonian

$$H_{eff} = H_S + H_N + H_K \tag{4.30}$$

$$H_S = \sum_k \left[\sum_\sigma \xi_{kS} c^\dagger_{k\sigma S} c_{k\sigma S} + \Delta(c^\dagger_{k\uparrow} c^\dagger_{-k\downarrow} + c_{-k\downarrow} c_{k\uparrow}) \right] \tag{4.31}$$

$$H_N = \sum_{k\sigma} \xi_{kN} c^\dagger_{k\sigma S} c_{k\sigma S} \tag{4.32}$$

$$H_K = \sum_{kk'\alpha\alpha'} \left[J_{\alpha\alpha'} \sum_{\sigma\sigma'} c^\dagger_{k\sigma\alpha} \boldsymbol{S} \cdot \boldsymbol{\sigma}_{\sigma\sigma'} c_{k'\sigma'\alpha'} + W_{\alpha\alpha'} \sum_\sigma c^\dagger_{k\sigma\alpha} c_{k'\sigma\alpha'} \right] \tag{4.33}$$

with $\alpha \in S, N$. Just before in the Schrieffer-Wolff transformation evaluated the self interaction terms J_{SS} and W_{SS}. The corresponding self-interactions for the metal is simply given by the limit $\Delta \to 0$ and replacement of t_S with t_N. For lowest order in Δ/U, where we in effect fully ignore Δ treating the superconductor as a metal we can also write the connecting term J_{NS} and W_{NS} in the above same form, with the tunnel couplings given by $t_S t_N$. So all the effective couplings are given as

$$J_{\alpha\alpha} = \frac{t_\alpha t'_\alpha}{U} \frac{4}{1-\delta^2}, \qquad W_{\alpha\alpha} = \frac{t_\alpha t'_\alpha}{U} \frac{-2\delta}{1-\delta^2} \tag{4.34}$$

An important thing to notice is that for $\delta << 1$ J is approximately constant and W linear. Now if we approximate the spin to be classical then the sign change of W must in effect flip which spectral peak is enhanced as $W \to -W$ makes $\delta z \to -\delta z$ in Eq.(3.31).

Now we will utilize the classical-spin approximation in order to solve this model. First we clearly see from the expression for J and W and our classical-spin discussion that the unitless quantity determining the YSR physics is

$$C = \pi \nu_F \frac{t_S^2}{U} \tag{4.35}$$

as it is the proportional to both J and W with $\pi\nu_F$ from the superconducting Green-function. In the next sections we will fully consider the transport through such a system, but lets first analyse the spectral function. By keeping only H_S, J_{SS}, and W_{SS} we plot the spectral function and YSR energy ω_0 using δ as a parameter. This is done in Fig.4.4 for different values of C, in units of Δ and by letting $|\boldsymbol{S}| = 1$ for simplicity.

The shapes seen in Fig.4.4 are seen everywhere in YSR quantum dot experiments. The round-shape, for weak YSR wherein the spin is not yet screened, is known as the eye. Now that we have discussed the Hamiltonian and the YSR state in this setup we will begin to consider transport which is what can measured in experiments.

Commonly one applies a current through the above system from metal to superconductor and measure the conductance. In experiments the above mentioned bias asymmetry appears quite clearly [23] and for one used to calculating transport in normal metallic systems this will come as no surprise since the spectral function directly links to conductivity and contains this asymmetry. Next we will find that this picture is too simple, and that sub-gap conductance is not necessarily proportional to the spectral function.

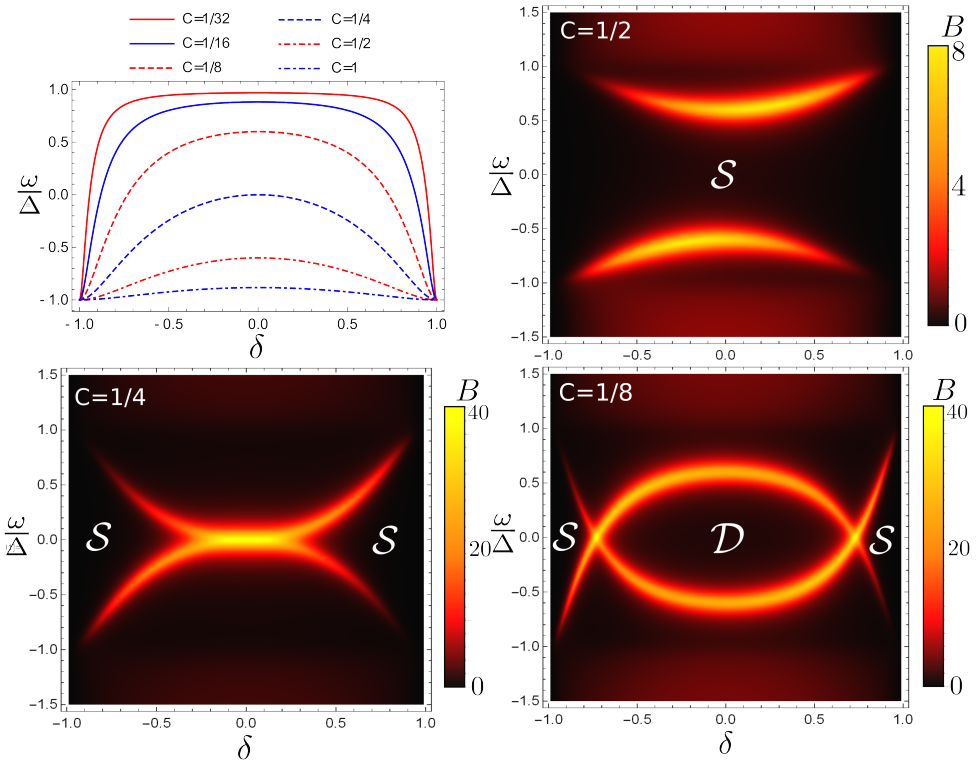

Figure 4.4: In the top left corner we plot $|\omega_0|$ eq.(3.19) as a function of δ for different C. For $C = 1/4$ we see it crosses zero as expected since then $\alpha = 4C = 1$ at $\delta = 0$ where $W_{SS} = 0$. For very small C the YSR state stays close to the gap as expected. In the color-plots we consider the spectral function as defined in eq.(3.24) also as functions of δ and for different C. Here, one can also clearly see the asymmetry arising when moving out of $\delta = 0$. All plots are made with $|\boldsymbol{S}| = 1$.

5 Transport

In this section we will derive non-equilibrium transport for a SDN system. We will use two different but similar approaches. First based on the calculation done by [7] we derive an exact mode which accounts for all interactions within the classical-spin framework. This model will turn out to be hard to apply and even harder to obtain an intuition off.
Later on based on the brilliant approach of [24] and [13] one can reduce the difficulties significantly by using the simplified Greens function from Section.3 and by ignoring contributions from the metallic probe, which yields a structure similar to transport through a resonant level. Thereby we obtain simple intuitive equations which allows one to understand the nature of YSR transport in greater detail.

The more advanced model can in that sense be used as a benchmark for the reduced form allowing us to test its limits, and even more importantly allowing one to consider the probe's impact on the physics for the case of high t_N.

5.1 Exact Calculations

The following section follows closely the calculations done in [7]. Taking the Anderson Hamiltonian for a SDN, eq.(4.2), and writing it in 4×4 Nambu space yields,

$$\begin{aligned} H_A &= H_S + H_N + H_d + H_t \\ H_\alpha &= \frac{1}{2}\sum_{kk'\alpha} \Psi^\dagger_{\alpha k}\left[\xi_{\alpha k}\tau_z + \Delta_\alpha \tau_x\right]\Psi_{\alpha k} \\ H_t &= \frac{1}{2}\sum_{\alpha k} t_\alpha(\Psi^\dagger_{\alpha k}\tau_z\Phi + \Phi^\dagger\tau_z\Psi_{\alpha k}) \\ H_d &= \sum_\sigma \epsilon_d n_{d\sigma} + U n_{d\uparrow}n_{d\downarrow} \end{aligned} \tag{5.1}$$

where $\alpha \in S, N$, $\Delta_N = 0$ and we are using the standard basis from Section.2.2 for $\Psi_{\alpha k}$ and we define

$$hi = \left(d^\dagger_\uparrow, \quad d_\downarrow, \quad d^\dagger_\downarrow, \quad d_\uparrow\right) \tag{5.2}$$

for the dot. The τ_z on the tunneling terms is necessary to fix signs from Nambu notation. Now defining current as the change of charge do to tunneling processes in and out of the superconductor,

$$I = \dot{Q}_S(t) = e\dot{n}_S(t) = \frac{-e}{2ih}\sum_k \left[H_t(t), \Psi^\dagger_{Sk}(t)\tau_z\Psi_{Sk}(t)\right] \tag{5.3}$$

$$= \frac{et_S}{4ih}\sum_{kk'}\left(\left[\Psi^\dagger_{Sk'}(t)\tau_z\Psi_{Sk'}(t), \Psi^\dagger_{Sk}(t)\tau_z\Phi(t)\right] - \text{h.c}\right) \tag{5.4}$$

where we used $n_S = 1/2(\Psi^\dagger_{Sk}\tau_z\Psi_{sk})$, from here we will assume all operators are evaluated at time t. Considering the commutator, suppressing S index for clarity and writing out the Nambu space yields,

$$\Psi^\dagger_{Sk'}\tau_z\Psi_{Sk'}\Psi^\dagger_{Sk}\tau_z\Phi = (c^\dagger_{k'\uparrow}c_{k'\uparrow} - c_{-k'\downarrow}c^\dagger_{-k'\downarrow} + c^\dagger_{k'\downarrow}c_{k'\downarrow} - c_{-k\uparrow}c^\dagger_{-k'\uparrow})(c^\dagger_{k\uparrow}d_\uparrow - c_{-k\downarrow}d_\downarrow + c^\dagger_{k\downarrow}d_\downarrow - c_{-k\uparrow}d_\uparrow) \tag{5.5}$$

Taking the commutator of each of these therms yields the current

$$I = \frac{-et_S}{2ih}\sum_k\left[c^\dagger_{k\uparrow}d_\uparrow + c_{k\downarrow}d^\dagger_\downarrow + c^\dagger_{k\downarrow}d_\downarrow + c_{k\uparrow}d^\dagger_\uparrow - \text{h.c}\right] = \frac{-et_s}{i2h}\sum_k\left[\Psi^\dagger_{Sk}\Phi - \text{h.c}\right] \tag{5.6}$$

$$= \frac{et_S}{2ih}\sum_k \text{Tr}\left[\Phi\Psi^\dagger_{Sk} - \Psi_{Sk}\Phi^\dagger\right] \tag{5.7}$$

where the trace arose as an inner product was converted to a outer. As to obtain a observable we take the thermodynamic average of the current,

$$\begin{aligned} \langle I\rangle &= \frac{et_S}{2ih}\sum_k \text{Tr}\left[\langle\Phi\Psi^\dagger_{Sk}\rangle - \langle\Psi_{Sk}\Phi^\dagger\rangle\right] = \frac{et_S}{2h}\text{Tr}\left[\mathcal{G}^<_{dS}(0) - \mathcal{G}^<_{Sd}(0)\right] \\ &= \frac{et_S}{h}\text{TrRe}\left[\mathcal{G}^<_{dS}(0)\right] \end{aligned} \tag{5.8}$$

where we have used the definition of the lesser Greens function $\mathcal{G}^{<}_{Sd}(t-t') = -i\langle\Psi_{Sk}(t)\Phi^{\dagger}(t')\rangle$ and used the relation $\left[\mathcal{G}^{<}_{ab}\right]^{*} = -\mathcal{G}^{<}_{ba}$. Next we need to evaluate these lesser Greens functions. Using our results from equations of motion eq.(2.14) we obtain

$$\mathcal{G}_{dS} = \mathcal{G}_{dd} t_S \tau_z \mathcal{G}_{0S} \tag{5.9}$$

now a quick way to obtain $\mathcal{G}_{dd}$ is to consider the equation of motion for $\mathcal{G}_{SS}$,

$$\mathcal{G}_{SS} = \mathcal{G}_{0S} + \mathcal{G}_{0S} t_S \tau_z \mathcal{G}_{dS} \tag{5.10}$$

Inserting the equation for $\mathcal{G}_{dS}$ then yields,

$$\mathcal{G}_{SS} = \mathcal{G}_{0S} + \mathcal{G}_{0S} t_S \tau_z \mathcal{G}_{dd} t_S \tau_z \mathcal{G}_{0S} = \mathcal{G}_{0S} + \mathcal{G}_{0S} T_{SS} \mathcal{G}_{0S} \tag{5.11}$$

where we define the T matrix following convention. Therefore we obtain $\mathcal{G}_{dd}$ as

$$t_S^2 \mathcal{G}_{dd} = \tau_z T_{SS} \tau_z \tag{5.12}$$

So the dot's Greens function is fully determined by the superconductors T matrix. Inserting back into Eq.(5.9)

$$\mathcal{G}_{dS} = \frac{1}{t_S} \tau_z T_{SS} \mathcal{G}_{0S} \tag{5.13}$$

which we use to get a expression for the current

$$\langle I \rangle = \frac{e}{h} \mathrm{Tr} \mathrm{Re} \left[\tau_z T_{SS} \mathcal{G}_{0S}\right]^{<} = \frac{e}{h} \int_{-\infty}^{\infty} d\omega \mathrm{Tr} \mathrm{Re} \left[\tau_z T_{SS}(\omega) \mathcal{G}_{0S}(\omega)\right]^{<} \tag{5.14}$$

where in the last step we fourier transformed. Very importantly this current is expressed without any reference to the dot. This allows us to solve for T_{SS} using our Kondo Hamiltonian obtained from Schrieffer-Wolff transformation instead, thereby obtaining an effective model for the center of the Coulomb diamond.

Writing out our Hamiltonian for this system in the simple form,

$$H = \frac{1}{2} \sum_{\alpha k k'} \Psi_{k\alpha} \left[(\xi_{\alpha k} \tau_z + \Delta_\alpha \tau_x)\delta_{kk'} + A_{\alpha\alpha}\right] \Psi_{\alpha k'} + \frac{1}{2} \sum_{kk'} \left[\Psi^{\dagger}_{kS} A_{SN} \Psi_{kN} + \mathrm{h.c}\right] \tag{5.15}$$

with

$$A_{\alpha\alpha'} = JS\sigma_z + W\tau_z \tag{5.16}$$

We start by defining the Greens function for the decoupled N and S space,

$$G_{SS} = \left[G_{0S}^{-1} - A_{SS}\right]^{-1} \quad \text{and} \quad G_{NN} = \left[G_{0N}^{-1} - A_{NN}\right]^{-1} \tag{5.17}$$

then calculating the contribution from coupling the two

$$\begin{aligned} \mathcal{G}_{SS,eff} &= \mathcal{G}_{SS} + \mathcal{G}_{SS} A_{SN} \mathcal{G}_{NS} \\ &= \mathcal{G}_{SS} + \mathcal{G}_{SS} A_{SN} \mathcal{G}_{NN} A_{NS} \mathcal{G}_{SS,eff} \end{aligned} \tag{5.18}$$

which we recognize as a Dyson series thereby yielding

$$\mathcal{G}_{SS,eff} = \left[\mathcal{G}_{0S}^{-1} - A_{SS,eff}\right]^{-1} \quad \text{with} \quad A_{SS,eff} = A_{SS} + A_{SN}\mathcal{G}_{NN}A_{NS} \tag{5.19}$$

from which we define a new T matrix,

$$\begin{aligned} \mathcal{G}_{SS,eff} &= \mathcal{G}_{0S} + \mathcal{G}_{0S}A_{SS,eff}\mathcal{G}_{SS,eff} = \mathcal{G}_{0S} + \mathcal{G}_{0S}T_{SS}\mathcal{G}_{0S} \\ &\Rightarrow T_{SS} = A_{SS,eff}\mathcal{G}_{SS,eff}\mathcal{G}_{0S}^{-1} \end{aligned} \tag{5.20}$$

which is a nice formula for our purpose. Putting this definition into eq.(5.14) yields

$$\left[T_{SS}\mathcal{G}_{0S}\right]^{<} = \left[A_{SS,eff}\mathcal{G}_{SS,eff}\right]^{<} = A^{a}_{SS,eff}\mathcal{G}^{<}_{SS,eff} + A^{<}_{SS,eff}\mathcal{G}^{r}_{SS,eff} \tag{5.21}$$

where we used Langreth rules [25] obtained by use of contour ordered Greens functions which is done in Appendix.A. We need to consider each of these objects in detail before moving on. Since they consist of fractions of Greens functions one cannot simply use Langreth rules, but if we instead return to the relevant Dyson series we can obtain new Dyson like equations by use of Langreth rules. We start with,

$$\begin{aligned} \mathcal{G}^{<}_{NN} &= \left[\mathcal{G}_{0N} + \mathcal{G}_{0N}A_{NN}\mathcal{G}_{NN}\right]^{<} \\ &= \mathcal{G}^{<}_{0N} + \mathcal{G}^{r}_{0N}A_{NN}\mathcal{G}^{<}_{NN} + \mathcal{G}^{<}_{0N}A_{NN}\mathcal{G}^{a}_{NN} \\ &= \frac{1}{1 - \mathcal{G}^{r}_{0N}A_{NN}}\mathcal{G}^{<}_{0N}\left(1 + A_{NN}\mathcal{G}^{a}_{NN}\right) \end{aligned} \tag{5.22}$$

where we used that the impurity potential $A_{\alpha\alpha}$ is time independent so $A^r = A^a$ and $A^< = A^> = 0$ and it the last step solved the Dyson like equation. With this result we can express one of the key components

$$A^{<}_{SS,eff} = \left[A_{SS} + A_{SN}\mathcal{G}_{NN}A_{SN}\right]^{<} = A_{SN}\mathcal{G}^{<}_{NN}A_{SN} = A_{SN}\frac{1}{1 - \mathcal{G}^{r}_{0N}A_{NN}}\mathcal{G}^{<}_{0N}\left(1 + A_{NN}\mathcal{G}^{a}_{NN}\right)A_{NS} \tag{5.23}$$

this is one piece of the puzzle. Next we consider

$$\begin{aligned} \mathcal{G}^{<}_{SS,eff} &= \left[\mathcal{G}_{0S} + \mathcal{G}_{0S}A_{SS,eff}\mathcal{G}_{SS,eff}\right]^{<} \\ &= \mathcal{G}^{<}_{0S} + \mathcal{G}^{r}_{0S}A^{r}_{SS,eff}\mathcal{G}^{<}_{SS,eff} + \mathcal{G}^{r}_{0S}A^{<}_{SS,eff}\mathcal{G}^{a}_{SS,eff} + \mathcal{G}^{<}_{0S}A^{a}_{SS,eff}\mathcal{G}^{a}_{SS,eff} \\ &= \frac{1}{1 - \mathcal{G}^{r}_{0S}A^{r}_{SS,eff}}\left[\mathcal{G}^{<}_{0S} + \mathcal{G}^{r}_{0S}A^{<}_{SS,eff}\mathcal{G}^{a}_{SS,eff} + \mathcal{G}^{<}_{0S}A^{a}_{SS,eff}\mathcal{G}^{a}_{SS,eff}\right] \\ &= \mathcal{G}^{r}_{SS,eff}A^{<}_{SS,eff}\mathcal{G}^{a}_{SS,eff} + \frac{1}{1 - \mathcal{G}^{r}_{0S}A^{r}_{SS,eff}}\mathcal{G}^{<}_{0S}\left(1 + A^{a}_{SS,eff}\mathcal{G}^{a}_{SS,eff}\right) \end{aligned} \tag{5.24}$$

Putting these pieces together we obtain the matrix needed to find the total current in eq.(5.14),

$$\begin{aligned}
&[A_{SS,eff}\mathcal{G}_{SS,eff}]^< = A^r_{SS,eff}\mathcal{G}^<_{SS,eff} + A^<_{SS,eff}\mathcal{G}^a_{SS,eff} \\
&= A^r_{SS,eff}\left[\mathcal{G}^r_{SS,eff}A^<_{SS,eff}\mathcal{G}^a_{SS,eff} + \frac{1}{1-\mathcal{G}^r_{0S}A^r_{SS,eff}}\mathcal{G}^<_{0S}\left(1+A^a_{SS,eff}\mathcal{G}^a_{SS,eff}\right)\right] + A^<_{SS,eff}\mathcal{G}^a_{SS,eff} \\
&= \left(1+A^r_{SS,eff}\mathcal{G}^r_{SS,eff}\right)A^<_{SS,eff}\mathcal{G}^a_{SS,eff} + A^r_{SS,eff}\frac{1}{1-\mathcal{G}^r_{0S}A^r_{SS,eff}}\mathcal{G}^<_{0S}\left(1+A^a_{SS,eff}\mathcal{G}^a_{SS,eff}\right) \qquad (5.25)\\
&= (1+T^r_{SS}\mathcal{G}^r_{0S})A^<_{SS,eff}\mathcal{G}^a_{SS,eff} + T^r_{SS}\mathcal{G}^<_{0S}(1+A^a_{SS,eff}\mathcal{G}^a_{SS,eff}) \\
&= T^r_{SN}\mathcal{G}^<_{0N}\left(1+A_{NN}\mathcal{G}^a_{NN}\right)A_{NS}\mathcal{G}^a_{SS,eff} + T^r_{SS}\mathcal{G}^<_{0S}(1+A^a_{SS,eff}\mathcal{G}^a_{SS,eff}) \\
&= T^r_{SN}\mathcal{G}^<_{0N}A^a_{NS,eff}\mathcal{G}^a_{SS,eff} + T^r_{SS}\mathcal{G}^<_{0S}(1+A^a_{SS,eff}\mathcal{G}^a_{SS,eff})
\end{aligned}$$

where we defined,

$$T^r_{SN} = (1+T^r_{SS})A_{SN}\frac{1}{1-\mathcal{G}^r_{0N}A_{NN}} \quad \text{and} \quad A^a_{NS,eff} = A_{NS} + A_{NN}\mathcal{G}^a_{NN}A_{NS} \qquad (5.26)$$

Now with all this in check we are finally ready to do full current calculations. Here we present the full expression and summarize all terms appearing in it,

$$\langle I\rangle = \frac{e}{h}\int d\omega \mathrm{ReTr}\tau_z\left[T^r_{SN}\mathcal{G}^<_{0N}A^a_{NS,eff}\mathcal{G}^a_{SS,eff} + T^r_{SS}\mathcal{G}^<_{0S}(1+A^a_{SS,eff}\mathcal{G}^a_{SS,eff})\right] \qquad (5.27)$$

where the fundamental quantities are

$$A^{r/a}_{NS,eff} = A_{NS} + A_{NN}\mathcal{G}^{r/a}_{NN}A_{NS} \qquad A^{r/a}_{\alpha\alpha,eff} = A_{\alpha\alpha} + A_{\alpha\beta}\mathcal{G}^{r/a}_{\beta\beta}A_{\beta\alpha} \qquad (5.28)$$

$$\mathcal{G}^{r/a}_{0S} = -\pi\nu_F\frac{(\omega\pm i\eta)+\Delta\tau_x}{\sqrt{\Delta^2-(\omega\pm i\eta)^2}} \qquad \mathcal{G}^{r/a}_{SS,eff} = \left[(\mathcal{G}^{r/a}_{0S})^{-1} - A^{r/a}_{SS,eff}\right]^{-1} \qquad (5.29)$$

$$\mathcal{G}^{r/a}_{0N} = \mp i\pi\nu_F \qquad \mathcal{G}^{r/a}_{NN} = \left[(\mathcal{G}^{r/a}_{0N})^{-1} + A_{NN}\right]^{-1} \qquad (5.30)$$

$$T^{r/a}_{SS} = A^{r/a}_{SS,eff}\frac{1}{1-\mathcal{G}^{r/a}_{0S}A^{r/a}_{SS,eff}} \qquad T^{r/a}_{SN} = (1+T^{r/a}_{SS})A_{SN}\frac{1}{1-\mathcal{G}^{r/a}_{0N}A_{NN}} \qquad (5.31)$$

$$\mathcal{G}^<_{0N} = 2i\pi\nu_F n_F(\omega - eV\tau_z) \qquad \mathcal{G}^<_{0S} = (\mathcal{G}^r_{0S} - \mathcal{G}^a_{0S})n_F(\omega) \qquad (5.32)$$

where we have chosen to apply the bias eV to the metallic side and obtained the metallic Greens functions by taking $\Delta \to 0$. We raise the Fermi level of the N side as current is defined as change of electrons on the S side, then positive bias yields positive current.

Lastly in this project we are more focused on conductance than current, so we define the differential conductance as

$$\sigma(V) = \frac{d\langle I\rangle}{dV} = \frac{2\pi\nu_F e}{h}\int d\omega \mathrm{ImTr}\left[\tau_z T^r_{SN}(\omega)\frac{dn_F(\omega - eV\tau_z)}{dV}A^a_{NS,eff}(\omega)\mathcal{G}^a_{SS,eff}(\omega)\right] \qquad (5.33)$$

For zero temperature the Fermi function yields a delta function and cancels the ω integral. In order to make this equation independent of ν_F this factor will be absorbed into A as to form a unitless scale. Taking from Schrieffer-Wolff we obtain effective parameters

$$\pi\nu_F A_{\alpha\alpha'} = \pi\nu_F J_{\alpha\alpha'}S\sigma_z + \pi\nu_F W_{\alpha\alpha'}\tau_z \qquad (5.34)$$

which we will use as our scales in plotting,

$$\pi\nu_F J_{\alpha\alpha'} S = \pi\nu_F \frac{t_\alpha t_{\alpha'}}{U}\hat{J} = \hat{t}_\alpha \hat{t}_{\alpha'}\hat{J} \quad \text{and} \quad \pi\nu_F W_{\alpha\alpha} = \pi\nu_F \frac{t_\alpha t_{\alpha'}}{U}\hat{W} = \hat{t}_\alpha \hat{t}_{\alpha'}\hat{W} \tag{5.35}$$

with $\hat{J}$, $\hat{W}$ and $\hat{t}_\alpha = \sqrt{\pi\nu_F/U}t_\alpha$ being unitless quantities. We will now show and discuss a number of results obtained by solving eq.(5.33) on Mathematica. We will not go through a full treatment but for more information and analytical expressions obtained in certain limits one can check out [7]. First we consider the case of week metallic coupling and no potential scattering $\hat{W} = 0$. This is done in Fig.5.1 where we clearly see conduction peaks precisely situated at the YSR energy. This matches what one would expect from considering the YSR spectral functions from our analysis of the Greens functions for the dot-superconductor system. Back then we needed to add an artificial broadening which now is replaced by broadening provided by the metallic lead.

When we considered spectral functions we found they had varying peak heights, but in Fig.5.1 we obtain the surprising result that for low couplings all peaks precisely conducts $2e^2/h$, which hints at something highly resonant going on and not just lowest order transport which should be proportional to the spectral function. Also the broadening increases as both $\hat{J}$ and $\hat{t}_N$ increases as expected since the metallic lead is then more strongly coupled to the superconductor. We see that for large $\hat{t}_N$ we encounter higher conductance than $2e^2/h$ for multiple peaks but we attribute this to simple overlap of YSR peaks. Lastly the conductance from out-of gap quasi-particles also increases for higher coupling to superconductor. For $\hat{t}_N = 0.75$ and $\hat{J} = 1.75$ we see that the coupling have become strong enough to engulf the whole gap and then we instead see a hill on a constant background. We saw earlier that the addition of a potential scattering term rendered the symmetric spectral functions asymmetric, so one would expect asymmetric conductance for low order transport. Therefore we analyze the case of finite $\hat{W}$ while keeping $\hat{t}_N$ small.

In Fig.5.2 we see a lot of interesting physics appearing. First the peak height is no longer locked to e^2/h even though there is no overlap between YSR, instead $2e^2/h$ acts as a upper bound. For $\hat{J} = \hat{W}$ no sub-gap features appears at all, and it seems that the closer $\hat{J}$ is to $\hat{W}$ the smaller are the conduction peaks. Maybe most surprisingly none of the peaks are bias asymmetric, while we know for a fact that the spectral function is. This hints strongly to the fact that transport is non-equilibrium and requires higher orders to function.

This result was very surprising as one normally relies on the spectral function for information about conductance patterns. Further expanding our confusion we found that increasing η from analytical continuation to a non-infinitesimal value allows bias asymmetric peaks to appear if $\bar{W} \neq 0$. For a critical η one than obtains conductance peaks that apart from a constant factor is similar to the associated spectral function. These effects are shown for a single case in Fig.5.3. It should be noted that this happens generically for all parameters when both $\hat{J} \neq 0$ and $\hat{W} \neq 0$ where the resulting asymmetry can be either small or large dependent on the underlying spectral function. In order to understand these effects we expanded Eq.(5.33) in the parameter $\hat{t}_N$ and obtained conductance in different order of $\hat{t}_N$. These calculations revealed that, for all cases, lowest orders in $\hat{t}_N$ always in symmetry corresponded to the related spectral function. If calculations are done in the symmetrical regime we found that higher orders of $\hat{t}_N$ will diverge, therefore one needs to sum all orders to obtain anything converging which in effect symmetries the conductance. Correspondingly in the asymmetrical regime we find that higher-order terms quickly go to zero and that the lowest orders fully describe conductance. So when η is infinitesimal higher order processes dominates transport. This also informs us that

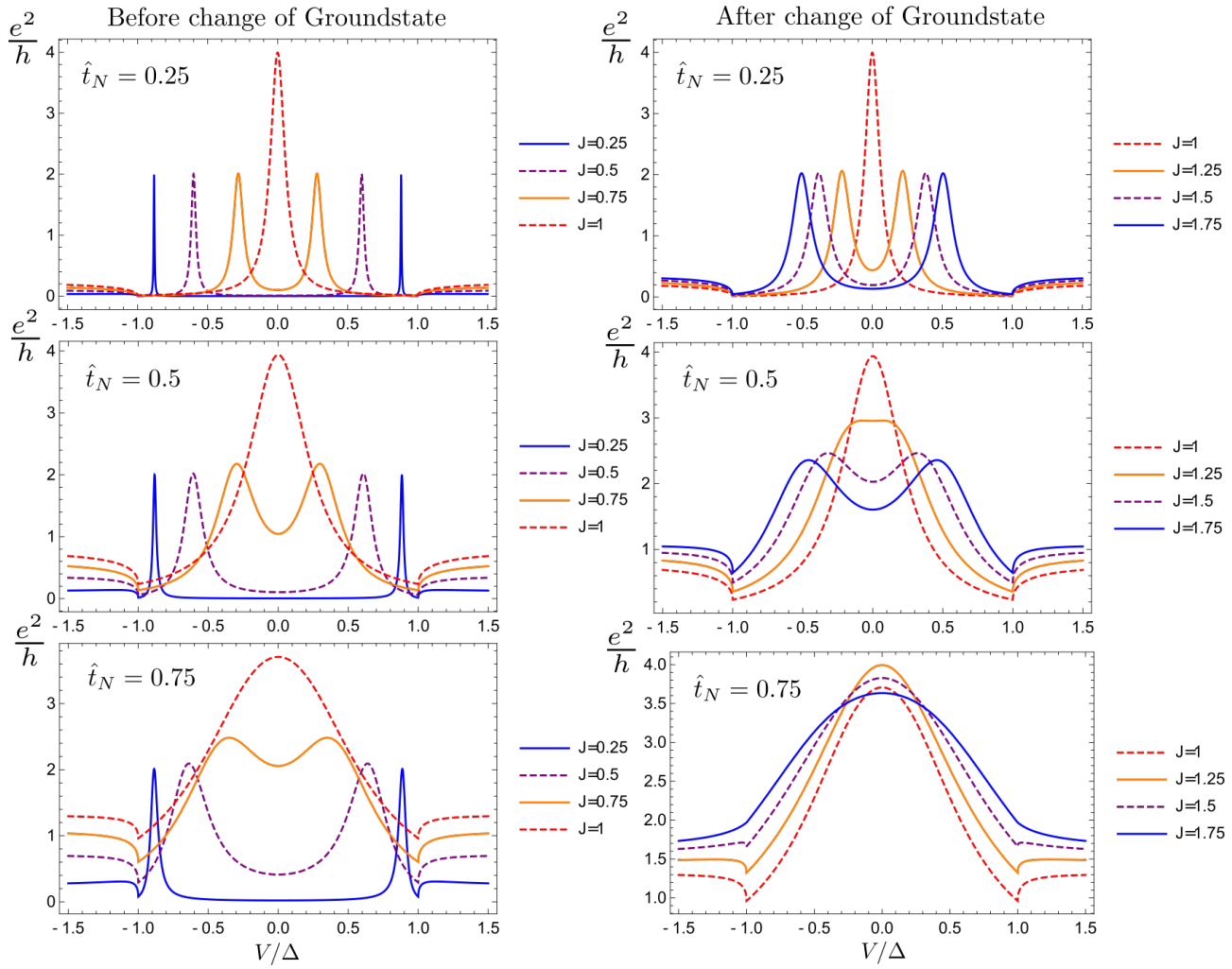

Figure 5.1: In these figures we plot conductance calculated using eq.(5.33) with parameters $\hat{t}_S = 1$, $\hat{W} = 0$ and all in units of Δ. These parameters are chosen such that $\hat{J}$ mimics the behavior of α in Fig.3.3 and as in that case the change of groundstate occurs at $\hat{J} = 1$. The peaks are all situated precisely at the YSR energy ω_0. In the lower panels we increase the metallic coupling t_N, thereby increasing metallic broadening. In all these plot we have analytically continued $\omega \to \omega \pm i\eta$ with $\eta = 10^{-7}\Delta$ included for technical reasons.

one should be very careful when using perturbative methods, such as low order master equations, to investigate transport through YSR states.

Instead of going down the long and tedious road of understanding this model in depth we will shift to the more transparent Resonant-level Model derived in the next section.

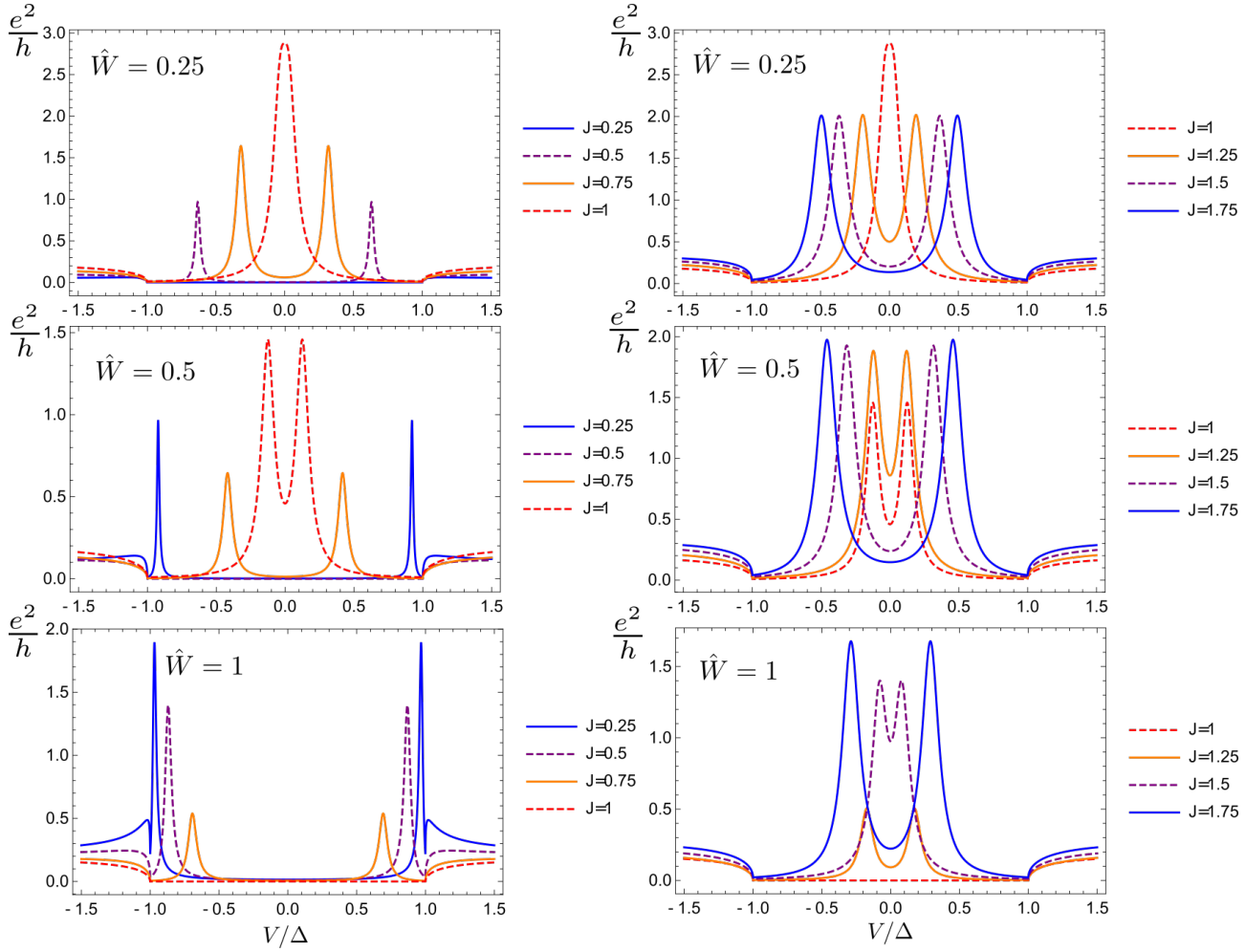

Figure 5.2: In these figures we consider conductance calculated using Eq.(5.33) with parameters $\hat{t}_S = 1$, $\hat{t}_N = 0.25$ and all in units of Δ. As to have correspondence we use the same $\hat{J}$ as in Fig.5.1, but the two sides do not correspond to a groundstate as changing $\hat{W}$ increases the crossing point. We increase the potential scattering $\hat{W}$ going downwards and notice that for $\hat{W} = \hat{J}$ there is no peak. In all these plots we have analytically continued $\omega \to \omega \pm i\eta$ with $\eta = 10^{-7}\Delta$.

5.2 Resonant-level Model

The model, which we have named the Resonant-level model, is based on the calculations of [24] and [13]. The basis of the model is using the simplified Hamiltonian eq.(3.36) and since we consider the metal to only weakly couple to the dots, we disregard terms $A_{NN} \approx 0$. For such an model we have

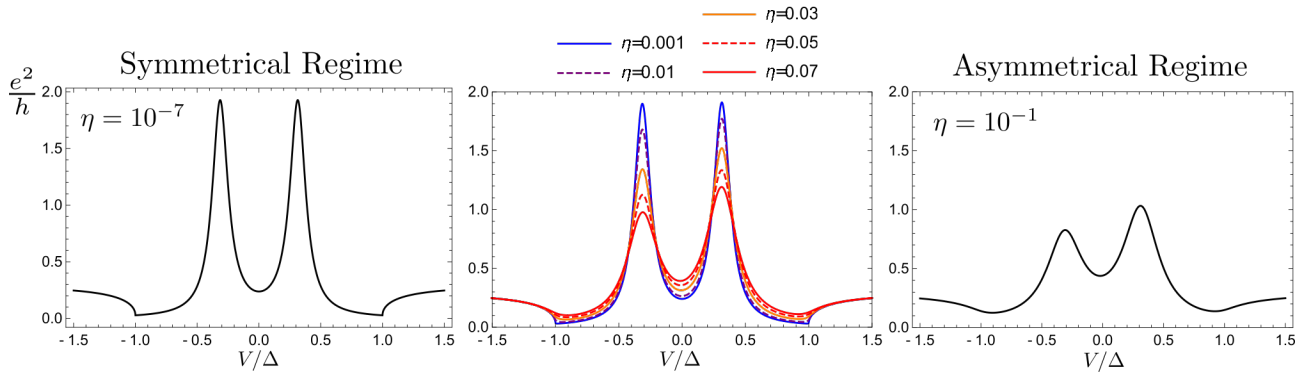

Figure 5.3: In these figures we plot conductance calculated using Eq.(5.33) with parameters $\hat{t}_S = 1$, $\hat{t}_N = 0.25$, $\hat{J} = 1.5$ and $\hat{W} = 0.5$ and all in units of Δ. In these plots we drive from a bias symmetrical regime into aa bias asymmetrical regime by increasing the analytical continuation parameter η from $\omega \to \omega \pm i\eta$. The result is surprising as one usually assumes that η only affects broadening.

the Hamiltonian

$$H = H_S + H_N + H_t \tag{5.36}$$

$$H_S \approx H_{eff} = -\omega_0 \gamma_\uparrow^\dagger \gamma_\uparrow + \omega_0 \gamma_\downarrow^\dagger \gamma_\downarrow \tag{5.37}$$

$$H_N = \sum_{k\sigma} \xi_k c_{Nk\sigma}^\dagger c_{Nk\sigma} \tag{5.38}$$

$$H_t = \sum_{\sigma} A_{NS\sigma}(c_{N\sigma}^\dagger c_{S\sigma} + \text{h.c.}) \tag{5.39}$$

where no k index on c_α means momentum summed and A_{NS} obtains a spin index as it is no longer cast in Nambu space. In order to compute the whole problem in terms of γ operators we rewrite the tunnel Hamiltonian using the relations $c_{S\uparrow} = (\hat{v}\gamma_\uparrow + \hat{u}\gamma_\downarrow^\dagger)$ and $c_{S\downarrow} = (\hat{v}\gamma_\downarrow - \hat{u}\gamma_\uparrow^\dagger)$,

$$H_t = A_{NS\uparrow}\left[c_{N\uparrow}^\dagger\left(\hat{v}\gamma_\uparrow + \hat{u}\gamma_\downarrow^\dagger\right) + \text{h.c}\right] + A_{NS\downarrow}\left[c_{N\downarrow}^\dagger\left(\hat{u}\gamma_\downarrow - \hat{v}\gamma_\uparrow^\dagger\right) + \text{h.c}\right] \tag{5.40}$$

This Hamiltonian can then be sorted into the two independent operators $\gamma_\uparrow$ and $\gamma_\downarrow$ and one can work out transport through both states, but we do a short-cut for clarity. Noticing that the Greens-function for both $\gamma_\uparrow$ and $\gamma_\downarrow$ yielded symmetrical spectral contributions and knowing from exact transport that the conductance is also symmetrical for both subspaces, we choose to only consider one channel and then multiply by a factor 2 in the end. We choose $\gamma_\uparrow$ and obtain

$$H_t = \hat{v}A_{NS\uparrow}c_{N\uparrow}^\dagger\gamma_\uparrow + \hat{u}A_{NS\downarrow}c_\downarrow^\dagger\gamma_\uparrow^\dagger + \text{h.c} \tag{5.41}$$

$$= \hat{v}A_{NS\uparrow}c_{N\uparrow}^\dagger\gamma_\uparrow - \hat{u}A_{NS\downarrow}\gamma_\uparrow^\dagger h_{N\downarrow} + \text{h.c} \tag{5.42}$$

where we define the hole operators $c_\downarrow^\dagger = h_\downarrow$. In this form we have no anomalous transport terms and if apply a bias eV to the metallic side we end up with the Hamiltonian,

$$H = H_e + H_\gamma + H_h + H_t \tag{5.43}$$

$$H_e = \sum_k (E_k - eV) c_{k\uparrow}^\dagger c_{k\downarrow}, \qquad H_h = -\sum_k (E_k - eV) h_{k\downarrow}^\dagger h_{k\downarrow} \tag{5.44}$$

$$H_\gamma = -\omega \gamma^\dagger \gamma, \qquad H_t = \hat{v} A_{NS\uparrow} c_\uparrow^\dagger \gamma - \hat{u} A_{NS\downarrow} \gamma^\dagger h_\downarrow + \text{h.c} \tag{5.45}$$

where we have suppressed the indexes N and $\uparrow$ on γ.

This is the effective model of two systems h and c coupled together through a resonant level γ. Such models are well known and offer us a reference point in which we can understand YSR transport. Here the electron/hole tunnel-couplings to the resonant level are proportional to the electron/hole spectral weight $\hat{u}$ and $\hat{v}$ of the YSR state.

Now in this language it is already clear why all conductance is symmetrical, even for asymmetrical

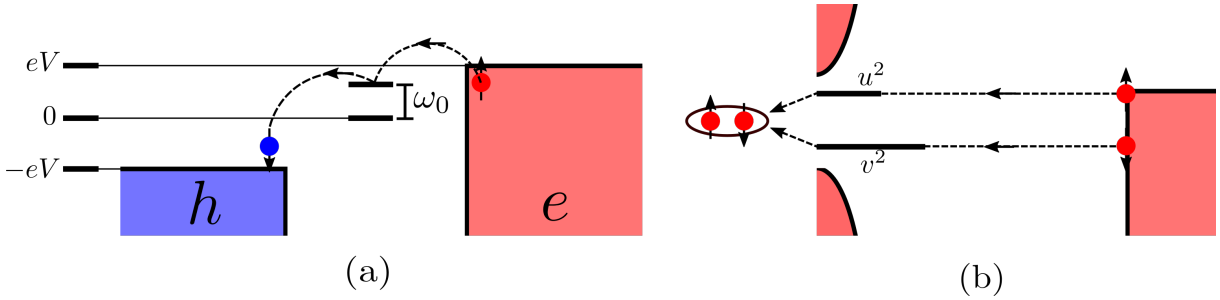

Figure 5.4: Representation of the symmetrical Andreev process. In (a) one sees the transport process in the Resonant level model, where a electron jumps onto the site thereby exciting it and the jumps along as a hole, in total removing to charges from the metal. In (b) one sees a more realistic way of considering the same process. Two electrons move in and form a cooper-pair mediated by the YSR-state.

spectral functions, if nothing further is added to the model. The only way to remove electrons from the metal is to transport them through the resonant level into the hole sector as shown in Fig.5.4. This process corresponds to the Andreev reflection well know in the literature.

Importantly both for negative and positive bias one needs to transport through both the electron u and hole v peak, which is clear in the model. This means that both bias conductance peaks ends up uv proportional and thereby symmetric.

Next we do current calculations and see if we can obtain results agreeing with the discussion. First as we have joined superconductor-dot into one YSR state its more natural to define current through the metal. We define it as,

$$\langle I \rangle = 2(\langle I_h \rangle - \langle I_e \rangle) \tag{5.46}$$

The sign is chosen as we want to compare this model to the exact calculation from before, so we want a electron leaving the metal to yield a positive current and the factor 2 is included as we only considered

$\gamma_\uparrow$. We define these currents independently

$$\langle I_e\rangle = e\langle \dot{n}_e\rangle = \frac{ie}{h}\langle[H_t, \sum_k c^\dagger_{k\uparrow}c_{k\downarrow}]\rangle = \frac{ie}{h}\sum_k \hat{v}A_{NS\uparrow}(\langle\gamma c^\dagger_{k\uparrow}\rangle - \langle c_{k\uparrow}\gamma^\dagger\rangle) \tag{5.47}$$

$$= \frac{e\hat{v}A_{NS\uparrow}}{h}(G^<_{\gamma e}(0) - G^<_{e\gamma}(0)) \tag{5.48}$$

$$\langle I_h\rangle = -\frac{e\hat{u}A_{NS\downarrow}}{h}(G^<_{\gamma h}(0) - G^<_{h\gamma}(0)) \tag{5.49}$$

where we use normal G to make it clear that these Greens functions are not in any Nambu space. Similar to before consider the Greens functions equation of motion,

$$G_{\gamma e} = G_{\gamma\gamma}\hat{v}A_{NS\uparrow}G_{0e} \quad \Rightarrow \quad G^<_{\gamma e}(0) = \int\frac{d\omega}{2\pi}(G^r_{\gamma\gamma}(\omega)\hat{v}A_{NS\uparrow}G^<_{0e}(\omega) + G^<_{\gamma\gamma}(\omega)\hat{v}A_{NS\uparrow}G^a_{0e}(\omega)) \tag{5.50}$$

$$G_{\gamma h} = -G_{\gamma\gamma}\hat{u}A_{NS\downarrow}G_{0h} \quad \Rightarrow \quad G^<_{\gamma h}(0) = -\int\frac{d\omega}{2\pi}(G^r_{\gamma\gamma}(\omega)\hat{u}A_{NS\downarrow}G^<_{0h}(\omega) + G^<_{\gamma\gamma}(\omega)\hat{u}A_{NS\downarrow}G^a_{0h}(\omega)) \tag{5.51}$$

where we used Langreth rules and the fact that the interaction is time independent. The normal metal Greens functions are given by

$$G^{r/a}_{0e}(\omega) = \pm i\pi\nu_F, \quad G^{r/a}_{0h}(\omega) = \pm i\pi\nu_F, \quad G^<_{0e/h}(\omega) = 2i\pi\nu_F n_F(\omega \mp eV) \tag{5.52}$$

where the plus in the lesser Greens function refers to electron and minus too hole components. Putting it all together yields

$$\langle I_e\rangle = \frac{ie\bar{v}^2A^2_{NS\uparrow}}{h}\int d\omega\left[G^<_{\gamma\gamma}(\omega) - n_F(\omega - eV)(G^r_{\gamma\gamma} - G^a_{\gamma\gamma})\right] \tag{5.53}$$

$$\langle I_h\rangle = \frac{ie\bar{u}^2A^2_{NS\downarrow}}{h}\int d\omega\left[G^<_{\gamma\gamma}(\omega) - n_F(\omega + eV)(G^r_{\gamma\gamma} - G^a_{\gamma\gamma})\right] \tag{5.54}$$

now the only component we need to solve for is the full YSR Greens function. We know that the non-interacting YSR Greens functions is given by eq.(3.33), which in the normalized form is,

$$\hat{G}_{0\gamma} = \frac{u^2 + v^2}{\omega - \omega_0} \tag{5.55}$$

We then do equation of motion using eq.(2.12),

$$\begin{aligned} G_{\gamma\gamma} &= \hat{G}_{0\gamma} + \hat{G}_{0\gamma}\bar{v}A_{NS\uparrow}G_{e\gamma} - \hat{G}_{0\gamma}\bar{u}A_{NS\downarrow}G_{h\gamma} \\ &= \hat{G}_{0\gamma} + \bar{v}^2A^2_{NS\uparrow}\hat{G}_{0\gamma}G_{0e}G_{\gamma\gamma} + \bar{u}^2A^2_{NS\downarrow}\hat{G}_{0\gamma}G_{0h}G_{\gamma\gamma} \end{aligned} \tag{5.56}$$

Before going onwards one can already here see that every YSR Greens function is paired up with a $\bar{u}^2$ or $\bar{v}^2$ in both Eq.(5.56) and Eq.(5.53) which means that we can remove all hats without consequence as $\hat{u}^2\hat{G}_{0\gamma} = u^2G_{0\gamma}$ with $G_{0\gamma} = (\omega - \omega_0)^{-1}$. So the normalization of u and v fully cancels. From here we define the effective couplings as

$$\Gamma_e = \pi\nu_F v^2A^2_{NS\uparrow} \qquad \Gamma_h = \pi\nu_F u^2A^2_{NS\downarrow} \tag{5.57}$$

We use Langreth rules on Eq.(5.56) to obtain Greens functions

$$G^{r/a}_{\gamma\gamma}(\omega) = \frac{1}{\omega - \omega_0 \mp i(\Gamma_e + \Gamma_h)} \tag{5.58}$$

and using that $G^{<}_{0\gamma} = 0$ we obtain for the full lesser Greens function

$$\mathcal{G}^{<}_{\gamma\gamma} = \left[\hat{G}_{0\gamma} + \bar{v}^2 A^2_{NS\uparrow}\hat{G}_{0\gamma}G_{0e}G_{\gamma\gamma} + \bar{u}^2 A^2_{NS\downarrow}\hat{G}_{0\gamma}G_{0h}G_{\gamma\gamma}\right]^{<} \tag{5.59}$$

$$\Rightarrow (1 - v^2 A^2_{NS\uparrow}G^r_{0\gamma}G^r_{0e} - u^2 A^2_{NS\downarrow}G^r_{0\gamma}G^r_{0e})G^{<}_{\gamma\gamma} = v^2 A^2_{NS\uparrow}G^r_{0\gamma}G^{<}_{0e}G^a_{\gamma\gamma} + u^2 A^2_{NS\downarrow}G^r_{0\gamma}G^{<}_{0h}G^a_{\gamma\gamma}$$

$$\Rightarrow G^{<}_{\gamma\gamma}(\omega) = 2i\frac{\Gamma_e n_F(\omega - V) + \Gamma_h n_F(\omega + V)}{(\omega + \omega_0)^2 + (\Gamma_e + \Gamma_h)^2} \tag{5.60}$$

and lastly before inserting into Eq.(5.53) we need to calculate

$$G^r_{\gamma\gamma} - G^a_{\gamma\gamma} = 2i\mathrm{Im}G^r_{\gamma\gamma} = \frac{2i\Gamma_e + 2i\Gamma_h}{(\omega + \omega_0)^2 + (\Gamma_e + \Gamma^2_h)} \tag{5.61}$$

and we obtain the current by inserting

$$I_e = \frac{e\Gamma_e}{h}\int d\omega \frac{2\Gamma_h n_F(\omega - V) - 2\Gamma_h n_F(\omega + V)}{(\omega - \omega_0)^2 + (\Gamma_e + \Gamma_h)^2} \tag{5.62}$$

$$I_h = \frac{e\Gamma_h}{h}\int d\omega \frac{2\Gamma_e n_F(\omega + V) - 2\Gamma_e n_F(\omega - V)}{(\omega - \omega_0)^2 + (\Gamma_e + \Gamma_h)^2} \tag{5.63}$$

In the end we obtain

$$I = 2(I_h - I_e) = \frac{8e}{h}\int d\omega \frac{\Gamma_e\Gamma_h n_F(\omega + V) - \Gamma_e\Gamma_h n_F(\omega - V)}{(\omega + \omega_0)^2 + (\Gamma_e + \Gamma_h)^2} \tag{5.64}$$

Finding conduction for $T = 0$ ew obtain the following expression

$$\sigma(V) = \frac{d\langle I\rangle}{dV} = \frac{8e^2}{h}\left[\frac{\Gamma_e\Gamma_h}{(V - \epsilon_0)^2 + (\Gamma/2)^2} + \frac{\Gamma_e\Gamma_h}{(V + \epsilon_0)^2 + (\Gamma/2)^2}\right] \tag{5.65}$$

where we defined the broadening $\Gamma = 2(\Gamma_e + \Gamma_h)$. This model precisely matches the form expected for a resonant level. One can think about transport through the following steps: the magnetic moment of the dot induces a localized YSR bound state in the superconductor, then a electron can tunnel through the dot and excite this induced state if the bias is higher than ω_0. Now the electron is stuck, as the YSR state is localized it cannot move away and it does not have enough energy to join the free-moving quasi particles at the gap Δ, so the state is blocked and no further electrons can be added to the YSR state. A way around this problem is if another electron joins the first in the superconductor then they can form a Cooper-pair become mobile and leave the YSR state, opening for repetitions of this process.

We will now compare results from this model with the results obtained from exact calculations. We will concentrate on the resonances $V = \pm\omega_0$. In this case the two Lorenztian peaks in Eq.(5.65) becomes equal in height so one can simply consider one of them

$$\sigma(\pm\omega_0) = \frac{8e^2}{h}\frac{\Gamma_e\Gamma_h}{(\Gamma_e + \Gamma_h)^2} \tag{5.66}$$

First of all when there is no potential scattering $W = 0$ it is clear that $A^2_{NS\uparrow} = A^2_{NS\downarrow}$ and $u^2 = v^2$ as we are in the particle-hole symmetric point. Then $\Gamma_e = \Gamma_h$ and we obtain the simple result,

$$\sigma(\pm\omega_0) = \frac{8e^2}{h}\frac{\Gamma_e^2}{(2\Gamma_e)^2} = \frac{2e^2}{h} \tag{5.67}$$

Which precisely matches what we saw from the exact calculations on Fig.5.1 for low $\bar{t}_N$. This also supports the validity of this model. For $\hat{t}_N$ small then $A_{NN} \propto \hat{t}_N^2$ is small, which is neglected in the resonant level model and higher order terms in $A_{NS} \propto \hat{t}_N$ are also small, so the metal's renormalization by the SC is small, allowing us to set $H_S \approx H_{eff}$, thereby forgetting about most of the SC without penalty.

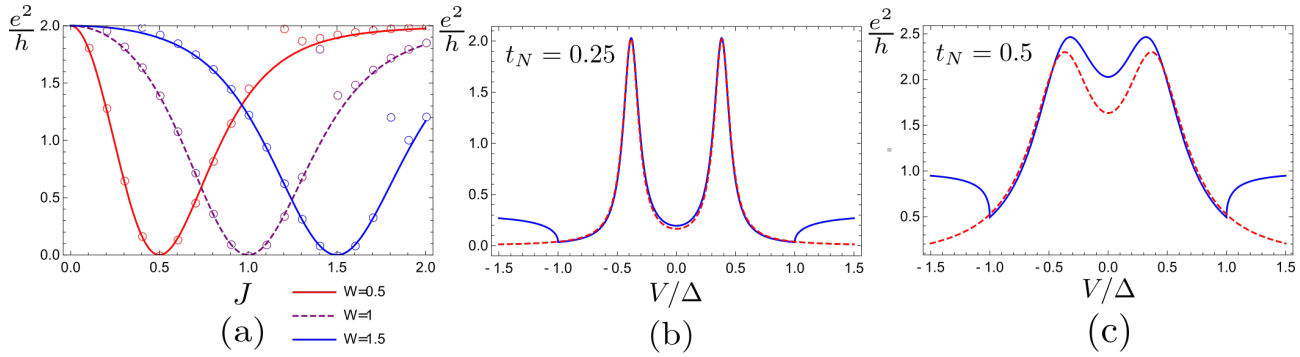

Figure 5.5: In (a) we consider peak heights at resonance using Eq.(5.66) with $\hat{t}_S = 1$ and $\hat{t}_N = 0.25$. Notice that it drops to zero for $\hat{W} = \hat{J}$ and converges toward $2e^2/h$ away from this point. The empty circles on top are numerically found peak height from Eq.(5.33). As our model only considers one peak it fails when the peaks get close to crossing at $V = 0$. In (b) we compare the Resonant level (Red, Dashed) model with exact calculation obtained with Eq.(5.33) (Blue, Full). Parameters are $\hat{t}_S = 1$, $\hat{J} = 1.5$, $\hat{W} = 0$ and $\hat{t}_N = 0.25$. In (c) we again compare, with parameters $\hat{t}_S = 1$, $\hat{J} = 1.5$, $\hat{W} = 0$ and $\hat{t}_N = 0.5$. Here the coupling to the metal is strong enough for the resonant model to fail.

In Fig.5.5 we investigate how this new resonant level model, eq.(5.65) compares with our results from exact calculations, Eq.(5.33). We find that for small $\hat{t}_N$ and η infinitesimal our model matches well with the exact calculations if one only considers sub-gap features. As expected out of gap behavior is lost as we have expanded around the sub-gap peaks.

5.3 Resonant level with Relaxation

In the previous sections we found how the resonant-level model reproduced the alway symmetric conduction peaks. Next we investigate how adding of a finite analytical continuation η rendered the exact model asymmetrical. From the previous analysis it is clear that another way of transport must have been opened, as cooper-pair transport must always be bias symmetric.

Let us consider the bare YSR Greens function but with some non-zero imaginary value $i\Gamma_r$ in the denominator as if it had been analytically continued

$$\bar{G}^{r/a}_{\gamma 0}(\omega) = \frac{1}{\omega + \omega_0 \mp i\Gamma_r} \tag{5.68}$$

How can such a term arise? We saw before that coupling the state to a metallic lead broadened it by $\Gamma_e + \Gamma_h$, so maybe coupling to some different state leaves it broadened? This was considered by [13] and we follow the same thought. We write up the Dyson series yielding a Greens function like

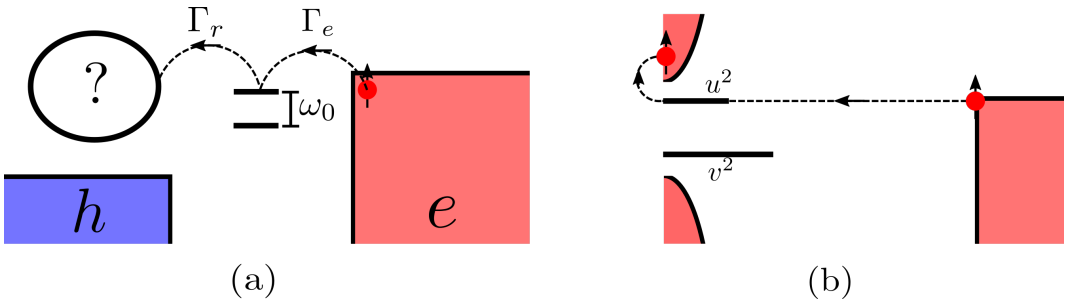

Figure 5.6: Representation of the new relaxation process. In (a) one sees the transport process in the Resonant level model, where a electron jumps onto the site thereby exciting it and then jumps along into something unknown, in the mathematical model this unknown is undetermined. In (b) one sees our interpretation of what is going on, we expect that the YSR state can relax into the quasi-particle continuum, which is a process demanding a energy transfer so a third particle is needed.

$\bar{G}^{r/a}_{0\gamma}(\omega)$,

$$\bar{G}_{0\gamma} = G_{0\gamma} + G_{0\gamma} i\Gamma_r \bar{G}_{0\gamma} \tag{5.69}$$

here one could assume that

$$i\Gamma_r = h_{\gamma\alpha} G_{0\alpha} h_{\alpha\gamma} \tag{5.70}$$

where α is some different state we have not included in our model. Since this effect somehow should be current carrying it should happen internally in the superconductor as not to put charges back in the metallic lead. Therefor we imagine it independent of bias which we have added to the metallic lead. So we assume

$$i\Gamma^<_r = 2i\Gamma_r n_{F/B}(\omega - \omega_\alpha) \tag{5.71}$$

which is to say that the α particles are centered at energy ω_α from the Fermi surface, where we assume ω_α to be independent of V. Doing the same manipulations as before yields the modified result

$$G^<_{\gamma\gamma}(\omega) = \frac{2i\Gamma_e n_F(\omega - eV) + 2i\Gamma_h n_F(\omega + eV) + 2i\Gamma_r n_F(\omega - \omega_\alpha)}{(\omega + \omega_0)^2 + (\Gamma_e + \Gamma_h + \Gamma_r)^2} \tag{5.72}$$

and

$$G^r_{\gamma\gamma}(\omega) - G^a_{\gamma\gamma}(\omega) = \frac{2i(\Gamma_e + \Gamma_h + \Gamma_r)}{(\omega + \omega_0)^2 + (\Gamma_e + \Gamma_h + \Gamma_r)^2} \tag{5.73}$$

then calculating the current again yields new contributions corresponding to the new transport process

$$\langle I \rangle = \frac{4e}{h} \int d\omega \frac{2\Gamma_e\Gamma_h n_F(\omega_h) - 2\Gamma_e\Gamma_h n_F(\omega_e) + \Gamma_r(\Gamma_h - \Gamma_e) n_F(\omega_\alpha) + \Gamma_e\Gamma_r n_F(\omega_e) - \Gamma_h\Gamma_r n_F(\omega_h)}{(\omega + \omega_0)^2 + (\Gamma_e + \Gamma_h)^2} \tag{5.74}$$

from which we obtain the differential conduction

$$\sigma = \frac{d\langle I\rangle}{dV} = \frac{4e^2}{h}\left[\frac{2\Gamma_e\Gamma_h + \Gamma_h\Gamma_r}{(V-\epsilon_0)^2 + (\Gamma/2)^2} + \frac{2\Gamma_e\Gamma_h + \Gamma_e\Gamma_r}{(V+\epsilon_0)^2 + (\Gamma/2)^2}\right] \tag{5.75}$$

which opens the possibility for asymmetrical conduction.

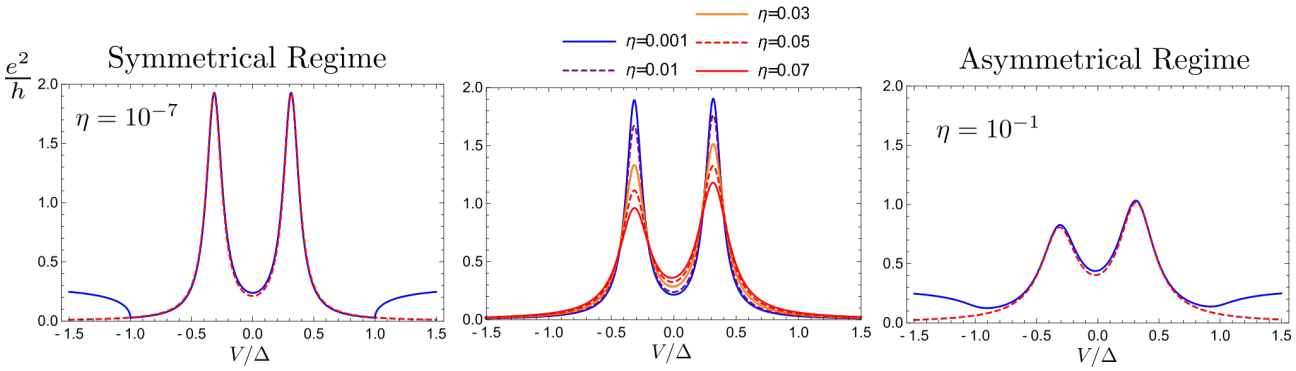

Figure 5.7: In these figures we consider conductance calculated using Eq.(5.75) with parameters $\hat{t}_S = 1$, $\hat{t}_N = 0.25$, $\hat{J} = 1.5$ and $\hat{W} = 0.5$ and all in units of Δ. In these plots we drive from an bias symmetrical regime into an bias asymmetrical regime by increasing Γ_r where we have set $\Gamma_r = \eta$. In the left and right most plot the resonant level model is plotted (Red,Dashed), while the exact model is (Blue,Full). In the middle one see only the resonant level model.

In Fig.5.7 we show how one can go from the symmetrical regime where $2\Gamma_e\Gamma_h > \Gamma_{e/h}\Gamma_r$ to the asymmetrical regime where $2\Gamma_e\Gamma_h < \Gamma_{e/h}\Gamma_r$. We find an excellent agreement for sub-gap physics and for small metallic coupling. To compare the two models one should simply set $\Gamma_r = \eta$.

An important thing to remember is that all usual sub-gap transport is through Cooper-pairs which is proportional to $t_S^4 t_N^4$ as there are no sub-gap states to relax into the continuum. This order is similar to $\Gamma_e\Gamma_h \propto t_S^4 t_N^4$, while the relaxation current through the YSR state is proportional to $\Gamma_r t_S^2 t_N^2$. Also all out-off gap transport is proportional to $t_S^2 t_N^2$ as single electrons are transported into the quasi-particle continuum similar in fashion to metal-metal transport.

This allows us to talk about two regimes for superconductor-dot-metal structures. If $\Gamma_{e/h} >> \Gamma_r$ then we are in the Cooper-pair regime where one would expect to see all conducting sub-gap features to appear on measurements and always bias-symmetrical. The YSR state should appear symmetrical with high peak conduction around $2e^2/h$ probably lowered by temperature broadening which does not affect the symmetry.

If $\Gamma_{e/h} << \Gamma_r$ we are in the relaxation regime where all two particle (Cooper-pair) transport is suppressed compared to the YSR peak. In this regime we expects the YSR to appear as asymmetric bias-peaks with asymmetry determined by W. Other features inside of the gap, such as charge state degeneracy lines, are expected to be weak or non-visible as they conduct through Cooper-pairs as their is no state in the superconducting gap which can relax and thereby open a single electron channel.

If one had control over t_N in experiments tuning between these two regimes should be possible, so long Γ_r is not huge, since the Cooper-pair term is of higher power in t_N than the relaxation term. The

advantage of doing it this way is that the YSR physics, which is mostly determined by superconducting self-interactions, is invariant. So one should be able to tune from a bias asymmetrical conductance picture into a bias symmetrical one without affecting the sub-gap states.

5.4 SDN Patterns

Now returning to consider how these models yields conduction patters for S-D-N system. From our Schrieffer-Wolff transformation we found that deep inside the charge sector and for $t_\alpha^2/U << 1$ and $\Delta/U << 1$ we get the following interactions,

$$A_{\alpha\alpha} = J_{\alpha\alpha'} S\sigma_z + W_{\alpha\alpha'}\tau_z \quad \text{with} \quad W_{\alpha\alpha'} = -\frac{t_\alpha t_{\alpha'}}{U}\frac{2\delta}{1-\delta^2}, \quad J_{\alpha\alpha'} = \frac{t_\alpha t_{\alpha'}}{U}\frac{4}{1-\delta^2} \tag{5.76}$$

where we defined $\delta = -1 - 2/U\epsilon_d$. Before we can calculate we need to determine the spin S. A single state in odd occupancy has spin-$1/2$, but also reminding ourselves that we use a classical-spin approximation for a truly quantum mechanical system we need to correct S a bit. As the full quantum mechanical system is hard to work on without the use of powerful numerical techniques as NRG, a full correspondence is beyond our reach, instead we compare to a quantum perturbativ technique developed with the Yosida anzats [26]. In [6] it was found that perturbatively, with and without potential scattering W, one obtain the same YSR energie ω_0 using a classical-spin and Yosida anzats if one uses $3J_{Classical} = J_{Yosida}$.

The Yosida anzats consists of replacing the superconductor's wavefunction with the wavefunction of a single quasi-particle and then calculating the exchange singlet and triplet states energies, which are formed by the quasi-particles interaction with the dot-state. The factor 3 is associated with the 3 states of the triplet. So following this procedure we will set $S = 3/2$ from here on out in order to compare with experiments, which are truly quantum mechanical. Using these parameters we plot expected conductance in Fig.5.8. Notice the difference between the Relaxation regime and Cooper-pair regime both the discussed bias asymmetry and the dramatic drop in conductance. These features we will look for in experiments to determine what kind of transport we should consider.

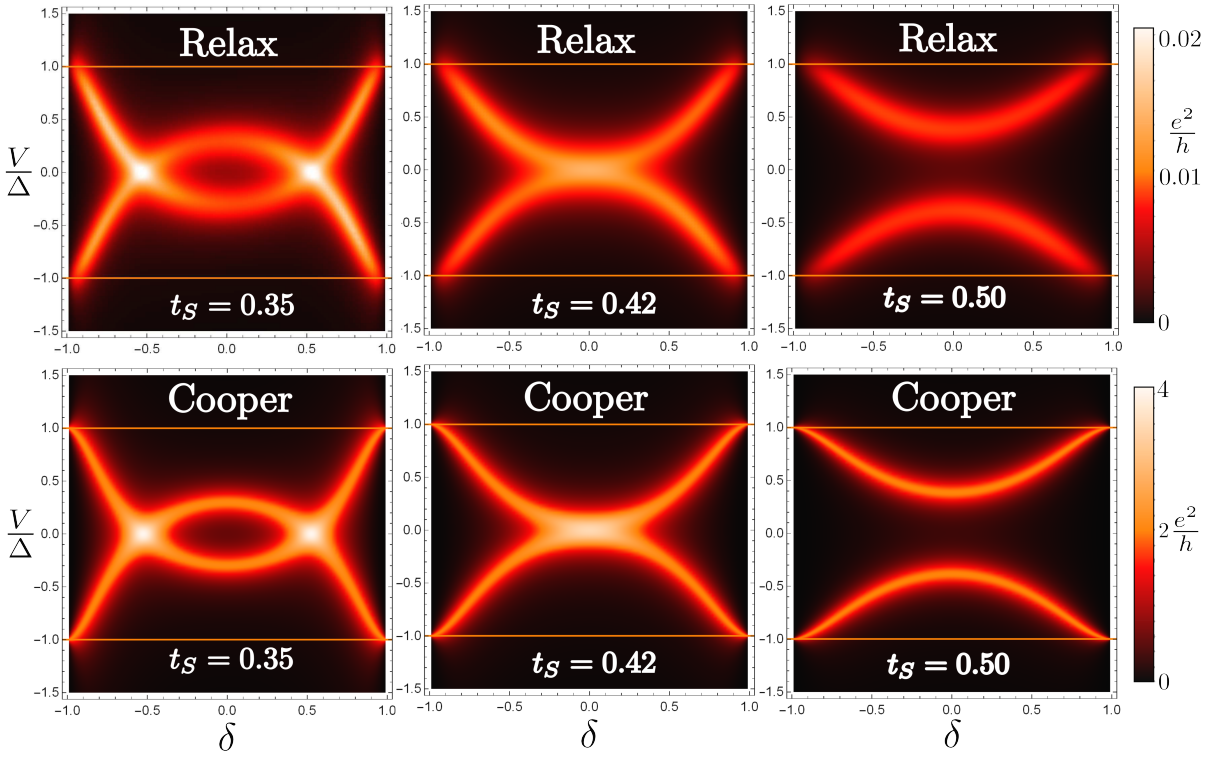

Figure 5.8: Here we plot conductance as a function of δ and bias using Eq.(5.75). δ corresponds to occupancy, which follows chemical potential on the dot μ. The three top most diagrams are in the relaxation dominated regime with $\hat{t_N} = 0.01$ and $\Gamma_r = 0.15$. Conductance lies between 0 and $0.02e^2/h$. The bottom three are in the Cooper-pair regime with $\hat{t_N} = 0.15$ and $\Gamma_r = 10^{-7}$. Conductance is always $2e^2/h$ at resonance. All parameters are in units of Δ and the orange-lines corresponds to $\pm\Delta$.

In experiments one can capacitively couple a lead to the dot and thereby control the chemical potential of the dot, which is equivalent to controlling ϵ_d. In real systems a quantum dot is often some kind of harmonic well with high enough level spacing to separate different levels. Then as one increases μ levels are filled one by one and we will expects YSR signatures in each odd occupancy sector within the gap. In 5.9 we show data from [23] to make the reader familiar with YSR signatures.

In the figure one clearly sees that every second sector shows stronger recognizable YSR features similar to Fig.5.8, while every second sector shows weaker eye structures often reaching all the way to the gap. These correspond to even occupancy, while the stronger corresponds to odd. In the far right side one even sees indication of a screened groundstate where the eye is opened and a crossing has occurred. From the low conductance and the visible asymmetry of the YSR state we would expect this experiment to occur in the relaxation regime in regards to transport.

A problem with asymmetry obtained by the Classical-Spin approximation is that the asymmetry is feeble compared to experimentally observed asymmetry, where one peak can be many factors larger then the other. We do not currently know the precise reason but mostly these strong asymmetries are observed far from center of the coulomb diamonds where our Schrieffer-Wolff transformed models are

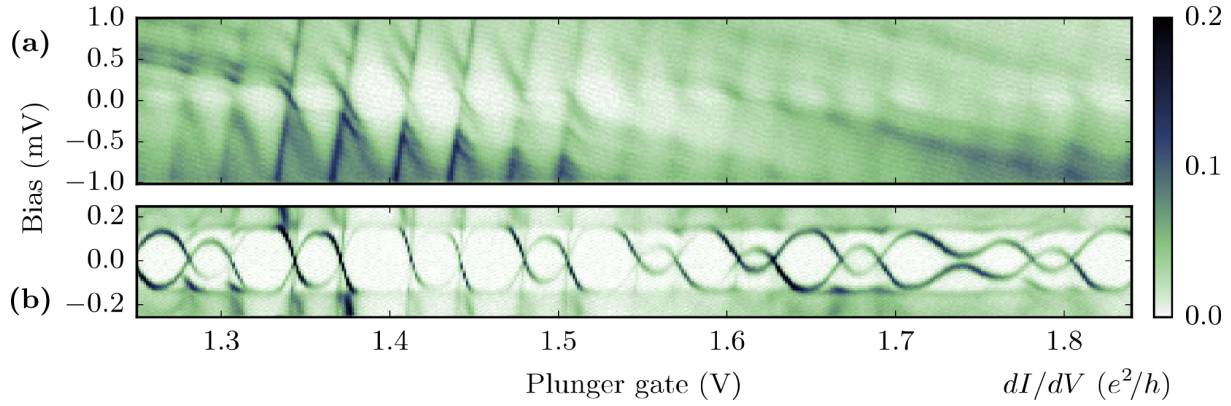

Figure 5.9: Here we show data from [23] obtained by A. Jellingaard et Al. The above diagram is made with a applied B-field in order to render both leads metallic so one can see clear coulomb diamonds. In the bottom we see in gap conductance at zero B-field with $T = 0.35mk$ in a SDN system.

bound to fail. This failure also becomes apparent in Section.8 where we analyze data using Classical-Spin.

6 Double-dot system

We have arrived at the main focus of this thesis, the treatment of superconductor-dot-dot-metal (SDDN) systems. Following collaboration with experimentalists at QDEV, mainly K. Groove Rasmussen and J. Nygaard, we have analyzed data obtained from double quantum-dot nanowire devices. In Fig.6.1 we present a schematic of the setup to provide the reader with an physical picture, a full description of the experiments will not be provided but a similar experiment is described in [23]. A great

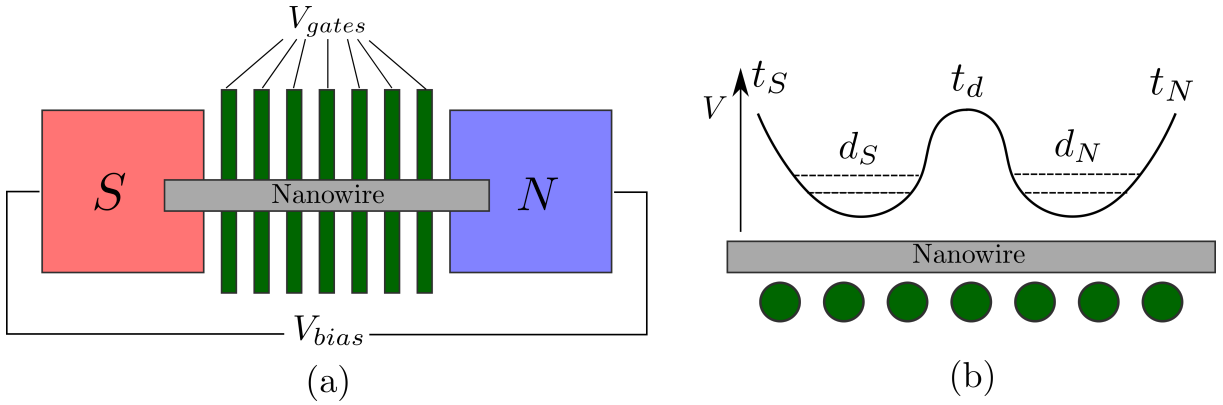

Figure 6.1: A schematic of the setup used in experiments. (a) A nanowire connects a superconducting lead (red) with an metalic lead (blue). Under the nanowire several capacitively coupled gates are placed orthogonal to the wire. (b) Side view of the wire. By controlling the bottom gates one can tune coulomb potentials in the nanowire. In our setup two potential wells are constructed d_S and d_N labeled by the lead they lie next to. The bottom gates also allows control of the tunnel-couplings between dots and leads.

advantage of this setup is its tuneability. By controlling the capacitively coupled bottom gates one has control over tunnel couplings and depth of wells which correspond to local chemical potentials of the dots. The disadvantage is that separation of parameters is not guaranteed, since tuning of a single bottom gat would alter the whole structure of the potential. So when one tries to tune a tunnel coupling the whole well could "splash" around. Writing up the full Anderson Hamiltonian for such a system

$$H = H_d + H_L + H_t \tag{6.1}$$

$$H_d = \sum_{\alpha=S,N}\left[\sum_\sigma \epsilon_\alpha n_{\alpha\sigma} + U_\alpha n_{\alpha\uparrow}n_{\alpha\downarrow}\right] + \sum_{\sigma\sigma'} U_d n_{S\sigma}n_{N\sigma'}$$

$$H_L = \sum_{\alpha k}\left[\sum_\sigma \xi_{\alpha k} c^\dagger_{\alpha k\sigma}c_{\alpha k\sigma} + \Delta_\alpha(c^\dagger_{\alpha k\uparrow}c^\dagger_{\alpha -k\downarrow} + c_{\alpha -k\downarrow}c_{\alpha k\uparrow})\right], \tag{6.2}$$

$$H_t = \sum_{\alpha k\sigma} t_\alpha c^\dagger_{\alpha k\sigma}d_{\alpha\sigma} + t_d\sum_\sigma d^\dagger_{S\sigma}d_{N\sigma} + \text{h.c}$$

here $n_{S/N}$ refers to electrons on d_S and d_N and as before $\Delta_N = 0$. The dots are considered to be coupled to their nearest neighbor so d_S is decoupled from lead N and similarly d_N is decoupled from

the superconductor. Apart from having two dots the only change in the Hamiltonian compared to the single dot Anderson model eq.(4.2) is the addition of a interdot coulomb interaction U_d which represents electrons on separate dots feeling each others charge. This coupling is assumed to be small compared to U_S and U_N. With this Hamiltonian we are able to develop models for such system but a problem occurs in comparing to experiments. In real systems the term U_d capacitively couples the two dots whereby dot-α feels the charge from the other dot's gate. This means that change of the bottom gate of one dot changes the occupancy of both dots.

6.1 Interdot Capacitive Coupling

This section will present a short discussion of the interdot capacitive coupling necessary to understand double dot systems. We will not go into full detail and we mostly rely on [27] for derivations. For starters consider the total charge on a single quantum dot connected to a bottom gate $Q_1 = C_g(V_1 - V_g)$ where C_g is the capacitive coupling to the gate, V_1 potential on the dot and V_g potential on the gate. Only if their is a difference will charge accumulate on the dot.

In expanding to two dots, and labeling as in our experiment, the total charge becomes

$$Q_S = C_{gS}(V_S - V_{gS}) + C_m(V_S - V_N) \tag{6.3}$$

$$Q_N = C_{gN}(V_N - V_{gN}) + C_m(V_N - V_S) \tag{6.4}$$

where C_{gS} relates to U_S, C_{gN} to U_N and C_m to U_d as they relate how difficult it is to change charge. From these equations one can calculate the total electrostatic energy stored in such a system which corresponds to a Hamiltonian, this is done in [27] and here we merely take the result,

$$H_{elec} = \frac{U_S}{2}\left(n_S - V_{gS}\right)^2 + \frac{U_N}{2}\left(n_N - V_{gN}\right)^2 + U_d(n_S - V_{gS})(n_N - V_{gN}) \tag{6.5}$$

here the different U's can be related to the capacitive couplings from above, but in our experiment they are simply measured. Now for our theoretical Anderson model eq.(6.3) to be relatable to experiment the electrically stored energy on the dot-gate system should correspond to the dot energy from Anderson $H_d = H_{elec}$ apart from factors not dependent on n_α as dynamics are determined by energy differences between states. Equating these two Hamiltonians yields the linear equations

$$\epsilon_\alpha = -U_\alpha\left(V_{g\alpha} - \frac{1}{2}\right) - U_d V_{\bar{\alpha}} \tag{6.6}$$

where $\alpha \in S, N$ and $\bar{\alpha}$ means the other dot. This equation shows that when one tunes the gate under a dot occupancy of both dots changes. Mostly we will work in the regime where $U_d/U_\alpha << 1$ such that tuning of one dot does not disturb the second much.

6.2 Honeycomb diagrams

In double dot experiments one typically deals in what is known as honeycomb diagrams. These are normally measured by plotting zero-bias conductance as a function of dot-bottom gates in a 2d plot. For our point of view variation of dot-bottom gates corresponds to variation of electron occupancy the on respective dot's. In Fig.6.2 we see actual data from experiments. The regime these measurements

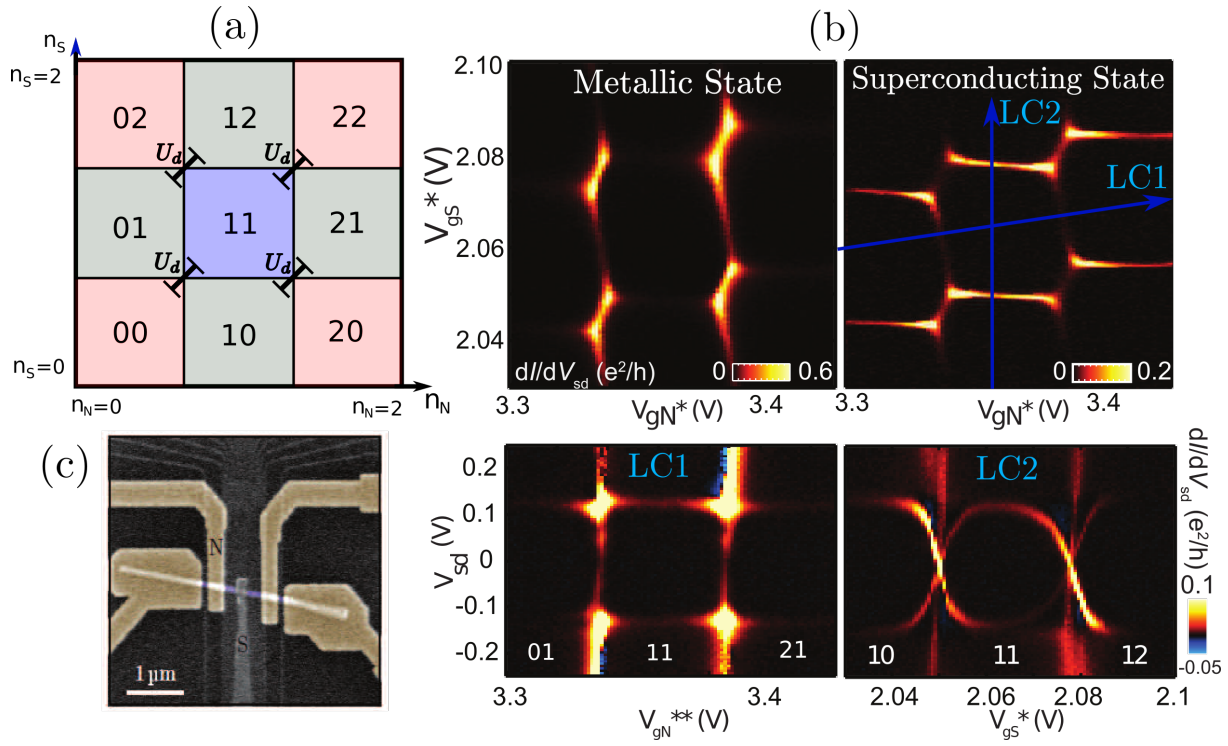

Figure 6.2: (a) A picture of how charge sectors appear under variation of n_S and n_N. The interdot coulomb coupling U_d separates charge sectors with the difference of a electron on both dots as shown. (b) The top two plots are experimental data of zero-bias conductance taken from a device. To the left with the superconducting lead being metallic and to the right it being superconducting. Bottom gates V_g are marked with asterisks to remind the reader that typically multiple gates are varied at a times. In the superconducting state two line-cuts are shown corresponding to change of source-drain bias as a function of bottom-gate along the cut. (c) Scanning electron microscopy of a typical device. In the experiments only one side of the device is used.

are done in, we denote as the weak-coupling regime or honeycomb regime. Weak coupling in the sense that couplings to both leads are so small that leads do not disturb dot spectrum and therefore it makes sense to talk about dot occupancy and charge. Also the interdot tunnel coupling t_d is very small such that only U_d interrupts the honeycomb's charge sectors. We will now discuss the visible transport.

When both leads are in the metallic state transport is simple. Both leads act as probes and one can separate transport into three types: 1): Fully sequential, this occurs whenever both dots are in a degenerate occupancy state where it is energetically free to add an electron to both dots. In Fig.6.2 one can see 4 light spots of high conductance in the metallic state at these sequential spots. 2): Partially sequential, this happens when one dot is degenerate so it can freely change occupancy, but electrons still have to tunnel through the second dot. Here dot-S and dot-N lines of degenerate occupancy can vary in conductance as one dot is typically easier to tunnel trough then the other. In Fig.6.2 for the metallic state on can see lines of dot-N degeneracy, which is weaker than the full sequential spots. 3):

Lastly there is cotunneling which is the full tunneling through both dots happening at all places away from degeneracy. As tunnel couplings are weak in this regime such transport is highly suppressed. Now we will move on to the case of one lead being superconducting.

First of all one does not see a huge impact on the honeycomb diagram, which structure is still visible in the superconducting honeycomb. Remembering that the S-lead is now a hard gapped superconductor this result might seem odd. Conductance in general is also smaller than the metallic case. Our explanation, following the language developed in the previous sections, is as follows: Since the systems now consist of two dots with all couplings small, Cooper-pair transport in which two electrons are transported through the entire system to form a Cooper-pair is highly suppressed compared to single electron transport. But single electron transport is only valid in the relaxation process where one can excite a YSR bound state which then relaxes into the continuum, which means that transport depends on the presence of a YSR at the given bias and gate.

These states are formed whenever one of the dots is at an occupancy yielding a magnetic moment, but as t_d must be small, to obtain a simple honeycomb, the superconductor does not feel the presence of dot-N and YSR states only forms from dot-S interactions. Therefore one sees conductance at dot-S degeneracy lines where the YSR state crosses zero. In the line cuts from Fig.6.2 one clearly sees YSR states when varying dot-S bottom gates. As the superconductor is only weakly coupled one sees a large "eye" in accordance with theory for small coupling $\alpha \propto \nu_F t_S^2/U_S$. In the variations of dot-N no such states can be seen, but a weaker sub-gap needle is observed precisely at degeneracy. This could either be attributed to a proximity induced type bound state [1], as discussed in the introduction or simply increased Cooper-pair transport as one dot is degenerate, opening for partial-sequential Cooper-pair transport.

Generally what one sees in these pictures is that the phase boundaries, which in the metallic case were formed by sequential tunneling lines, are replaced with YSR crossings. Both of these indicates a phase-transition of the dot and in conduction measurements act as boundaries between different groundstates. Later we will see that this continues to be true in the superconducting case even when couplings t_S and t_d are large.

When bias is larger than the gap situated at $\Delta = 0.14$ meV one probes the superconducting quasiparticles instead of the gap and the superconductor behaves as a metallic lead with a weird density of states.

In this case we were able to give a simple explanation, but only because coupling were weak making this system behave effectively as a single dot coupled to a superconductor. When the couplings are increased we have to leave our simple models behind as the superconductor then feels dot-N also. Especially in the 11 charge sector care must be taken as more complicated interactions occurs when YSR screening begins to compete with singlet-triplet formation between dots.

Here our classical-spin calculations based on Schrieffer-Wolff based Kondo models becomes cumbersome. First of all, the model only properly describes the physics deep inside of the coulomb diamond and is difficult to extrapolate to all areas of the honeycomb. Secondly, each charge sector would demand independent Schrieffer-Wolff calculations and as we have to consider two dots high order calculations would be needed. For example to obtain a term wherein the superconductor self-interacts through dot-N at least a fourth order Schrieffer-Wolff transformation would be needed.

In the next section we will develop a simple model based on a completely different approach. This model turns out to be directly solvable and allows us to obtain spectrum for the superconductor-dot-

dot system and when the metallic lead is weakly coupled, acting only like a probe, this is enough to give a qualitative understanding of transport.

7 Zero-Band-Width model

In this section we will develop the Zero-Band-Width (ZBW) model, which is a method used to solve the Superconductor-Dot systems numerically. First and foremost this model is an alternative to full Numerical Renormalization Group (NRG) calculations which are known for properly describing YSR physics in such setups [23, 28].

The NRG approach is based on logarithmic discretization of energy to form a Wilson chain. Starting from highest k one will then integrate out one site at a time until a converging result is obtained. Such an approach yields the correct spectrum in the YSR problem but a number of difficulties remain. First and foremost the method is numerical cumbersome requiring both skill and computer power. Secondly an out of equilibrium version of NRG has not yet been developed which makes NRG unable to reveal much about transport. NRG provides fine spectral properties, but as discussed in the transport section sub-gap conduction is not proportional to the YSR spectral function.

ZBW will provide an easy to apply alternative to NRG as it can be solved by direct diagonalization. The ZBW method corresponds to replacing the whole BCS superconductor with a single quasi-particle site with energy Δ. This approximation is inspired by Yosida's variational anzats [26] where to lowest order the superconductor is in effect also replaced by a single site. The YSR physics are then captured by the triplet/singlet formation happening between this single site and the dot. The singlet will win some energy thereby entering the gap and as the spins are opposite pointing this corresponds to a screened state. The three triplet states are pushed up far away from the gap. Using a reduced Kondo model the energies of these states were calculated in [10]. But as we seek a model for all charge sectors we numerically do the same for the full Anderson model. The name Zero-Bandwidth comes from the fact that by replacing the whole quasi-particle band with a single state one is effectively treating the band as having no width.

Similar ZBW models have been explored in metallic systems with regards to the Kondo problem [22]. There the ZBW is a poor approximation as the Kondo problem exist on all scales and the lowest energy state does not determine the full physical picture. Beginning this investigation we expected the same to be true for superconducting systems but it turns out that ZBW yields surprisingly good results almost to the limit of being able to use ZBW to extract parameters. As one can see in Appendix.C ZBW predicts qualitatively the same results as NRG, which is believed to yield the full solution, in almost all regimes. Only in regions of large coulomb interaction U and large coupling to superconductor Γ will ZBW fail.

Our picture for why ZBW provides such a close comparison to NRG is the following. A BCS superconductors spectral function is empty in the gap and then diverges precisely at $\pm\Delta$ and afterwards it flattens out returning to a metallic like density of states. Therefore lower energy states then Δ are irrelevant and Cooper pairs can also be disregarded as they are spin-less and magnetically inactive. Therefor the first and largest contributions arise from the peaks at $\pm\Delta$ which is what we capture with a ZBW model. The ZBW approach was first explored in [6]. Here we will extend his analysis and in the end apply the model to the double-dot system described earlier.

It should be stated that similar to NRG there does not exist a way to extend ZBW to transport calculations and we need to return to classical-spin calculations to discuss transport.

7.1 Single-Dot ZBW

We start with the simple system of a superconductor coupled to a single quantum dot as a testing ground for our new model. For a single quantum dot we expect the physics to be simple and follow the same guide-lines as the classical-spin model yielding a fine model to compare to.

Our model Hamiltonian based on the Anderson Hamiltonian eq.(4.2) is,

$$H = H_S + H_d + H_t \tag{7.1}$$

$$H_S \approx H_{ZBW} = \Delta c_\uparrow^\dagger c_\downarrow^\dagger + \Delta c_\downarrow c_\uparrow \tag{7.2}$$

$$H_d = \sum_\sigma \epsilon_d n_\sigma + U n_\uparrow n_\downarrow \tag{7.3}$$

$$H_t = t \sum_\sigma c_\sigma^\dagger d_\sigma + \text{h.c} \tag{7.4}$$

This model consists of two fermion sites with spin degeneracy in each. Therefor the total Hilbert space is $2^4 = 16$ dimensional which can be diagonalized exactly. We then compare this model to the classical spin model using Eq.(3.19) with,

$$\alpha = \pi\nu_F \frac{3t^2}{2U} \frac{4}{1-\delta^2} \quad \text{and} \quad \beta = \pi\nu_F \frac{t^2}{U} \frac{-2}{1-\delta^2} \tag{7.5}$$

where the factor $3/2$ is needed to make the classical-spin behave quantum for low t^2/U as discussed in the transport Section.5. The results are plotted in Fig.7.1. One clearly sees the similar behavior for

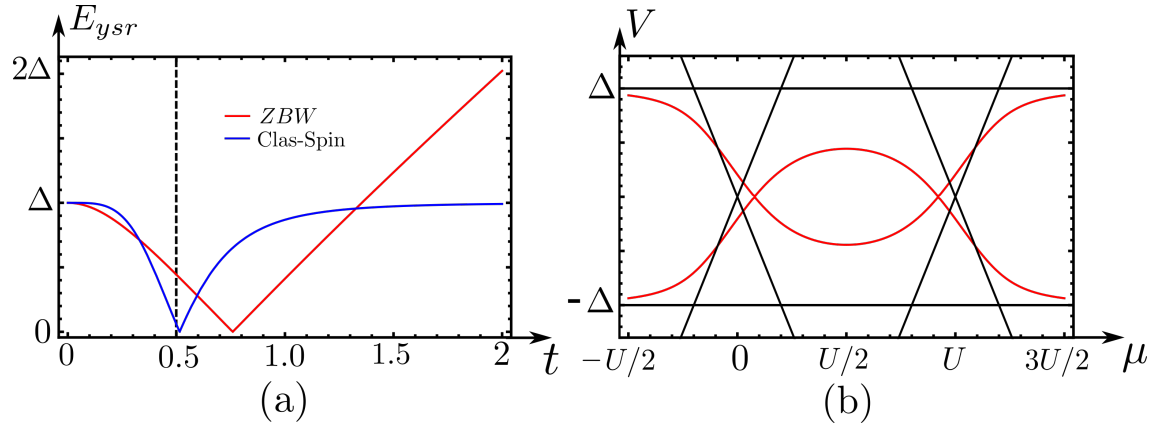

Figure 7.1: (a) Here we plot the YSR energy at the particle-hole symmetric point $\epsilon_d = -U/2$ for the Classical Spin (Blue) and ZBW (Red) model as a function of tunnel coupling to the superconductor. Here we have chosen $U = 5$ and everything in units of Δ. We see ZBW behaves unphysical in crossing Δ. The line indicates t used in (b). (b) A picture of the lowest excitation excluding degeneracies for the ZBW model for $t = 0.5$ and $U = 5$ in units of Δ. Here $\mu = -\epsilon_d$ is the chemical potential. Black lines are the coulomb diamond and gap.

both ZBW and classical spin. They disagree about when the change of ground state appears and for large t one clearly see how ZBW fails by crossing Δ. The behavior is similar for other choices of U.

The failure of ZBW is related to its missing gap. For both classical spin and NRG the YSR state is unable to cross Δ as it anti-crosses with the bulk states and so it converges towards Δ for high coupling. But as there are no bulk states for ZBW the crossing occurs. In the second plot we see that ZBW reproduces familiar shapes, here for example we see the "eye" shape where the coupling is not strong enough to screen the impurity yet. We also see that the degeneracy points for $V = 0$, which before stemmed from the coulomb diamond, now occur almost at the same spot but is the tail of a YSR state. For transport in the relaxation regime one would only see the YSR structure and not the diamond.

Next in Fig.7.2 we compare the first excitation from ZBW with classical spin YSR. For small coupling t we see that they match quite well but for large t they separate. It should be stated that the two models behavior is generally the same in the sense that as t increases from 0 an "eye" shape forms, then closes leading to a "hill" which merges with the gap. They differ in the fact that the ZBW crosses the gap as shown in Fig.7.2. But following these observation one could state that we are simply com-

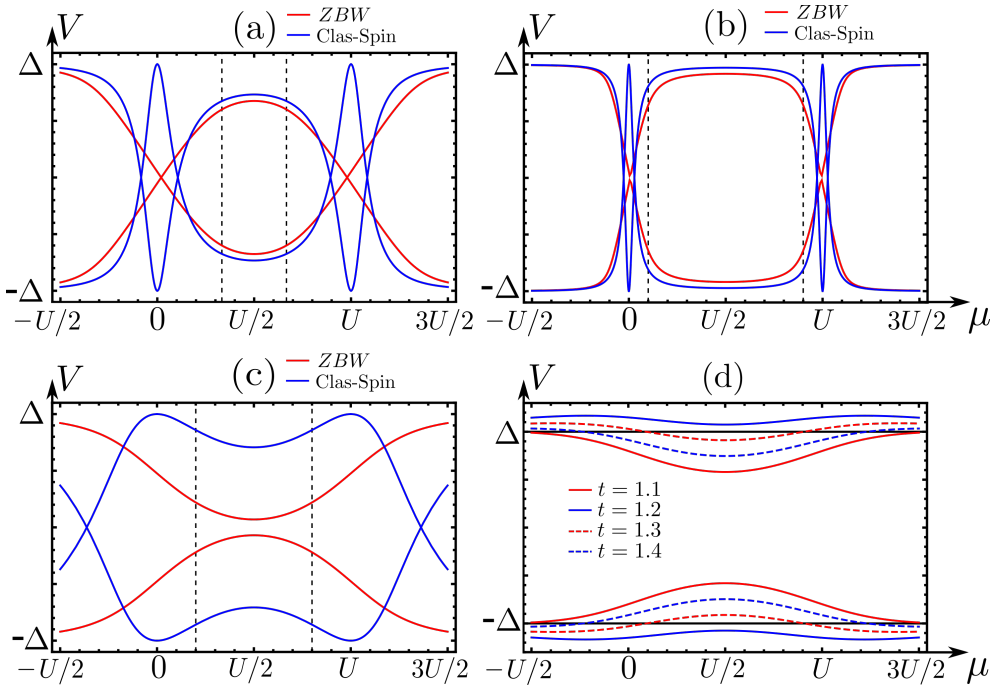

Figure 7.2: Here we plot lowest level excitations as a function of chemical potential. In (a) $U = 3$ and (b) $U = 10$ both with $t = 0.25$ in units of Δ. The dotted lines are the limits to classical spin calculation set by Schrieffer-Wolff at $U \pm \mu = \Delta$, only within these lines can classical spin be trusted. In (c) $U = 5$ and $t = 0.8$ in units of Δ. In this plot one sees large disagreement between the models. At (d) we consider ZBW at $U = 5$ close to the crossing of Δ for varies t. One clearly see how the full level cross Δ.

paring two approximate models with each other without knowing if both are failing. Therefore we compare ZBW to full NRG calculations taken from [29] in Appendix.C. There we see that NRG and ZBW behave very similar except that the ground state change happens faster for NRG. These results

in addition to results from Double-Dot ZBW lead us to believe that if one disregards the precise value of t then ZBW is equivalent to full NRG. Therefor using ZBW one can quickly obtain results in a qualitative sense for YSR systems. Before going into full double-dot ZBW we will present an extension which fixes the crossing problem for ZBW.

7.2 Extended ZBW

Following the line of reason for development of the Wilson chain in NRG we believe that ZBW could be improved by extending the model with more states in the "chain". In a sense we develop the bulk at Δ by adding more sites to the superconductor which fixes the ZBW crossing problem for high t.

The problem here is that this expansion is uncontrolled and we have no way to fix the new arising tunnel couplings between superconducting sites other than comparing to one site ZBW. Therefor in this section we will only provide a short analysis just to show that if the right approach is chosen there is hope for improving ZBW and verifying that the missing bulk is indeed what gives the crossing problem.

The recipe is simple: add sites in the superconductor only keeping the first site coupled to the dot. Constructing such a model it was quickly realized that two superconducting sites fail, and one have to go to three sites to obtain a working model.

We do not fully understand why but we believe it is related to singlet-doublet formation between the sites removing them from Δ. We therefor utilize the following extension

$$H_S = \sum_{i=1}^{3} \left(\Delta c_{i\uparrow}^\dagger c_{i\downarrow}^\dagger + \Delta c_{i\downarrow} c_{i\uparrow} \right) + \sum_\sigma \left(t_1 c_{1\sigma}^\dagger c_{2\sigma} + t_2 c_{2\sigma}^\dagger c_{3\sigma} + \text{h.c} \right) \tag{7.6}$$

Next as before we plot YSR energy in the particle-hole symmetrical point as a function of increasing superconducting coupling t and compare to ZBW in Fig.7.3.

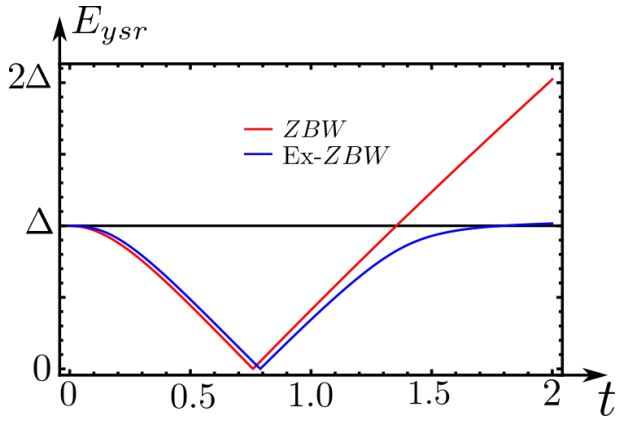

Figure 7.3: Comparison between single site ZBW and extended ZBW at $U = 5$ and $t_1 = t_2 = 0.3$ in units of Δ. Notice that the extended version still crosses but now for higher t.

We see how the extended model fixes the crossing. What happens is that the dot hybridizes with the first site to form the YSR state, while the other two sites still hang at Δ. But when it tries to cross

later it anti-crosses with the two sites. As two sites are a poor approximation to a full bulk the crossing still occurs for higher t.

7.3 Double-Dot ZBW

In this section we use the ZBW model to do a full treatment of the superconductor-dot-dot system. We will use the non-extended version of ZBW in order to have as simple a model as possible. Similar to the section on double-dot systems we will primarily deal with two kinds of data. honeycomb diagrams which are conduction plot of all occupation sectors at zero bias, and line-cuts which represent conduction as function of occupancy along a line in the full honeycomb and source-drain bias.

As before we obtain our effective model by replacing the superconducting Hamiltonian by a single site,

$$H = H_S + H_d + H_t \tag{7.7}$$

$$H_d = \sum_{\alpha=S,N} \frac{U_\alpha}{2} \left(\sum_\sigma n_{\alpha\sigma} - V_\alpha \right)^2 + U_d \left(\sum_\sigma n_{S\sigma} - V_S \right) \left(\sum_\sigma n_{N\sigma} - V_N \right)$$

$$H_S = \Delta c_\uparrow^\dagger c_\downarrow^\dagger + \Delta c_\downarrow c_\uparrow \tag{7.8}$$

$$H_t = \sum_\sigma t_S c_{Sk\sigma}^\dagger d_{S\sigma} + t_d \sum_\sigma d_{S\sigma}^\dagger d_{N\sigma} + \text{h.c}$$

where we started by choosing the form eq.(6.5) for the Anderson Hamiltonian as they in real experiments vary the bottom gates and not the local chemical potential $\epsilon_d = -\mu$. So variations of V_α terms should directly correspond to variations of the real bottom gate $V_{g\alpha}$. For this model treating all combinations of parameters would be a challenge and we will therefor only discuss the subset relevant to the experimental results. Luckily a number of parameters can be extracted by other measurements restricting the number of free parameters we have to deal with. As a simple test we will show that our model can reproduce similar honeycomb and cuts as seen in Fig.6.2. For this device, measurements in the normal regime enabled height measurements of coulomb diamonds from which the parameters $U_N = 3.1$meV, $U_S = 2.9$meV and $U_d = 0.8$meV were obtained. The results of this analysis is shown in Fig.7.4

In these plots we first consider the case of small coupling $t_S = 0.01$meV to the superconductor in order to map out the bare honeycomb diagram. Here we see that the lowest excitation is a the gap except near degeneracy points where crossing occurs. In the next diagram we then increase the coupling to the superconductor to $t_S = 0.125$meV which in effect "softens" all transitions along the V_S lines while the sudden transitions along V_N are retained. Such behavior mimics the behavior expected from the analysis in Section.6 where we considered dot-S influenced by YSR physics while low t_d kept the dot-N unaffected.

In effect we obtain a clear correspondence between excitations obtained by the ZBW model and conductance highlights obtained in the experiment. Generally this is also what we expect when the metal is weakly coupled thus only acting as a probe not affecting the system.

In the last plot with $t_S = 0.40$meV we see that the honeycomb structure is replaced by two lines, if one considered conductance. This is the screened honeycomb where the "eye" in the line cut has crossed and becomes a hill instead. This indicates that the $V_S = 1$ state has been completely screened

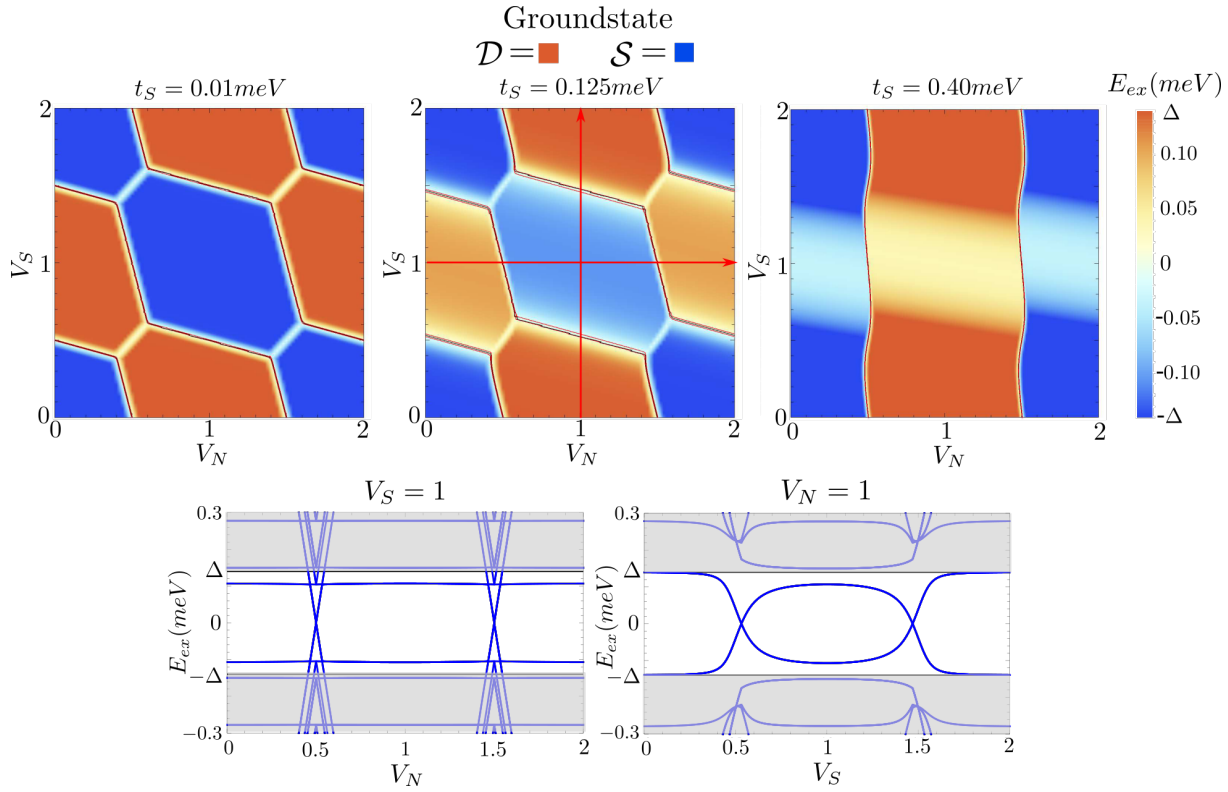

Figure 7.4: The top three plots are Honey-Comb diagrams with $t_S = 0.01$meV, $t_S = 0.125$meV and $t_S = 0.4$meV all sharing $U_S = 2.9$meV, $U_N = 3.1$meV, $\Delta = 0.14$meV and $t_d = 0.01$meV. The color scale shows distance to nearest excitation with sign chosen to represent ground-state, positive means Doublet ground state and negative Singlet ground state. Care should be taken in the 11-sector where singlet refers to approximate singlet/triplet degeneracy. Also contours at $E_{ex} = 0$ are highlighted. The red lines indicate the line-cuts shown in the bottom two plots. These show excitations apart from degeneracy. The blurred sections are out of gap where the model fails to account for bulk states and should therefore not be trusted.

into a singlet. From this one would not be able to see occupancy changes by varying V_S, so if one looked at data naivly one would believe only dot-N is present. In order to see that there is two dots one should raise the bias while doing honeycombs until the light regions would resurface.

Optimistic with the results from ZBW we move onto the hard problem of large couplings t_S and t_d. First let us consider the effects of increasing t_d, primarily leading to two effects: First the degeneracy between triplet and singlet in the 11-sector would be broken. Tunneling through nearby charge sectors, for example $\langle\uparrow_N,\downarrow_S| \to \langle\uparrow_N\downarrow_N,0| \to \langle\uparrow_N,\downarrow_S|$, leads to an effective exchange interaction for states of separate spin on each dot. Solving such a model by ignoring U_d, doing lowest order Schrieffer-Wolff and diagonalizing yields exchange energy,

$$E_T = 0, \qquad E_S \approx -\frac{4t_d^2}{U_S + U_N} \tag{7.9}$$

where E_T is the energy modifying the three triplet states and E_S the energy modifying the singlet state. Since the singlet state is spin-less it does not produce YSR physics. So YSR physics first occurs for the higher energy triplet states which will be screened to doublet.

Secondly for high t_d the superconductor can tunnel through dot-S, interact with dot-N and tunnel back to the superconductor, enabling screening of dot-N. This is a fourth order Schrieffer-Wolff term taking different forms for different configurations. But to lowest order in Schrieffer-Wolff the effective dimensionless strength of such a term is

$$\alpha_N \propto \pi\nu_F \frac{t_S^2 t_d^2}{U_S^2 U_N} \tag{7.10}$$

which is similar to the strength of the coupling α to a single dot except there is an additional factor t_S^2/U_S^2 coming from tunneling through dot-S twice.

This analysis enables us to characterize such systems by three parameters

$$\alpha_S = \pi\nu_F \frac{t_S^2}{U_S}, \qquad \alpha_N = \pi\nu_F \frac{t_S^2 t_d^2}{U_S^2 U_N}, \qquad E_S = \frac{4t_d^2}{U_S + U_N} \tag{7.11}$$

which explain the physics going on deep within sectors where charge is determined. First the four corner sectors where no dot is singularly occupied and therefor has no magnetic moments follow trivial behavior with no YSR physics. The sectors with $V_S = 1$ and $V_N = 0/2$ would contain YSR physics determined by α_S as dot-N is magnetically inactive. Similarly for $V_N = 1$ and $V_S = 0, 2$ with YSR coupling set by α_N. Lastly in the 11-sector one would have competition between singlet formation and triplet screening, where the primary scale for screening would be set by α_S as dot-S is easier to screen. It should be stated that this is only a lowest order analysis and the rest of the sectors out of these specific points follow complex behavior. Testing of these scales indicate that the α scales do not provide a consistent picture and keeping one of these invariant does not guarantee invariance of its respective YSR state as small changes still occur. We do not yet know if this arises as a failure of ZBW or if its because these scales are only accurate for small couplings as they are built on the classical-spin approximation. NRG investigations provided by R. Zitko also indicate that these scales are not fully determining the physics and that the relevant physics change when one changes parameters, but still keeps the related scale invariant. Even though such scale arguments fail we still believe the corresponding physical picture to be true in each sector which is supported by ZBW investigations.

We will now be moving on to discuss our primary focus which is data from a different device than the one just discussed. This device is similarly constructed as the one previously analyzed but for this device couplings are stronger. As before some parameters could be extracted by driving the superconducting lead metallic: $U_N = 2.5$meV, $U_d = 0.01$meV. But U_S was not extractable as the high coupling still present in the normal case blurred coulomb diamond features. Beginning our analysis we found out that the band crossing flaw of ZBW became more prevalent for large U_S and we therefore chose to work in the regime of $U_S = 0.8$meV corresponding to $U/\Delta \approx 5.5$ where such details are not interfering with the general picture. We also found no evidence of the triplet-singlet transition occurring in the data so we choose $t_d = 0.27$meV from which the triplet-singlet separation becomes $E_S = 0.177$meV which is above the gap and therefor out of the picture.

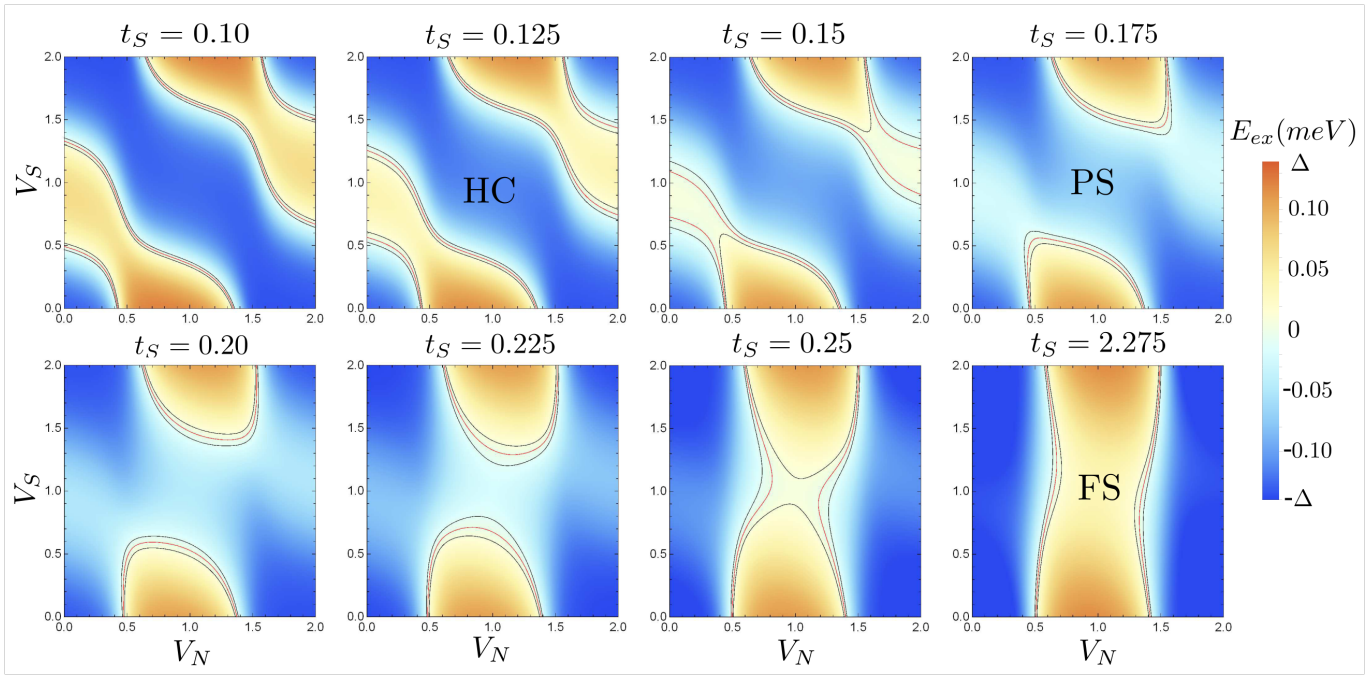

Figure 7.5: Here we see dynamics of the Honey comb diagram under increasing t_S. Parameters are $U_N = 2.5$meV, $U_S = 0.8$meV, $U_d = 0.1$meV, $\Delta = 0.14$meV and $t_d = 0.27$meV. The letters represent phase: HC = Honey Comb in which all dot states are visible. PS = Partially screened, this regime is where dot-S is screened but the joined triplet is not. FS = Fully screened, in this regime the triplet in the 11-sector is screened to a doublet and therefor it only looks like dot-N is present. The Red contour line is along the transition $E_{ex} = 0$ while the black is along $E_{ex} = \pm 0.01$meV.

Next we will show the evolution of the honeycomb starting from these parameters and for increasing t_S. This can be seen in Fig.7.5

What is seen is that for increasing t_S dot-S is screened before the 11-sector, which stems from the lower energy of the singlet state for high t_d. This opens up a regime which we call partially screened in the sense that dot-S is screened by itself but not when interacting with dot-N. If one increases t_S further the screened triplet state, which is a doublet since a screened spin 1 becomes spin $1/2$, will eventually obtain lower energy than the singlet state and we then enter the fully screened regime. Quantifying this analysis we construct a phase diagram for t_S and t_d shown in Fig.7.6. This phase diagram affirms us in our intuition that increasing t_d prolongs the existence of the partially screened regime as the exchange singlet becomes more and more energetically favorable to have as ground state in the 11-sector compared to screened triplet. The existence of these phases can be tested in a multitude of ways by controlling the tunnel couplings in the experimental setup. In Fig.7.7 one can see how experimentally one can tune the fully screened regime into the partially screened regime by varying the gate controlling t_d increasing the singlet-triplet separation.

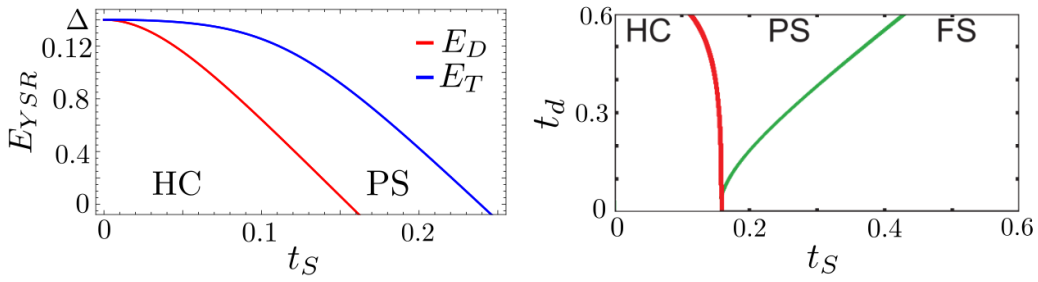

Figure 7.6: To the left we see two excitations: screened doublet in the 10-sector labeled E_D and the screened triplet in the 11-sector labeled E_T as a function of t_S with $t_d = 0.27$meV. In the region where E_D have crossed zero but E_T has not we call the partially screened regime. To the right is a phase diagram. Here the red line corresponds to E_D crossing 0 and the green line E_T crossing 0. All plots are with $U_S = 0.8meV$, $U_N = 2.5meV$, $U_d = 0.1meV$ and $\Delta = 0.14meV$ and factors are in units of meV

As seen for the single-dot ZBW the exact values of parameters should not be trusted, as the ZBW model does not fully agree with NRG, but we want to verify that the dynamics found by double-dot ZBW is qualitatively reasonable. Luckily R. Zikto was willing to provide us with honeycomb diagrams for us to compare too. These are shown in appendix.C. From this comparison it is clear that ZBW is capable of describing dynamics of such setups and the above results can indeed be trusted. Finally in order to truly test our understanding we went into detail and did a full comparison of experimental results from this device in the partial screened regime and with ZBW. In this analysis we fitted parameters by hand in order to match ZBW line cuts with experimental line cuts. The results are shown in Fig.7.8

These fits show the surprising strength of a model as simple as ZBW. Even though the theory was constructed from a hunch stemming from the Yosida's anzats we have obtained a model capable of. to a good degree, reproducing experimental results. To avoid bragging it should be stated that this was done by using three free parameters namely U_S, t_S and t_d and we cannot guarantee that our solution is unique. We have from the start limited U_S and it would not be hard to imagine that the true value is larger and would be able to produce similar line-cuts. Just to be pedantic one should also consider that in experiment the different sectors are ill-defined when no clear honeycomb is present and the line-cuts shown are therefor done using estimates of the gate on the other dot, not fully comparable to our line cuts which have precise defined gates for the second dot.

But apart from these details ZBW appears to be a powerful easy to use tool which can be used to obtain a quick quantitative picture. Here in the end we would like to state that the discussed screening of sectors in a honeycomb have been observed before for a system with two metallic leads and two quantum-dots [30]. Here there is no YSR physics going on, but instead the screening happens as Kondo screening of the magnetic moment. The big difference is that instead of crossing, the Kondo signatures stick at $V_{sd} = 0$ thereby forming a "flatland" in conductance instead of disappearing.

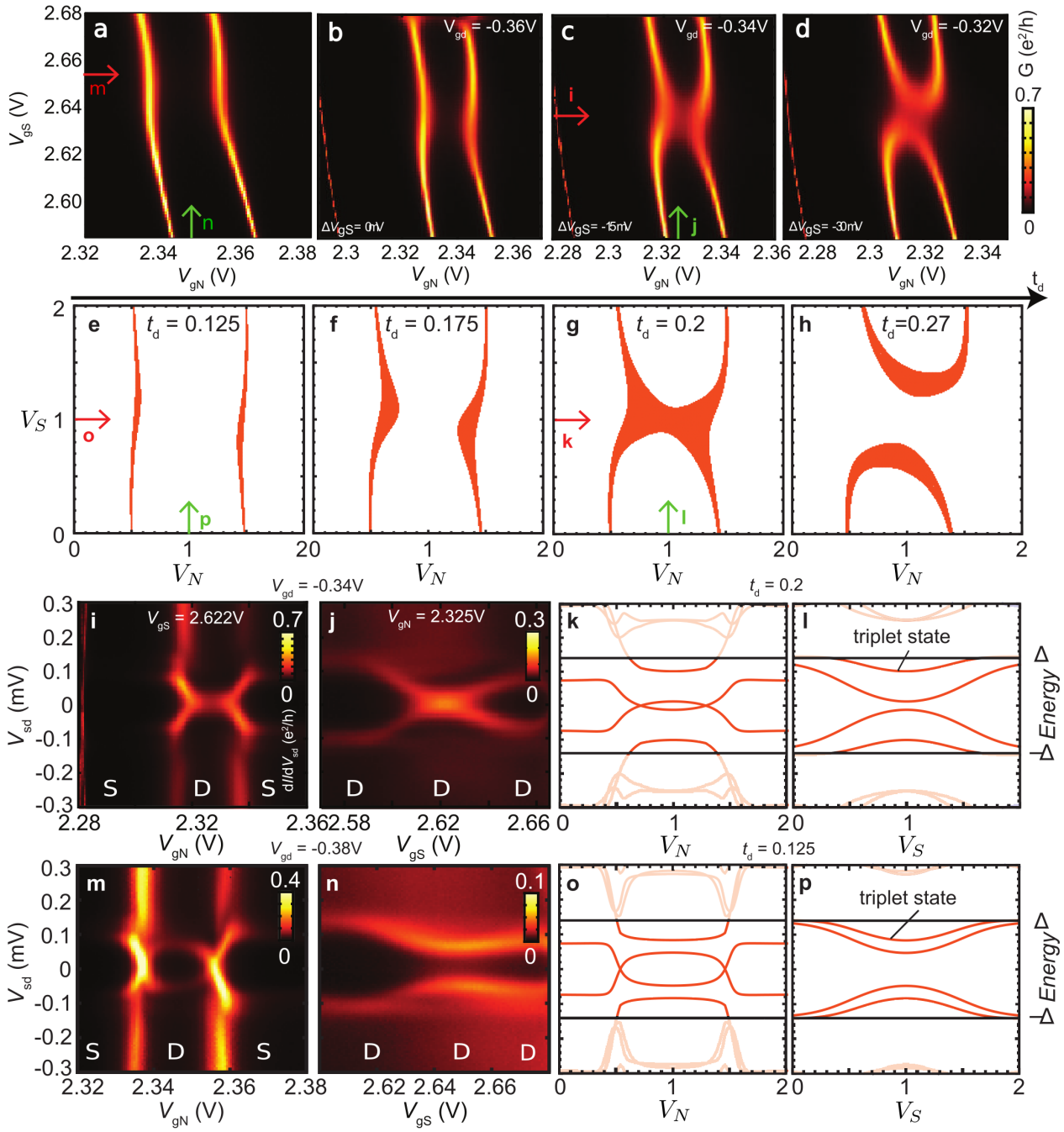

Figure 7.7: In figures a to d we see conduction at zero bias as a function of bottom gates for the two dots. From a to d the gate corresponding to the t_d coupling have been increased. In these plots we see the phase transition from fully screened to partially screened. In figures e to f we see theoretical plots where the colored areas correspond to excitations with $|E_{ex}| < 0.015$meV showing the phase boundaries as to give a clear correspondence to data. t_d is in units of meV . The rest of the plots are line-cuts with label shown on their corresponding honeycomb. Here we see the triplet state enter the gap for low t_d coupling. In Fig.7.8 we in depth investigate the same parameters as plot d here. The theoretical plots are done with: $U_N = 2.5$meV, $U_S = 0.8$meV, $U_d = 0.1$meV, $\Delta = 0.14$meV and $t_S = 0.22$meV. This plot was made in collaboration with K. Groove

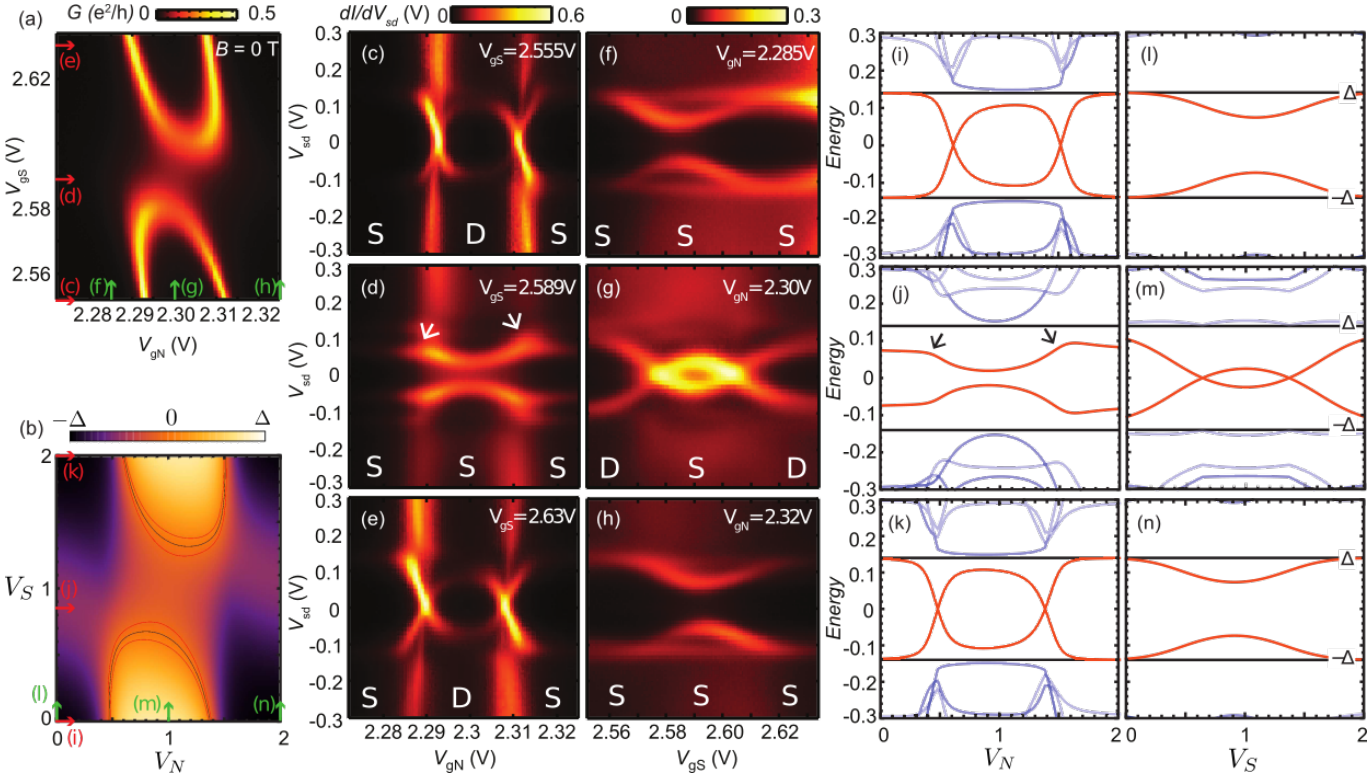

Figure 7.8: In figure (a) we see conduction at zero bias as a function of bottom gates for the two dots. In (b) we see a theoretical plot of excitations as a function of gate V_α obtained with ZBW following the previous convention. Notice that conduction occurs at boundaries between ground states. Next there are six line-cuts for both experimental and theoretical Honey-Combs, their label indicates a line on the corresponding honeycomb. In the experimental cuts they measure conduction as a function of source-drain bias, while for theory it is simply excitations with irrelevant out-of gap excitations colored Blue. The theoretical plots are done with: $U_N = 2.5$meV, $U_S = 0.8$meV, $U_d = 0.1$meV, $\Delta = 0.14$meV, $t_S = 0.22$meV and $t_d = 0.27$meV. This plot was made in collaboration with K. Groove

8 Classical-Spin for SDDN

With the use of ZBW we were able to completely map out the phases and visualize excitations for the SDDN system. But this is not all, as it is not proper to completely map an excitation plot to a conduction plot, we would like to complete the picture by doing transport calculations through such systems.

The problem is that we do not yet know how to expand ZBW into a non-equilibrium framework or in any way obtain transport equations. One could then return to NRG which, with a slight expansion, is able to compute spectral functions. In the literature it is quite common practice to simply calculate spectral functions and compare them to conduction data [2, 23, 28].

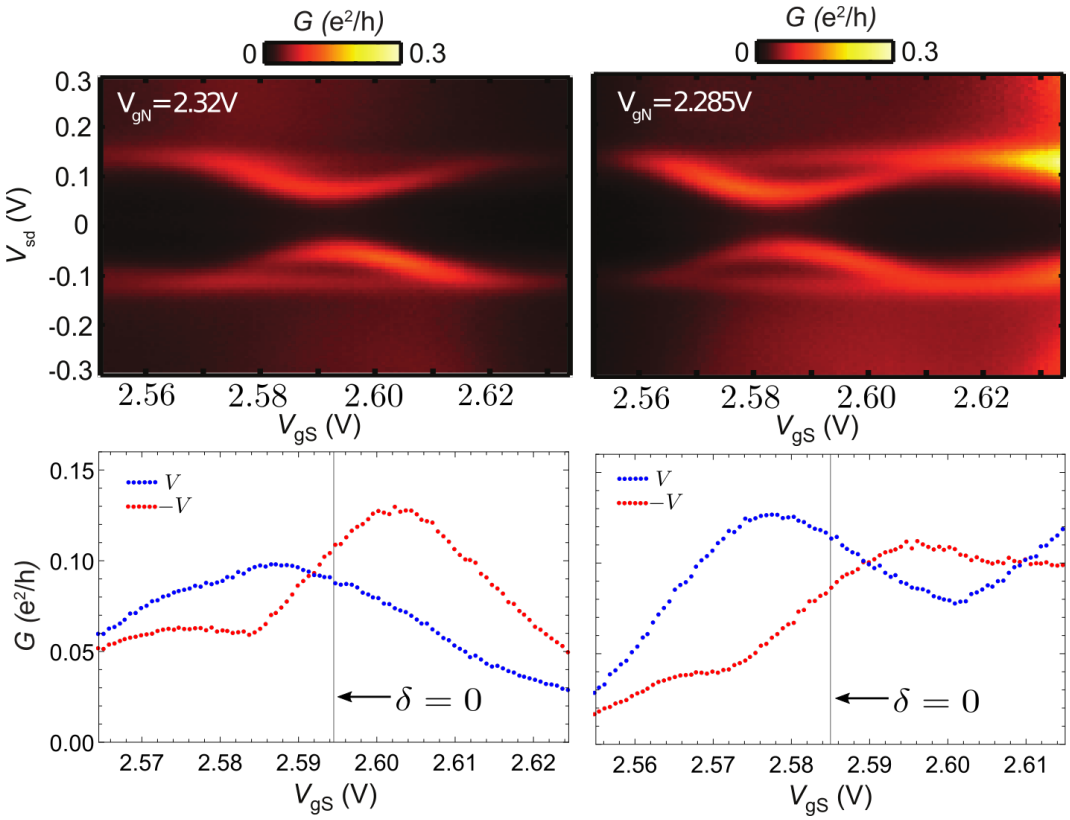

Figure 8.1: On the top left we see the line-cut corresponding to $n_N = 2$ and on top right line-cut $n_N = 0$. As the bottom gate varies one correspondingly varies n_S and we see a screened YSR state moving into the gap as n_S approaches 1. On the bottom two plots we see max-conductance of YSR peaks plotted as a function of bottom gate for dot-S. Lines in the middle represent particle-symmetrical points obtained by finding the point were YSR states are furthest into the gap. These plots where made in collaboration with K. Grove

Yet we saw, by doing classical-spin calculations, that one cannot simply compare spectral function to conduction. Importantly if there is no relaxation Γ_r then sub-gap transport will always turn out bias-symmetric for classical-spin calculations. Also simple problems like spin-dependent tunnel-

coupling, which is always the case in our calculations, will change conduction patterns away from spectral patterns.

Therefor in this section we will try to do transport calculations on the SDDQ system by use of classical-spin models. The problem here is that such models are derived deep inside a given charge sector and not for the whole Honey-comb. So we choose to focus on two specific sectors namely $n_S = 1$ with $n_N = 0$ or $n_N = 2$. The reason for this choice is simplicity as we keep dot-N magnetically inactive so we can focus on dot-S for contributions to YSR physics.

In Fig.8.1 we see a plot of line-cuts describing these two sectors when varying n_S. We notice the peak asymmetry when moving away from the particle-hole symmetrical point, described in the classical-spin picture as $\delta = 0$, where one peak is growing and one is falling. This asymmetry, in correspondence with conductance much lower than $2e^2/h$, strongly hints that we are in the relaxation dominated regime, as described in the transport Section.5, where non-resonant single-electron processes dominate conduction. We will later from an estimate of parameters show this is indeed the case. But an additional asymmetry shows up, namely that even for $\delta = 0$ conduction is not bias symmetric which would always be the case for single-dot transport. This could be a error in the experimental setup where positive or negative bias enhances conduction. But when considering $n_N = 0$ compared to $n_N = 2$ we see that the bias asymmetry changes sign enhancing the bottom YSR peak for $n_N = 0$ and top for $n_N = 2$. This systematic form indicates that it is not such an error.

Therefor we will now derive effective Kondo models for these two regions using Schrieffer-Wolff transformations. We will go up to third order as cotunneling through two dots is at least a third order process. So second order will be self-interaction mediated through the closest dot while third order will be tunneling connecting metal with superconductor.

Also we will be looking for terms breaking particle-hole symmetry at $\delta = 0$. Remembering that in the analysis for the single-dot we found that to all orders of Δ/U this symmetry was protected it must stem from something new in the double-dot system.

8.1 Second order perturbation - Self-interactions

Here we will calculate the second order contribution to the leads, which is effectively the leads self-interaction through their closest quantum dot. First of all we ignore the metallic leads contribution as we consider only weak coupling. We therefor go straight to the superconductors self-interaction through dot-S.

For tunnel operators and energies we use the full double-dot Anderson Hamiltonian shown in eq.(6.3). We start with the case of $n_N = 0$ for which the system is completely similar to the single-dot system as dot-N is always inactive and U_d never contributes. Therefor taking the results from single-dot calculation to lowest order in Δ/U_S from eq.(4.21)

$$H_{SS}^{(0)} = J_{SS}^{(0)} \sum_{kk'\sigma\sigma'} c_{Sk\sigma}^\dagger \boldsymbol{S} \cdot \boldsymbol{\sigma}_{\sigma\sigma'} c_{Nk'\sigma'} + W_{SS}^{(0)} \sum_{kk'\sigma} c_{Sk\sigma}^\dagger c_{Nk'\sigma'} \tag{8.1}$$

with

$$J_{SS}^{(0)} = \frac{t_S^2}{U_S} \frac{4}{1-\delta^2} \qquad W_{SS}^{(0)} = \frac{t_S^2}{U_S} \frac{-2\delta}{1-\delta^2} \tag{8.2}$$

here the index (0) indicates that it is for $n_N = 0$. The next order that contributes to this interaction would be of the fourth order and can be disregarded compared to second order. This explains why

the YSR result in this sector is so similar in nature to single-dot results as the YSR Hamiltonian is identical.

Next we consider the same for $n_N = 2$. Here dot-N is actually active through U_d since adding/subtracting an electron on dot-S would change the energy by $\pm 2U_d$ in addition to the contribution from dot-S itself. This only affects the energy denominators from the single-dot calculation in the following way

$$E_2^{(2)} = E_2 + 2U_d \qquad E_0^{(2)} = E_0 - 2U_d \tag{8.3}$$

here E_2 and E_0 refers to the energies of the intermediate state with 0 or 2 electrons on dot-S from the single-dot calculation. Now in Schrieffer-Wolff calculations, when disregarding the gap ($\Delta \approx 0$), these terms are always subtracted from the initial state $E_1 - E_2 = -\epsilon_S - U_S$ and $E_1 - E_0 = \epsilon_S$. Considering these relations together it is clear that if one shifts $\epsilon_S^{(2)} = \epsilon_S + 2U_d$ then the calculation are equivalent and one can reuse the previous result only with the following replacement,

$$\delta^{(2)} = \delta - \frac{4U_d}{U_S} \tag{8.4}$$

so in this constellation the particle hole symmetrical point is situated at $\delta^{(2)} = 0$. In the following deviations and comparisons we will not differentiate between $\delta^{(0)}$ and $\delta^{(2)}$ since the only difference experimentally is that the particle-hole symmetrical bias value is shifted between the two.

8.2 Third order perturbation - Effective coupling

In the double-dot systems one needs to consider third order Schrieffer-Wolff to account for transport in the region of fixed occupancy. Like before we choose to work in the 1 electron on dot-S, 0 electrons on dot-N configuration. Also when working with the superconductor in Bogouliubov basis the whole m block is diagonal and we only need to consider terms going trough two l states in eq.(B.14). We develop a model by following the same recipe as in Section.4, starting by finding all possible paths from superconductor to metal as shown in Fig.8.2. Using the notation $\langle \lambda, S, N|$ where λ is a supercon-

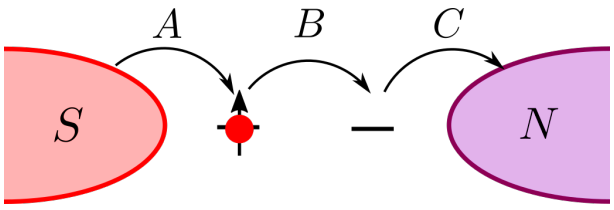

Figure 8.2: An visualization of the paths from S to N in third order Schrieffer-Wolff transformations. Paths for third order are as follows, where one should read from the right: 1) ACB. 2) CAB. 3) CBA.

ducting eigenstate state while S and N refers to dots. The possible paths are,

$$1) \quad \langle \lambda, \sigma, 0| \to \langle \lambda, 0, \sigma| \to \langle \lambda + e, 0, 0| \to \langle \lambda + e \mp qp, \sigma', 0| \tag{8.5}$$

$$2) \quad \langle \lambda, \sigma, 0| \to \langle \lambda, 0, \sigma| \to \langle \lambda \mp qp, \sigma', \sigma| \to \langle \lambda + e \mp qp, \sigma', 0| \tag{8.6}$$

$$3) \quad \langle \lambda, \sigma, 0| \to \langle \lambda \mp qp, \uparrow\downarrow, 0| \to \langle \lambda \mp qp, \sigma', \bar{\sigma}'| \to \langle \lambda + e \mp qp, \sigma', 0| \tag{8.7}$$

similar to what we did for second order where we use the notation qp for quasi-particle on superconductor and e for electron on metal and λ is the initial state. We use the approximation that all quasi-particles are taken from the gap ($E_{pq} \approx \Delta$) and electrons are taken from the Fermi surface of the metal ($E_e \approx 0$).

Additionally for clarity we will start by disregarding the gap ($\Delta \approx 0$) as all dot energies are of the order $U >> \Delta$. Hence the energy denominators from $\mp qp$ becomes identical and we in effect can calculate as if the superconductor was a metal, which we will do in the following calculations.

Using the Schrieffer-Wolff recipe we start by considering operator order

$$1) \quad H_A H_C H_B \Rightarrow C^{(1)} t_S t_d t_N \sum_{\sigma\sigma'} d^\dagger_{S\sigma'} c_{S\sigma'} c^\dagger_{N\sigma} d_{N\sigma} d^\dagger_{N\sigma} d_{S\sigma} = -C^{(1)} t_S t_d t_N \sum_{\sigma\sigma'} c^\dagger_{N\sigma} d^\dagger_{S\sigma'} d_{S\sigma} c_{S\sigma'} \tag{8.8}$$

$$2) \quad H_C H_A H_B \Rightarrow C^{(2)} t_S t_d t_N \sum_{\sigma\sigma'} c^\dagger_{N\sigma} d_{N\sigma} d^\dagger_{S\sigma'} c_{S\sigma'} d^\dagger_{N\sigma} d_{S\sigma} = -C^{(2)} t_S t_d t_N \sum_{\sigma\sigma'} c^\dagger_{N\sigma} d^\dagger_{S\sigma'} d_{S\sigma} c_{S\sigma'} \tag{8.9}$$

$$3) \quad H_C H_B H_A \Rightarrow C^{(3)} t_S t_d t_N \sum_{\sigma\sigma'} c^\dagger_{N\sigma} d_{N\sigma} d^\dagger_{N\sigma} d_{S\sigma} d^\dagger_{S\sigma'} c_{S\sigma'} = -C^{(3)} t_S t_d t_N \sum_{\sigma\sigma'} c^\dagger_{N\sigma} (d^\dagger_{S\sigma'} d_{S\sigma} - \delta_{\sigma\sigma'}) c_{S\sigma'} \tag{8.10}$$

where we used $d^\dagger_{N\sigma} d_{N\sigma} = 0$ as we consider the dot-N to be fixed in gate, so only term the identity from commutators appears. Here C is the respective energy denominator for a given path. These denominators are found using third order Schrieffer-Wolff transformation as seen in Appendix.B,

$$C = \frac{1}{2}\left(\frac{1}{(E_m - E_l)(E_m - E_{l'})} + \frac{1}{(E_{m'} - E_l)(E_{m'} - E_{l'})} \right) \tag{8.11}$$

$$C^{(1)} = \frac{1}{(\epsilon_S - \epsilon_N)(\epsilon_S)} \tag{8.12}$$

$$C^{(2)} = \frac{1}{(\epsilon_S - \epsilon_N)(-\epsilon_N - U_d)} \tag{8.13}$$

$$C^{(3)} = \frac{1}{(-U_S - \epsilon_S)(-\epsilon_N - U_d)} \tag{8.14}$$

where U_d is the interdot coulomb coupling. Now from the operator order it is clear that path $1)$ and $2)$ can be treated on the same basis therefor we begin by looking at their joined denominator, where we expand in U_d to first order,

$$C^{(1)} + C^{(2)} = \frac{1}{(\epsilon_S - \epsilon_N)\epsilon_S} - \frac{1}{(\epsilon_S - \epsilon_N)\epsilon_N} + \frac{U_d}{(\epsilon_S - \epsilon_N)\epsilon_N^2} = -\frac{1}{\epsilon_N \epsilon_S} + \frac{U_d}{(\epsilon_S - \epsilon_N)\epsilon_N^2} \tag{8.15}$$

$$C^{(3)} = \frac{1}{(\epsilon_S + U_S)\epsilon_N} - \frac{U_d}{(\epsilon_S + U_S)\epsilon_N^2} \tag{8.16}$$

Just like before we shift to spin basis using eq.(4.16) and obtain,

$$H_{SN} = J_{SN} \sum_{kk'\sigma\sigma'} c^\dagger_{Sk\sigma} \boldsymbol{S} \cdot \boldsymbol{\sigma}_{\sigma\sigma'} c_{Nk'\sigma'} + W_{SN} \sum_{kk'\sigma} c^\dagger_{Sk\sigma} c_{Nk'\sigma'} \tag{8.17}$$

where we obtain different terms for J_{SN} and W_{SN} as the operator ordering changes the sign of $C^{(3)}$. Lastly we shift to $\epsilon_S = -U_S/2(1+\delta)$ and $\epsilon_N = U_N/2$ specifying our charge sector. Inserting and manipulating yields,

$$J^{(0)}_{SN} = -t_S t_d t_N (C^{(1)} + C^{(2)} + C^{(3)}) = \frac{2t_S t_d t_N}{U_S U_N}\left[\frac{-4}{1-\delta^2} + \frac{4U_d}{U_N}\left(\frac{1}{1+\delta+\frac{U_N}{U_S}} + \frac{1}{1-\delta}\right)\right] \tag{8.18}$$

$$W^{(0)}_{SN} = -\frac{t_S t_d t_N}{2}(C^{(1)} + C^{(2)} - C^{(3)}) = \frac{2t_S t_d t_N}{U_S U_N}\left[\frac{2\delta}{1-\delta^2} + \frac{2U_d}{U_N}\left(\frac{1}{1+\delta+\frac{U_N}{U_S}} - \frac{1}{1-\delta}\right)\right] \tag{8.19}$$

from which its is clear that the last terms break particle-hole symmetry, as W_{SN} takes a non-zero value at $\delta = 0$.

In order for these new terms to be able to explain data, similar terms should exist for dot-N doubly occupied. Therefor we will go through the same motions as before starting with defining the three paths which can be seen in Fig.8.3,

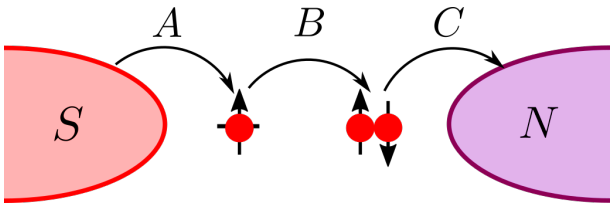

Figure 8.3: A visualization of the paths from S to N in third order Schrieffer-Wolff transformations. The paths for third order are as follows: 1) BCA. 2) ABC. 3) BAC.

$$1) \quad \langle \lambda, \sigma, \uparrow\downarrow| \rightarrow \langle \lambda \mp qp, \uparrow\downarrow, \uparrow\downarrow| \rightarrow \langle \lambda + e \mp qp, \uparrow\downarrow, \sigma'| \rightarrow \langle \lambda + e \mp qp, \bar{\sigma}', \uparrow\downarrow| \tag{8.20}$$

$$2) \quad \langle \lambda, \sigma, \uparrow\downarrow| \rightarrow \langle \lambda + e, \sigma, \bar{\sigma}| \rightarrow \langle \lambda + e, 0, \downarrow\uparrow| \rightarrow \langle \lambda + e \mp qp, \sigma', \uparrow\downarrow| \tag{8.21}$$

$$3) \quad \langle \lambda, \sigma, \uparrow\downarrow| \rightarrow \langle \lambda + e, \sigma, \sigma'| \rightarrow \langle \lambda + e \mp qp, \uparrow\downarrow, \sigma'| \rightarrow \langle \lambda + e \mp qp, \bar{\sigma}', \uparrow\downarrow| \tag{8.22}$$

$$\tag{8.23}$$

We obtain the operator order,

$$1) \quad H_B H_C H_A \Rightarrow D^{(1)} t_S t_d t_N \sum_{\sigma\sigma'} d^\dagger_{N\sigma'} d_{S\sigma'} c^\dagger_{N\sigma'} d_{N\sigma'} d^\dagger_{S\sigma} c_{S\sigma} = D^{(1)} t_S t_d t_N \sum_{\sigma\sigma'} c^\dagger_{N\sigma'} (d^\dagger_{S\sigma} d_{S\sigma'} - \delta_{\sigma\sigma'}) c_{S\sigma} \tag{8.24}$$

$$2) \quad H_A H_B H_C \Rightarrow D^{(2)} t_S t_d t_N \sum_{\sigma\sigma'} d^\dagger_{S\sigma} c_{S\sigma} d^\dagger_{N\sigma'} d_{S\sigma'} c^\dagger_{N\sigma'} d_{N\sigma'} = D^{(2)} t_S t_d t_N \sum_{\sigma\sigma'} c^\dagger_{N\sigma'} d^\dagger_{S\sigma} d_{S\sigma'} c_{S\sigma} \tag{8.25}$$

$$1) \quad H_B H_A H_C \Rightarrow D^{(3)} t_S t_d t_N \sum_{\sigma\sigma'} d^\dagger_{N\sigma'} d_{S\sigma'} d^\dagger_{S\sigma} c_{S\sigma} c^\dagger_{N\sigma'} d_{N\sigma'} = D^{(3)} t_S t_d t_N \sum_{\sigma\sigma'} c^\dagger_{N\sigma'} (d^\dagger_{S\sigma} d_{S\sigma'} - \delta_{\sigma\sigma'}) c_{S\sigma} \tag{8.26}$$

here we used $d^\dagger_{N\sigma} d_{N\sigma} = 1$ as this dot is always occupied. These expressions are very similar to the

case of $n_N = 0$, but the energy denominators take a slightly altered form

$$D^{(1)} = \frac{1}{(-\epsilon_S - U_S - 2U_d)(\epsilon_N + U_N - \epsilon_S - U_S)} \tag{8.27}$$

$$D^{(2)} = \frac{1}{(\epsilon_N + U_N + U_d)(\epsilon_S + 2U_d)} \tag{8.28}$$

$$D^{(3)} = \frac{1}{(\epsilon_N + U_N + U_d)(\epsilon_N + U_N - \epsilon_S - U_S)} \tag{8.29}$$

Remembering from our evaluation of the second order terms for $n_N = 2$ that we shifted ϵ_S by $2U_d$, we here shift both ϵ_S and ϵ_N with $2U_d$ and their respective U. So by doing the following shift $\hat{\epsilon}_\alpha = \epsilon_\alpha + U_\alpha + 2U_d$ we obtain

$$D^{(1)} = \frac{1}{(-\hat{\epsilon}_S)(\hat{\epsilon}_N - \hat{\epsilon}_S)} \tag{8.30}$$

$$D^{(2)} = \frac{1}{(\hat{\epsilon}_N - U_d)(\hat{\epsilon}_S - U_S)} \tag{8.31}$$

$$D^{(3)} = \frac{1}{(\hat{\epsilon}_N - U_d)(\hat{\epsilon}_N - \hat{\epsilon}_S)} \tag{8.32}$$

These expressions compare to the empty dot-N denominators and as in that case, we simply expand in U_d and substitute $\hat{\epsilon}_S = -U_S/2(-1+\delta)$ where the sign is from the U_S shift earlier and $\hat{\epsilon_N} = -U_N/2$ to obtain,

$$J^{(2)}_{SN} = t_S t_d t_N (D^{(1)} + D^{(2)} + D^{(3)}) = \frac{2t_S t_d t_N}{U_S U_N}\left[\frac{4}{1-\delta^2} - \frac{4U_d}{U_N}\left(\frac{1}{1+\delta} + \frac{1}{1-\delta+\frac{U_N}{U_S}}\right)\right] \tag{8.33}$$

$$W^{(2)}_{SN} = \frac{t_S t_d t_N}{2}(-D^{(1)} + C^{(2)} - D^{(3)}) = \frac{2t_S t_d t_N}{U_S U_N}\left[\frac{-2\delta}{1-\delta^2} - \frac{2U_d}{U_N}\left(\frac{1}{1+\delta} - \frac{1}{1-\delta+\frac{U_N}{U_S}}\right)\right] \tag{8.34}$$

So with these equation we find an important difference between $n_N = 0$ and $n_N = 2$ namely the U_d dependent term. This term specifically breaks particle-hole symmetry at $\delta = 0$. An easy way to see this is to consider W_{SN} for $\delta = 0$ yielding

$$W^{(0)}_{SN}(\delta = 0) = \frac{4t_S t_d t_N U_d}{U_S U_N^2}\left(\frac{1}{1+\frac{U_N}{U_S}} - 1\right) = -\frac{4t_S t_d t_N U_d}{U_S U_N}\frac{1}{U_N + U_S} \tag{8.35}$$

$$W^{(2)}_{SN}(\delta = 0) = -\frac{4t_S t_d t_N U_d}{U_S U_N^2}\left(1 - \frac{1}{1+\frac{U_N}{U_S}}\right) = -\frac{4t_S t_d t_N U_d}{U_S U_N}\frac{1}{U_N + U_S} \tag{8.36}$$

Now from these calculations it seems like $W(\delta = 0)$ is identical for $n_N = 0$ and $n_N = 2$, but as the transport only depends on $A^2_{\sigma SN} = (J \pm W)^2$ the important sign is the one separating W and J. So since $J^{(0)}(\delta = 0) = -J^{(2)}(\delta = 0)$ the symmetry is actually broken in the opposite direction for $n_N = 0$ and $n_N = 2$.

8.3 Transport

With effective Kondo models for these occupancies we now can do full conductance calculations using our classical-spin model. For starters we will try to extract parameters. As a lot of quantities are unknown or only poorly estimated this is a crude estimation and we will therefor not be too concerned in simplifying. We start by disregarding the particle-hole symmetry breaking term by setting $U_d = 0$. Then the double-dot model becomes completely similar to the single-dot model with the adjustment $t_{N1} = 2t_d t_N/U_N$ where 1 refers to single-dot.

Then taking our conductance formula eq.(5.75) from the Resonant-Level calculation and considering it for $T \neq 0$ as in the experiment we get,

$$\sigma(V) = \frac{4e^2}{h}\int d\omega \left[\frac{2\Gamma_e\Gamma_h + \Gamma_e\Gamma_r}{(\omega+\omega_0)^2 + (\Gamma/2)^2}\frac{dn_F(\omega - V)}{dV} + \frac{2\Gamma_e\Gamma_h + \Gamma_h\Gamma_r}{(\omega+\omega_0)^2 + (\Gamma/2)^2}\frac{dn_F(\omega + V)}{dV}\right] \tag{8.37}$$

with the definitions $\Gamma_e = \pi\nu_F v^2 A^2_{\uparrow NS}$ and $\Gamma_h = \pi\nu_F u^2 A^2_{\downarrow NS}$. For $\delta = 0$, $\Gamma_e = \Gamma_h$ as $u = v$ and $A_{\uparrow NS} = A_{\downarrow NS}$. In this case the two Lorentzians are completely similar and we therefor choose to work with only the positive,

$$\sigma_+(V) = \frac{4e^2}{h}\int d\omega \frac{\Gamma_h\Gamma/2}{(\omega+\omega_0)^2 + (\Gamma/2)^2}\frac{dn_F(\omega + V)}{dV} \tag{8.38}$$

$$= \frac{4e^2}{h}\int d\omega \frac{\Gamma_h\Gamma/2}{(\omega+\omega_0)^2 + (\Gamma/2)^2}\frac{1}{4T}\text{sech}\left(\frac{1}{2}T(\omega - V)\right)^2 \tag{8.39}$$

where we used the definition $\Gamma = 2\Gamma_e + 2\Gamma_h + 2\Gamma_r$. This expression is the envelope of a Lorentzian with a *Sech*^{2} distribution divided by T. The exact result of such an envelope is a so called tri-gamma function as seen in [31]. For our range of parameters we find that this envelope can be approximated to a Lorentzian where one simply adds temperature to the width yielding,

$$\sigma_+(V) = \frac{4e^2}{h}\frac{\Gamma_h\Gamma_T/2}{(V-\omega_0)^2 + (\Gamma_T/2)^2} \tag{8.40}$$

$$\sigma_+(\omega_0) = \frac{8e^2}{h}\frac{\Gamma_h}{\Gamma_T} \tag{8.41}$$

with $\Gamma_T = \Gamma + 2T$ being the measured Lorentzian width. Next we are ready to do some ballpark estimates. First as seen on Fig.8.1 the peak conductance at $\delta = 0$ can be estimated to be $\sigma_+(\pm\omega_0) \approx (0.08 \sim 0.13)e^2/h$ and K. Groove fitted the peak to a Lorentzian using different methods and obtained a estimate of the width $\Gamma_T \approx (30 \sim 50)\ \mu$eV. Using these two results we estimate,

$$\Gamma_h = \sigma_+(\omega_0)\frac{h\Gamma_T}{8e^2} \tag{8.42}$$

$$\Gamma_h = \Gamma_e \approx (0.3 \sim 0.8)\mu\text{eV} \tag{8.43}$$

By measuring another sample in the coulomb regime the temperature is estimated to be $T = 80\text{mK} \approx 8\mu$eV from which we can find Γ_r from the total width

$$\frac{\Gamma_T}{2} = \Gamma_r + T + 2\Gamma_h \tag{8.44}$$

$$\Gamma_r \approx (6 \sim 16)\mu\text{eV} \tag{8.45}$$

So we found that $\Gamma_{e/h}$ is a factor ten smaller than Γ_r, supporting our idea that we indeed are in the relaxation regime dominated by single electron transport. It is also clear from data that we have bias asymmetrical conductance supporting this claim. We do not yet know what this relaxation rate stems from and we will later present a short discussion on the topic.

Next writing out Γ_e by use of Eq.(8.18) for $U_d = 0$ and Eq.(3.29) we obtain

$$\Gamma_e(\delta = 0) = \pi\nu_F v^2 A^2_{\uparrow NS} = 8\pi^2\nu_F^2\Delta\frac{\alpha}{(1+\alpha^2)^2}\frac{t_S^2 t_d^2 t_N^2}{U_S^2 U_N^2}(4S)^2 \tag{8.46}$$

Then similar to earlier when we used classical-spin approximation we do the substitution $S = 3/2$. We then fit the YSR energy using Eq.(3.19) to obtain $t_S = 0.25m$eV as seen on Fig.8.4 which is also the fit we used to find the particle-hole symmetrical points shown in Fig.8.1. From these plots we determined that for $n_N = 0$ the interval $\delta \in [-1, 1]$ corresponds to $V \in [2.555V, 2.615V]$, while for $n_N = 2$ it corresponds to $V \in [2.5645V, 2.6245V]$

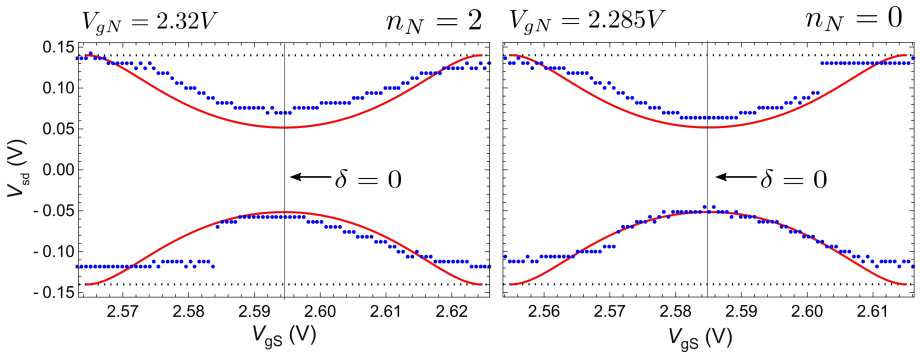

Figure 8.4: In these two plots we fit the YSR energy found using Eq.(3.19) to the conductance peaks along the line-cuts also shown in Fig.8.1. The classical-model model is varied along $\delta \in [-1, 1]$ from left to right in both plots thereby corresponding occupancy with bottom-gate bias. This definition of the δ interval is the one used from now on.

The rest of the parameters are taken from ZBW (See Fig.7.8) therefor we can estimate the effective metallic coupling to be $t_N = (0.09 \sim 0.11)$meV where we have set $\nu_F = 1$ as it lives similarly on all tunnel couplings. From this we find $\pi\nu_F\frac{t_N^2}{U_N} << 1$ supporting that the metals contributions to the physics are negligible. Next we will try to use our model to discuss behavior out of the particle-hole symmetrical point and compare it to the line-cuts made through honey-comb diagrams. First of all it should be stated that such a comparison is not completely kosher as variations of δ correspond to variations of occupancy n_S. The problem is that experimental line-cuts corresponds to variations of bottom gates which change occupancy of both dots at the same time due to the inter-dot coupling U_d as discussed in section.6. But for $U_d << U_S, U_N$ the inter-dot interaction is weak and line-cuts almost correspond to occupancy variations.

Here we will utilize our full model for the $n_N = 0$ and $n_N = 2$ sector with self-interaction A_{SS} given by the second order interaction and coupling A_{NS} given by the third order interaction without neglecting U_d. Plots are shown in Fig.8.5 where one can see that particle-hole symmetry is broken precisely at $\delta = 0$. This effect comes from the U_d term in A_{NS} and symmetry is restored for $U_d = 0$.

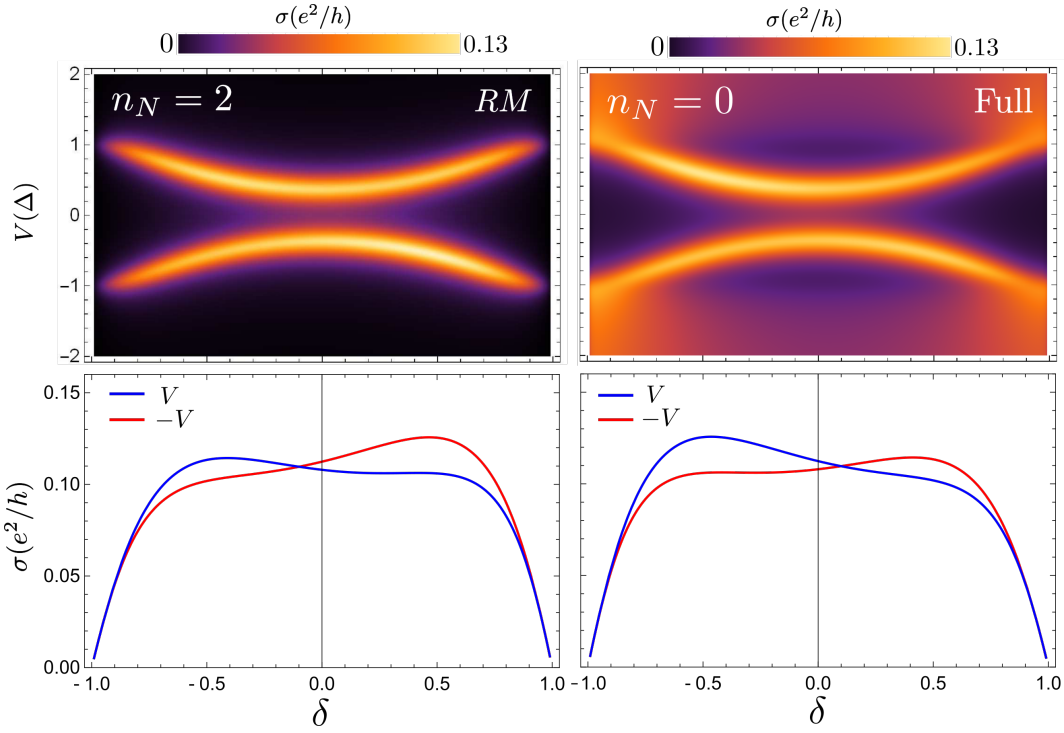

Figure 8.5: In the top two plots we plot conductance as a function of bias and δ corresponding to occupancy. Left is for $n_N = 2$ and right $n_N = 0$. Also to illustrate the difference, the left has been made using Resonant level Eq.(5.75) with temperature added to broadening through $\Gamma_r \to \Gamma_r + T$ such that $\Gamma = 43\mu$ eV and the right the exact conductance model Eq.(5.33) with analytical continuation $\Gamma = 2\eta = 43\mu$eV. Below we see plots of peak conductance precisely at the resonance $V = \pm\omega_0$ obtained using Eq.(5.75). Parameters are $U_S = 0.8$meV, $U_N = 2.5$meV, $U_d = 0.1$meV, $t_d = 0.27$meV, $t_S = 0.25$meV and $t_N = 0.1$meV.

Comparing this plot with Fig.8.1 we see that this corresponds to the enhancing effect seen in experiment.

In general when comparing the classical-spin transport calculations with the experimental results a few features stand out. First the bias asymmetry seen in experiment is captured by our classical spin model and explained through the relaxation process, but the amount of asymmetry seen in the experimental data is not mimicked by our model which underestimates it. Actually the underlying Green functions $\mathcal{G}_{SS}$ in the classical-spin calculation are more asymmetrical compared to conductance result. But the competition of magnetic J and potential W interaction in the effective coupling between metal and superconductor A_{NS} decreases the asymmetry. If only J or W is present in A_{NS} then $A^2_{\uparrow NS} = A^2_{\downarrow NS} = t^2$ which would render $\Gamma_e = v^2t^2$ and $\Gamma_h = u^2t^2$ such that one directly probes the spectral function as u^2 corresponds to the spectral functions positive peak height and v^2 its negative increasing asymmetry.

But as transport really occurs through the dots it would be wrong to neglect such effects and furthermore the symmetry breaking at $\delta = 0$ is only found because we include such terms and does

not exist in any shape or form in the spectral function. One would have to consider self-interactions to fourth order in Schrieffer-Wolff transformations to obtain U_d dependent terms in the spectral function. We believe that the failure of our model, in the sense of direct correspondence with data, is more related to the following approximations:

First in approximating the spin to be classical we have lost the coupling between spin dependent tunneling J_{NS} and YSR state. Utilizing a full quantum mechanical treatment one would capture how J_{NS} dependent terms change the dot-spins, thereby affecting the YSR state. Also the classical-spin approximation is only found to be valid in the low coupling limit with $\alpha << 1$ which is before the singlet-doublet phase transition occurs, where we here extrapolate it far out of this regime.

Secondly the classical-spin model already exist within a approximation namely the Schrieffer-Wolff transformation which is only valid for low Δ/U and deep within the coulomb diamonds where occupancy is fixed. Much of the observed asymmetry occurs at the wings of the YSR state close to the degeneracy points where such a model breaks down and if one could calculate transport through an Anderson like model this weakness could be overcome.

This being said we still find that the classical-spin models are able to explain observed features such as asymmetry in bias and breaking of symmetry at the particle-hole symmetrical point. Also it haa allowed us to separate the concept of resonant cooper-pair transport from relaxation transport. Later we will present some ideas on how to test these concepts and a discussion of what drives the relaxation process.

9 Discussion and Outlook

Here we will present some prospects on the research done in this thesis and a discussion of relevant issues. Two prospects are found interesting enough to have their subsections, while the rest will be discussed here. We start by considering the ZBW model. From the work done in this thesis we believe it is clear that a ZBW approximation yields a full qualitative picture of YSR physics in quantum dot systems if one can avoid crossings of Δ. Unfortunately, these become more and more apparent for large U. The missing link for ZBW is to make the expansion controllable in the sense of finding a larger theory that can be controllably approximated to ZBW. With such an expansion by hand, it would be easier to obtain limits of the model without going through tedious testing of arbitrary parameters. To this author, the most sensible way to obtain such an expansion seems to be by generalizing Yosida's anzats [26], consisting of replacing the full superconductor with a few quasi-particles, to the full Anderson model and obtain parameters self-consistently. Such a derivation is probably not simple but would help significantly in quantifying ZBW. Secondly by determining the parameters self-consistently one would obtain relations for ZBW tunnel couplings which seems to be none comparable to NRG tunnel couplings as they need different values to produce similar physics.

For transport we find separation of transport into two regimes, Cooper-pair transport and relaxation transport, to be promising in regards to future work. First, the concept itself could be tested in a system with a controllable metallic coupling and small Γ_r. By increasing t_N one would increase the symmetrical contribution, $\Gamma_e\Gamma_h \propto t_N^4$, faster then the asymmetrical contribution, $\Gamma_{e/h}\Gamma_r \propto t_N^2$, which in the end would dominate, thereby yielding symmetrical conduction trough sub-gap features. Here Γ_r needs to be small, else the broadening of sub-gap features when increasing t_N would render sub-gab features none visible .The reason for tuning t_N being that the rest of YSR features, primarily induced by superconducting self-interactions, would be unmodified. Such an experiment have to our knowledge not been conducted in a quantum-dot setup. Secondly, we have only been able to find these two transport regimes in a classical-spin calculations, which leaves one to wonder if it this picture also works for a model using a quantum-mechanical spin. The mains differences being that the quantum-model would contain multiple states of spin and couple all spin interactions. In [7] they considered lowest order treatment of quantum spin-spin correlations and obtained symmetrical conductance for $\eta = 0$ and finite potential scattering, supporting the transport picture. But a treatment, focusing specifically on this separation of transport, in a quantum framework should be conducted in future work.

9.1 Relaxation

In the transport Section.5 we, out of the blue, introduced a relaxation parameter Γ_r only motivated by the fact that it could stem from a coupling to Hilbert-space, not considered in the calculations, and yielded bias asymmetric conductance. Also in extracting parameters for the specific device, discussed earlier, we found $\Gamma_r = (6 \sim 16)\mu$eV which constitutes approximately half of the total width of the sub-gap states, estimated to be $\Gamma = (30 \sim 50)\mu$eV at the particle-hole symmetrical point. This estimate shows that Γ_r is not a small parameter in the experiment and have a significant impact on the physics. Next we list up possible contribution to relaxations or similar effects,

- Soft-Gapped Superconductor.

- Relaxation induced by phonon coupling.
- Relaxation induced by coupling to classical field.

The first explanation that came to our minds, was that the superconductor we are working with have a soft-gap, in the sense that coupling to some not regarded field have broadened the normally almost divergent superconducting peaks. This means that quasi-particle excitations are present within the gap opening for metallic like transport, as considered in a similar system in [32]. Such processes are traditionally described by as a quasi-particle lifetime τ, determining how often Cooper-pairs break up and reform [33]. But measurements done on different samples, with the same superconductor, showed hard gaps. Also, knowing that the superconductor we are working with is Aluminum, which have a high quasi-particle lifetime [33] and therefore a hard gap, we find no reason to believe that our superconductor should have a soft-gap.

Another mechanism could be that the relaxation stem from coupling to a phonon field, this was explored in [13] and in [34] where they considered coupling to a local phonon, induced by impurity sites as this was in a STM setup. The problem in calculating such contributions, is that the effects of regular phonons are already somewhat included in the BCS superconductor through the effective attractive field. Higher order terms is precisely what yields the quasi-particle lifetimes in [33], and we just before assumed this effect to be negligible.

Lastly, the conduction measurement are done by tuning a DC current to the bias one is probing, and then applying a small AC on top of that, in order to measure gradients from which the differential conduction is extracted. But application of a rapidly changing field could drive transitions between states in the system, if the time evolution is so rapid that it breaks the adiabatic theorem [35]. Thereby driving transitions in the superconductor, allowing the YSR state to relax into the quasi-particle bulk. The effects of applying such a field have yet to be investigated in this context.

Concluding this discussion we should state a very eluding property about this relaxation: Namely that the width of the sub-gap state seems to be independent of how far inside the gap the state is. This is weird as about half the width is from relaxation and the three proposed mechanisms should quite strongly depend on the distance to the gap. Because, it would then demand less energy to move the YSR state up to the bulk. The author do not currently have a explanation for this.

9.2 Zeeman Splitting

An interesting prospect of subdividing transport into the relaxation and Cooper-pair regime is a possible explanation of disappearing Zeeman splitted states seen at occupancy-phase transitions [23]. Our explanation follows these lines: In the regime where dominant transport is through relaxation $\Gamma_{e/h}\Gamma_r >> \Gamma_e\Gamma_h$ transport is mediated through the relaxation of a bound quasi-particle internally in the superconductor. This means that transitions between states on the dot, not involving a YSR excitation, must happen through formations of Cooper-pairs, since in that case no quasi-particle can relax. Transport is then of order $\Gamma_e\Gamma_h \propto t_N^4 t_S^4$, which for small t_N as generally assumed, is small. A specific example of this is the transition between two Zeeman split states, arising from a finite magnetic field. which occurs when one have doublet ground state. A schematic of this concept is shown in Fig.9.1. This explanation allows us to do a prediction. In the case of transport being dominated by relaxation we would assume that the Zeeman split lines will be none visible and YSR features to be asymmetric.

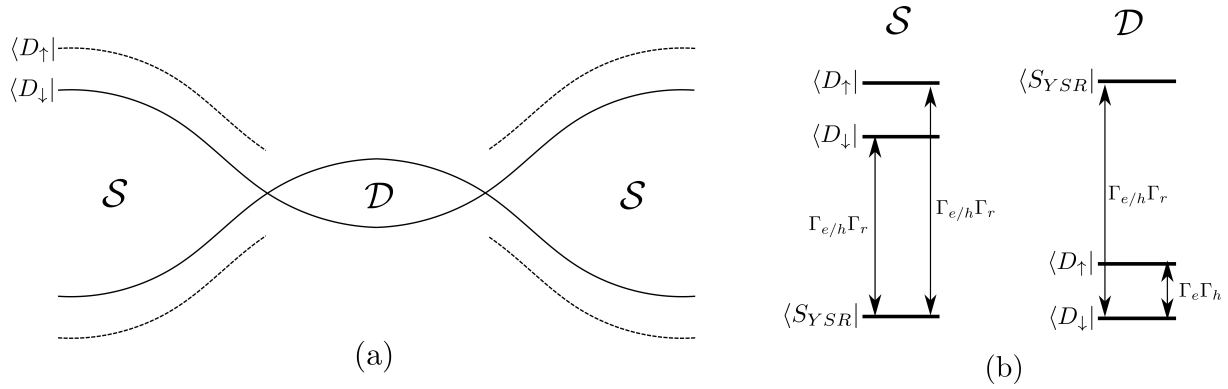

Figure 9.1: (a) Here we show a representation of how Zeeman split doublet lines disappear in conductance measurements. Singlet groundstate is marked by $\mathcal{S}$ and doublet with $\mathcal{D}$. (b) Here we show how the spectra look deep inside the singlet state and deep inside the doublet. Transitions are labeled with our expected dominant transition strength. In the relaxation regime the $|D_\downarrow\rangle$ to $|D_\uparrow\rangle$ transition would be weak.

But if transport is Cooper-pair dominated then we would expect the Zeeman split states to be visible and YSR features to be symmetric with high conductance.

10 Conclusion

We have in this thesis explained and used the basic formalism of Greens functions in Nambu space to solve the system of a classical local moment coupled to a BCS superconductor. From this we obtained bound sub-gap states, known as YSR states. We showed that by the addition of a potential scattering term these states obtain an effectively bias asymmetric spectral function. Lastly we expand around the resonance and obtain a simple Hamiltonian consisting only of two Bogoliubovs, describing the sub-gap part of the YSR physics.

Next we considered an experimental platform for realizations of YSR sub-gap states, namely the SDN system. Here we, by use of Schrieffer-Wolff transformations, showed that deep within the odd occupancy sector one obtains an effective spin-$1/2$ impurity model, which for all orders in Δ/U shows particle-hole symmetry represented by zero potential scattering $W = 0$. We then continued into transport calculations. Based on the Keldysh technique we consider applying a bias over the metal-superconductor structure, driving current through the quantum dot probing its states. Here we find that this system unmodified always yields bias symmetrical peaks of height $2e^2/h$, which we show stems from highly resonant transport. Including a relaxation rate into a simplified transport calculation yielded conductance showing the bias asymmetry expected from the YSR spectral function. This we classified into two regimes namely relaxation and Cooper-pair driven transport.

We then explained the basic concepts of SDDN systems and the different transport regimes expected in such setups. We found that in the regime of weak-coupling honeycomb diagrams and transport could be explained using the language from single-dot superconductor systems. We find that in conductions measurements the boundaries between different ground states are formed by YSR transitions, instead of coulombs diamonds as in the metallic case.

We then developed a ZBW model, in order to explain the behavior of SDDN systems for large couplings. We show that both single-dot and double-dot ZBW models matches, to a qualitative degree, NRG results, giving us confidence in this new approach. We then do an analysis of a specific device, where we classify a new regime which we call partially screened, formed in the competition between exchange singlet and YSR screening. Using ZBW we are able to fit data and dynamics to large extent and thereby extract parameters.

Lastly, to bring coherence to this story, we use our Schrieffer-Wolff based classical-spin approach on two line-cuts from the SDDN honeycomb. We specifically consider the regimes where the dot closest to the metal is kept magnetically inactive, thereby obtaining an almost single-dot model. Almost, in the sense that we find a new term proportional to the interdot coulomb interaction, which breaks particle-hole symmetry at $\delta = 0$. Using this model we extract a number of parameters and classify the observed transport to be relaxation transport.

Appendices

A Contour Ordered Greens functions

It turns out that deriving relations between the different types of greens functions can be tedious, but by defining the contour ordered greens function this task will turn out to be much simpler. This section is based on the derivations done in [25]. We start by defining a new Greens function,

$$\mathcal{G}^C(t,t') = -i\langle T_C(c(t)c^\dagger(t')\rangle \tag{A.1}$$

where all other indices are hidden in the matrix structure. We only write time fully out. T_C is here the contour ordering operator which sorts operators based on order on the contour. The contour is defined as the integral from $-\infty + i\eta$ to $+\infty + i\eta$ then to $+\infty - i\eta$ and ending in $-\infty - i\eta$ where η is taken to be infinitesimal. Such a contour is shown at Fig.A.1

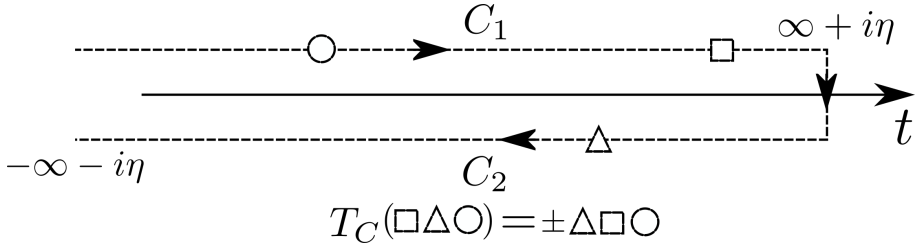

Figure A.1: A drawing of the contour C which one integrates along. One can decompose $C = C_1 + C_2$ where C_1 is the upper plane and C_2 the lower. The shapes represents time dependent operators which occurs somewhere along the contour. At the bottom one sees the definition of contour ordering T_C where it sorts the shapes dependent on their placement on the contour.

The trick is that one can by choosing on which contour a given t exist obtain a specific kind of Greens function. For example if both t and t' exist on the upper contour then the contour ordering operator T_C would sort them based on the value of t and t' with the lowest (earliest) coming first. This is per definition the time-ordered Greens function. But if t existed on the upper contour and t' on the lower then ordering would always put t first, thereby one obtains the lesser Greens function. These relations can be expressed as,

$$\mathcal{G}^C(t,t') = \begin{cases} \mathcal{G}^t(t.t') & \text{if} \quad t \in C_1, t' \in C_1 \\ \mathcal{G}^<(t.t') & \text{if} \quad t \in C_1, t' \in C_2 \\ \mathcal{G}^>(t.t') & \text{if} \quad t \in C_2, t' \in C_1 \\ \mathcal{G}^{\bar{t}}(t.t') & \text{if} \quad t \in C_2, t' \in C_2 \end{cases} \tag{A.2}$$

So it is clear that starting from contour ordered Greens functions the usual ones are easy to find.

Now in order for Contour ordered Greens function to be useful we need a perturbation scheme that is similar to that of usual Greens function. Normally one introduces Contour ordering to solve problems of time-dependent Hamiltonians, so for the sake of generality we introduce it in the same manner even though this thesis does not contain time dependency.

Consider the following Hamiltonian,

$$H = h + H_t(t) \tag{A.3}$$

where $h = h_0 + h_i$ where h_0 is diagonal and h_i contains interactions. Writing time evolution for a operator A in the Interaction picture,

$$A_H(t) = v^\dagger(t, t_0) A_h(t) v(t, t_0) \quad \text{with} \quad v(t, t') = T_t e^{-i\int_{t_0}^{t} dt' H_{th}(t')} \tag{A.4}$$

where the h index on both A and $H_t(t')$ refers to the interaction picture trivial evolution $A_h(t) = e^{ih(t-t_0)} A e^{-ih(t-t_0)}$. The trick of contour ordering is to notice that $u(t, t_0)$ evolves one from t_0 to t and $u^\dagger(t, t_0)$ evolves one back again. Setting $t_0 = -\infty$ and $t = \infty$ and shifting t, t_0 by $+i\eta$, as to force $v(t, t_0)$ to follow the upper contour and $v^\dagger(t, t_0)$ the lower, then precisely yields the contour path on Fig.A.1 so,

$$v^\dagger(t^*, t_0^*) v(t, t_0) = T_C e^{-i\int_C d\tau H_{th}(\tau)} = T_C S_C^{H_{th}} \tag{A.5}$$

where we use τ for time following the contour. An important byproduct of this is that all places where before one used normal time ordering can easily be replaced by contour ordering as,

$$A_h(t) = u^\dagger(t^*, t_0^*) A_{h_0} u(t, t_0) = T_C e^{-i\int_C d\tau h} A_{h_0} \tag{A.6}$$

with $u(t, t_0)$ being the normal time-evolution operator for an interacting Hamiltonian. With this discussion in place we are ready to consider the contour ordered Greens function,

$$\mathcal{G}^C(t, t') = -i\langle T_C(c(t) c^\dagger(t')\rangle = -i\langle T_C S_C^{H_{th}} [c_h(t) c_h^\dagger(t')]\rangle \tag{A.7}$$

following [25] we notice that before we are in a form where we can use Wick's theorem [19], we must separate h_0 from h_i so all time evolution is given by h_0, which is non-trivial as h_i resides in $S_C^{H_{th}}$ in a complicated manner. Here we just state the result,

$$G^C(t, t') = -i\langle T_C S_C^{H_{th_0}} S_C^{h_i} [c_{h_0}(t) c_{h_0}^\dagger(t')]\rangle \tag{A.8}$$

and since all time evolution in this form is governed by the quadratic h_0 one can apply Wicks theorem and make Dyson equations as usual, with the only difference being that the integrals arising from S_C terms are now contour integrals instead of regular time integrals.

This means that for every normal Dyson equation, obtained from Greens functions with normal timer ordering, their exist a corresponding contour version. This basically allows us to freely use relation for contour ordered Greens function for any Dyson series containing normal time ordered Greens functions. Now a typical beast one need to evaluate in transport theory is the lesser Greens function composed of two other Greens functions. We start by considering,

$$\mathcal{G} = \mathcal{G}_1 \mathcal{G}_2 \tag{A.9}$$

where 1 and 2 are for different Greens functions, we consider the correspondent contour equation

$$\mathcal{G}^C = \mathcal{G}_1^C \mathcal{G}_2^C \tag{A.10}$$

$$\mathcal{G}^<(t, t') = \int_C d\tau \mathcal{G}_1^C(t, \tau) \mathcal{G}_2^C(\tau, t') \tag{A.11}$$

where we in the last equation obtained the lesser by choosing t to be on the upper contour and t' on the lower. Here τ goes through the whole contour. Next, we divide the contour into two pieces

$$\int_C d\tau \mathcal{G}_1^C(t,\tau)\mathcal{G}_2^C(\tau,t') = \int_{C_1} d\tau \mathcal{G}_1^t(t,\tau)\mathcal{G}_2^<(\tau,t') + \int_{C_2} d\tau \mathcal{G}_1^>(t,\tau)\mathcal{G}_2^{\bar{t}}(\tau,t') \tag{A.12}$$

where C_1 is the positive part of the contour and C_2 the negative as shown of Fig.A.1. Next as the contours are just line integrals now we can evaluate them,

$$= \int_{-\infty}^{\infty} d\tau \mathcal{G}_1^t(t,\tau)\mathcal{G}_2^<(\tau,t') + \int_{\infty}^{-\infty} d\tau \mathcal{G}_1^>(t,\tau)\mathcal{G}_2^{\bar{t}}(\tau,t') \tag{A.13}$$

now since $\mathcal{G}^t = \mathcal{G}^> + \mathcal{G}^R$ and $\mathcal{G}^{\bar{t}} = \mathcal{G}^< - \mathcal{G}^A$ we can rewrite the above equation as

$$= \int_{-\infty}^{\infty} d\tau (\mathcal{G}_1^R(t,\tau)\mathcal{G}_2^<(\tau,t') + \mathcal{G}_1^<(t,\tau)\mathcal{G}_2^A(\tau,t)) \tag{A.14}$$

so in matrix form this equation becomes

$$\mathcal{G}^< = \mathcal{G}_1^R\mathcal{G}_2^< + \mathcal{G}_1^<\mathcal{G}_2^A \tag{A.15}$$

which a relation we are gonna use in section.5 alot. We also need the related equation for three Greens functions which easily follows from the above equation,

$$\begin{aligned}
\mathcal{G}^< &= [\mathcal{G}_1\mathcal{G}_2\mathcal{G}_3]^< \\
&= [\mathcal{G}_1\mathcal{G}_2]^R\mathcal{G}_3^< + [\mathcal{G}_1\mathcal{G}_2]^<\mathcal{G}_3^A \\
&= \mathcal{G}_1^R\mathcal{G}_2^R\mathcal{G}_3^< + \mathcal{G}_1^R\mathcal{G}_2^<\mathcal{G}_3^A + \mathcal{G}_1^<\mathcal{G}_2^A\mathcal{G}_3^A
\end{aligned} \tag{A.16}$$

This equation concludes our delve into contour ordered Greens functions as we now have the relations we need to derive transport.

B Schrieffer-Wolff Transformation

In order to examine our system in different charge configurations one can reduce the complicated Anderson-model to effective Kondo-models whenever one is far removed from charge degeneracies. This is done by use of quasi-degenerate-perturbation theory also known as the Schrieffer-Wolff transformation. The following derivations are based on [36]. We start off with a general Hamiltonian, H, and postulate that their exist a unitary transformation such that,

$$e^S H e^{-S} = \hat{H} \tag{B.1}$$

where $\hat{H}$ is block diagonal in two blocks which we label m and l. We then expand the left-hand side

$$\begin{aligned} e^S H e^{-S} &= \lim_{A\to 1} e^{AS} H e^{-AS} = \lim_{A\to 1} \left(H + [S,H]\, A + \frac{1}{2}\,[S,[S,H]]\, A^2 + \frac{1}{6}\,[S,[S,[S,H]]]\, A^3 \cdots \right) \\ &= \sum_j \frac{1}{j!}\,[S,H]^{(j)} \end{aligned} \tag{B.2}$$

where the second equal sign is from taylor expansion in A and $[A,B]^{(j)}$ is a short hand form of the previous equation, example $[A,B]^{(2)} = [A,[A,B]]$. Now we separate H

$$H = H^D + H^B + H^N \tag{B.3}$$

where H^D is a diagonal matrix H^B is block diagonal in the m,l blocks and H_N is the non-block-diagonal components connecting the m block to the l block. Since S rotates a block-diagonal matrix into a non-block-diagonal S can be chosen to be a non-block-diagonal matrix. In the beginning we chose $\hat{H}$ to be block diagonal. This allows us to separate the off-diagonal components, and put them to zero, from the diagonal components which must yield $\hat{H}$. From this we rewrite eq.B.2 into,

$$\hat{H} = \sum_j \frac{1}{(2j)!}\left[S, H^D + H^B\right]^{(2j)} + \sum_j \frac{1}{(2j+1)!}\left[S, H^N\right]^{(2j+1)} \tag{B.4}$$

$$0 = \sum_j \frac{1}{(2j)!}\left[H^N\right]^{(2j)} + \sum_j \frac{1}{(2j+1)!}\left[S, H^D + H^B\right]^{(2j+1)} \tag{B.5}$$

next as this is a perturbation theory we would like to consider it in powers of expansion. Assuming interactions are small H^D is considered to be order 0 and H_B and H_N are of order 1. S can be written $S = S^{(1)} + S^{(2)} + S^{(3)} + S^{(4)} \cdots$ where $S^{(n)}$ is of order n, now collecting all terms up to third order from the above equation yields,

$$\begin{aligned} \hat{H} &= H^D + H^B + [S^{(1)}) + S^{(2)}, H^N] + \frac{1}{2}[S^{(1)},[S^{(1)},H^D + H^B]] \\ &\quad + \frac{1}{2}[S^{(2)},[S^{(1)},H^D]] + \frac{1}{2}[S^{(1)},[S^{(2)},H^D]] \end{aligned} \tag{B.6}$$

$$0 = H^N + [S^{(1)} + S^{(2)}, H^D + H^B] + [S^{(3)}, H^D] + \frac{1}{2}[S^{(1)},[S^{(1)},H^N]] + \frac{1}{6}[S^{(1)},[S^{(1)},[S^{(1)},H^D]]] \tag{B.7}$$

in the last equation we sort terms in order and set each order equal to zero independently to obtain equations for S_1

$$H^N = -[S^{(1)}, H^D] \quad \Rightarrow \quad \langle m| H^N |l\rangle = (E_m - E_l) \langle m| S^{(1)} |l\rangle \tag{B.8}$$

$$\Rightarrow \langle m| S^{(1)} |l\rangle = \langle m| \frac{H^N}{E_m - E_l} |l\rangle \quad \Rightarrow \quad S^{(1)} = \frac{H^N}{E_L - E_R} \tag{B.9}$$

here E_m is the energy diagonal component of the m state and in the last step we promote $S^{(1)}$ to an operator by defining the operator $E_{L(R)}$ to be the energy of the state to the immediate Left(Right). In this manner we can construct Schrieffer-Wolff scheme in a operator formalism instead of the usual state formalism. Setting the second order term to zero yields an equation for $S^{(2)}$

$$[S^{(1)}, H^B] = -[S^{(2)}, H^D] \quad \Rightarrow \quad S^{(2)} = \frac{S^{(1)}H^B - H^B S^{(1)}}{E_L - E_R} \tag{B.10}$$

Next we sort $\hat{H}$ from eq.B.6 in powers as well,

$$\hat{H} = \hat{H}^{(0)} + \hat{H}^{(1)} + \hat{H}^{(2)} + \hat{H}^{(3)} \tag{B.11}$$

$$\hat{H}^{(0)} = H^D$$

$$\hat{H}^{(1)} = H^B$$

$$\hat{H}^{(2)} = [S^{(1)}, H^N] + \frac{1}{2}[S^{(1)}, [S^{(1)}, H^D]] = \frac{1}{2}[S^{(1)}, H^N]$$

$$\hat{H}^{(3)} = [S^{(2)}, H^N] + \frac{1}{2}[S^{(1)}, [S^{(1)}, H^B]] + \frac{1}{2}[S^{(2)}, [S^{(1)}, H^D]] + \frac{1}{2}[S^{(1)}, [S^{(2)}, H^D]] = \frac{1}{2}[S^{(2)}, H^N] \tag{B.12}$$

now evaluating the two last terms yields

$$\hat{H}^{(2)} = \frac{1}{2}\frac{H^N}{E_L - E_R}H^N + \frac{1}{2}H^N\frac{H^N}{E_R - E_L} \tag{B.13}$$

$$\hat{H}^{(3)} = \frac{1}{2}\left(\frac{\frac{H^N}{E_L-E_R}H^B}{E_L - E_R} - \frac{H_B\frac{H^N}{E_L-E_R}}{E_L - E_R}\right)H^N + \frac{1}{2}H^N\left(\frac{H^B\frac{H^N}{E_L-E_R}}{E_L - E_R} - \frac{\frac{H^N}{E_L-E_R}H^B}{E_L - E_R}\right)$$

which is the full expansion up to third order, in order to show that the operator form is equivalent to the expression in [36] one inserts complete basis between each operator and consider only terms connecting m with m',

$$\hat{H}^{(2)}_{mm'} = \frac{1}{2}\sum_l H^N_{ml}H^N_{lm'}\left(\frac{1}{E_m - E_l} + \frac{1}{E_{m'} - E_l}\right) \tag{B.14}$$

$$\begin{aligned}\hat{H}^{(3)}_{mm'} = &\frac{1}{2}\sum_{ll'} H^N_{ml}H^B_{ll'}H^N_{l'm'}\left(\frac{1}{(E_m - E_{l'})(E_m - E_l)} + \frac{1}{(E_{m'} - E_{l'})(E_{m'} - E_l)}\right) \\ &- \frac{1}{2}\sum_{lm''} H^B_{mm''}H^N_{m''l}H^N_{lm'}\left(\frac{1}{(E_m - E_l)(E_{m''} - E_l)}\right) \\ &- \frac{1}{2}\sum_{lm''} H^N_{ml}H^N_{lm''}H^B_{m''m'}\left(\frac{1}{(E_{m'} - E_l)(E_{m''} - E_l)}\right)\end{aligned} \tag{B.15}$$

Which is the expected form. Using the operator form allows one to obtain the relevant perturbation as expressed in operators without having to consider the intermediate states in other places then the energy denominators, which will prove a significant advantage with superconductors where particle conservation is broken and the possible number of intermediate states thereby increases. Schrieffer-Wolff perturbation is applicable when the coupling are small and/or the energy separation between the m and l states is large as the n order term is of order $n-1$ in energy differences between states in the denominator.

C Comparison between ZBW and NRG

Here we do a comparison between the ZBW model and full NRG. First for the single-dot system and then for double-dots. For the single-dot comparison we use plots from [29] where he plots single-dot NRG results for a number of parameters. In order to do a comparison we use [29] definition of Γ which is $\Gamma = 2\pi\nu_F t^2$ in units of Δ. What is clearly seen is the great agreement between the two models, almost to the degree that one could use ZBW to extract parameters. But one should be careful as the comparison worsens for large Γ and U. For very large values of Γ ZBW will begin to cross the gap as discussed in the main text, something never happening for NRG, so here the comparison is broken. In general when ZBW begins to fail it does not do so in a dramatic way (apart from the gap crossing) it simply becomes slower then NRG, meaning that one needs a larger Γ to obtain the same cuts. So if one only needs a qualitative analysis ZBW will do the job.

Next we do the comparison for the double dot model. In this case we are not interested in comparing parameters as it have already been established for single dot, that the models disagree about exact value. Instead we want to be sure that the dynamics found by ZBW is also found by NRG. For this purpose R. Zitko have provided us with a number of NRG plots for different values of Γ. He uses the definition $\Gamma = \pi\nu_F t^2$ which is different from the previous. In comparing with R. Zitko we use his definition of Γ. The double dot plots are done using the same convention as used in the main text ZBW sections, both for NRG and ZBW. The parameters used are $U_N = 2.5$meV, $U_S = 0.8$meV, $U_d = 0.1$meV, $\Delta = 0.14$meV and $t_d = 0.22$meV.

The structure of the plots are: ZBW plots at the top and NRG at the bottom for increasing Γ going to the right. We clearly see a good agreement between the models, when using $\Gamma_{ZBW} = 1/2\Gamma_{NRG}$. We are not sure if the factor 2 is merely coincidental or a disagreement in some definition along the derivations. But from our comparison for the single-dot it would be surprising if one could compare, using precisely the same Γ in both NRG and ZBW.

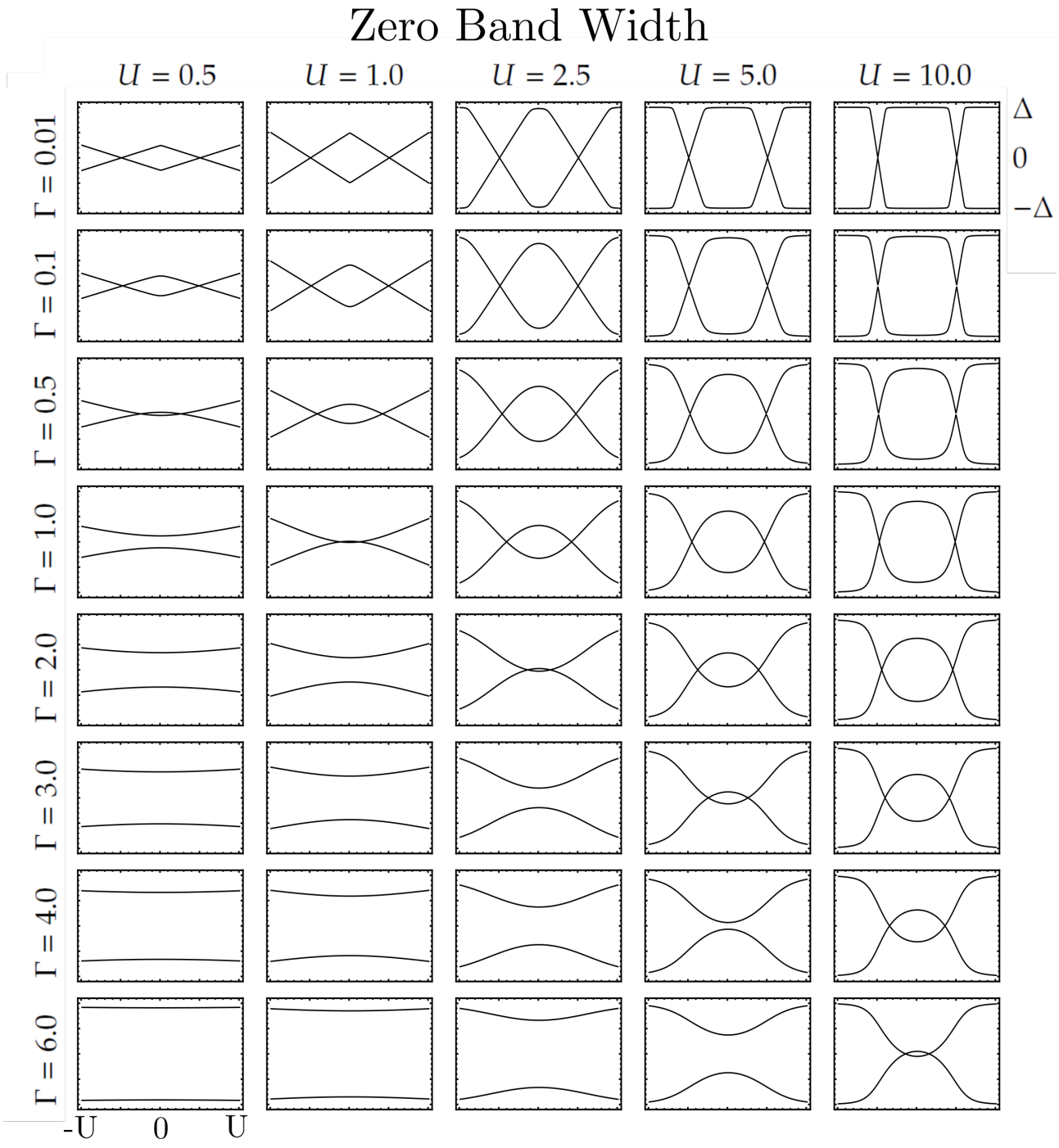
Zero Band Width
U = 0.5
U = 1.0
U = 2.5
U = 5.0
U = 10.0
Γ = 0.01
Γ = 0.1
Γ = 0.5
Γ = 1.0
Γ = 2.0
Γ = 3.0
Γ = 4.0
Γ = 6.0
Δ
0
−Δ
-U
0
U

Numerical Renormalization Group

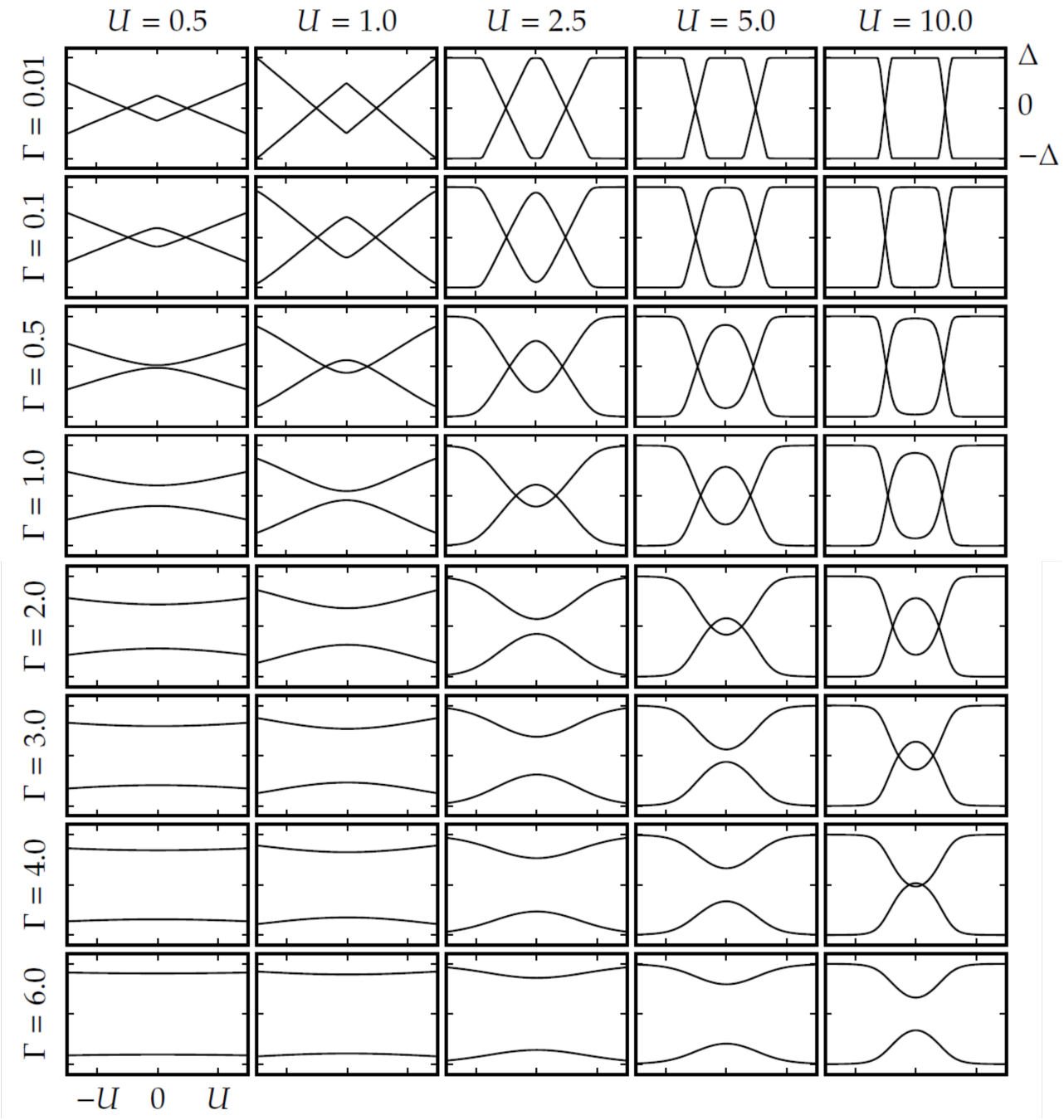

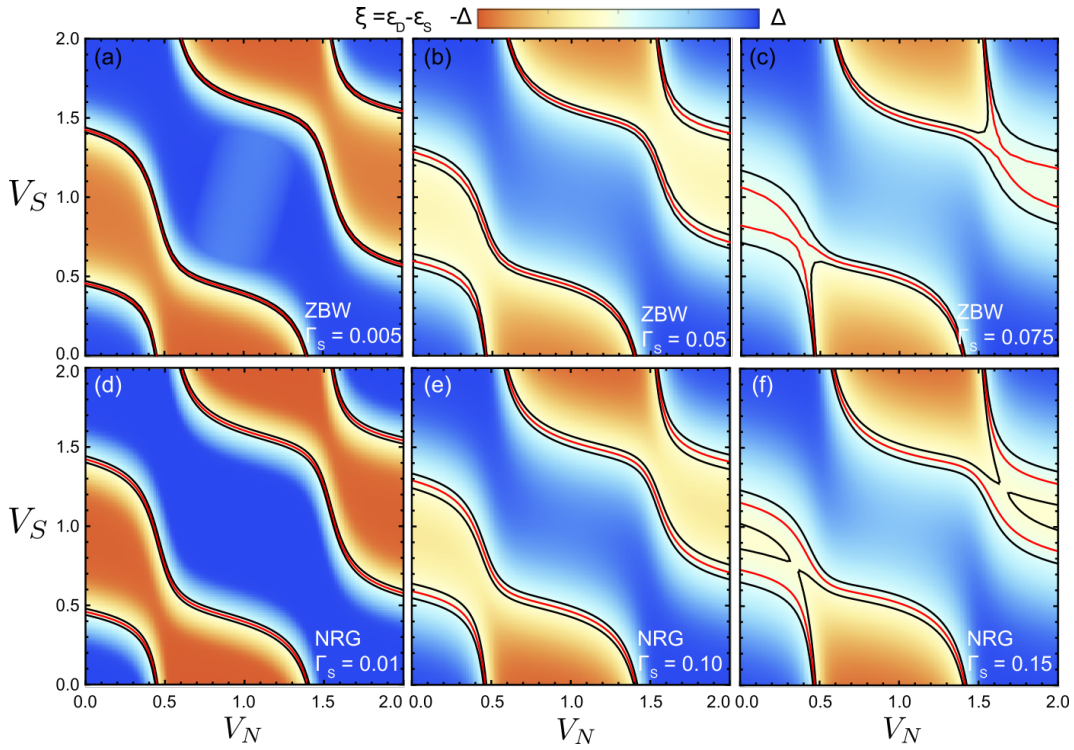
ξ =ε_D-ε_S -Δ Δ
(a)
(b)
(c)
(d)
(e)
(f)
ZBW Γ_S = 0.005
ZBW Γ_S = 0.05
ZBW Γ_S = 0.075
NRG Γ_S = 0.01
NRG Γ_S = 0.10
NRG Γ_S = 0.15
V_S
V_N
0.0
0.5
1.0
1.5
2.0

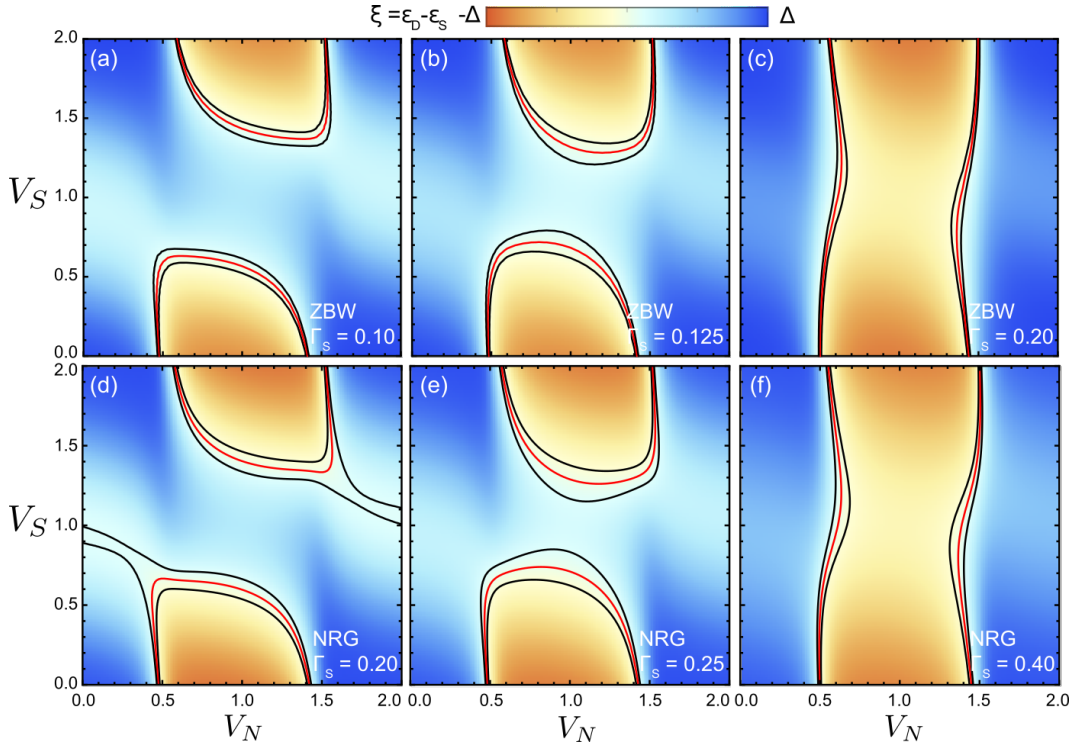
ξ =ε_D-ε_S -Δ Δ
(a)
(b)
(c)
(d)
(e)
(f)
ZBW Γ_S = 0.10
ZBW Γ_S = 0.125
ZBW Γ_S = 0.20
NRG Γ_S = 0.20
NRG Γ_S = 0.25
NRG Γ_S = 0.40
V_S
V_N
0.0
0.5
1.0
1.5
2.0

References

[1] Tobias Meng, Serge Florens, and Pascal Simon. Self-consistent description of andreev bound states in josephson quantum dot devices. *Phys. Rev. B*, 79:224521, Jun 2009.

[2] J-d Pillet. *Tunneling spectroscopy of the Andreev bound states in a carbon nanotube*. PhD thesis, l'Université Pierre et Marie Curie, december 2011.

[3] Luh Yu. Bound State in Superconductors with Paramagnetic Impurities. *Acta Phys. Sin.*, 21(1):75, 1965.

[4] Hiroyuki Shiba. Classical Spins in Superconductors. *Prog. Theor. Phys.*, 40(3):435–451, September 1968.

[5] A. I. Rusinov. Superconductivity near a paramagnetic impurity. *JETP Lett.*, 9(2):85–87, 1969. [Zh. Eksp. Teor. Fiz. **9**, 146 (1968)].

[6] Gediminas Kiršanskas, Moshe Goldstein, Karsten Flensberg, Leonid I. Glazman, and Jens Paaske. Yu-shiba-rusinov states in phase-biased superconductor–quantum dot–superconductor junctions. *Phys. Rev. B*, 92:235422, Dec 2015.

[7] V. Koerting, B. M. Andersen, K. Flensberg, and J. Paaske. Nonequilibrium transport via spin-induced subgap states in superconductor/quantum dot/normal metal cotunnel junctions. *Phys. Rev. B*, 82:245108, Dec 2010.

[8] J-d Pillet, C H L Quay, P Morfin, C Bena, A L Yeyati, and P Joyez. Andreev bound states in supercurrent-carrying carbon nanotubes revealed. *Nature Physics*, 6(11):1–5, 2010.

[9] Yoichi Tanaka, Norio Kawakami, and Akira Oguri. Correlated electron transport through double quantum dots coupled to normal and superconducting leads. *Phys. Rev. B*, 81:075404, Feb 2010.

[10] Gediminas Kiršanskas. *Electron Transport in Quantum Dots and Heat Transport in Molecules*. PhD thesis, Niels Bohr Institute, 2014.

[11] Ali Yazdani, B. A. Jones, C. P. Lutz, M. F. Crommie, and D. M. Eigler. Probing the local effects of magnetic impurities on superconductivity. *Science*, 275(5307):1767–1770, 1997.

[12] Gerbold C. Menard, Sebastien Guissart, Christophe Brun, Stephane Pons, Vasily S. Stolyarov, Francois Debontridder, Matthieu V. Leclerc, Etienne Janod, Laurent Cario, Dimitri Roditchev, Pascal Simon, and Tristan Cren. Coherent long-range magnetic bound states in a superconductor. *Nat Phys*, 11(12):1013–1016, Dec 2015. Letter.

[13] Michael Ruby, Falko Pientka, Yang Peng, Felix von Oppen, Benjamin W. Heinrich, and Katharina J. Franke. Tunneling processes into localized subgap states in superconductors. *Phys. Rev. Lett.*, 115:087001, Aug 2015.

[14] Akira Oguri, Yoichi Tanaka, and Johannes Bauer. Interplay between kondo and andreev-josephson effects in a quantum dot coupled to one normal and two superconducting leads. *Phys. Rev. B*, 87:075432, Feb 2013.

[15] Gabriel Sellier, Thilo Kopp, Johann Kroha, and Yuri S. Barash. π junction behavior and andreev bound states in kondo quantum dots with superconducting leads. *Phys. Rev. B*, 72:174502, Nov 2005.

[16] Eduardo J. H. Lee, Xiaocheng Jiang, Rok Žitko, Ramón Aguado, Charles M. Lieber, and Silvano De Franceschi. Scaling of subgap excitations in a superconductor-semiconductor nanowire quantum dot. *Phys. Rev. B*, 95:180502, May 2017.

[17] Falko Pientka, Leonid I. Glazman, and Felix von Oppen. Topological superconducting phase in helical shiba chains. *Phys. Rev. B*, 88:155420, Oct 2013.

[18] Michael Schecter, Karsten Flensberg, Morten H. Christensen, Brian M. Andersen, and Jens Paaske. Self-organized topological superconductivity in a yu-shiba-rusinov chain. *Phys. Rev. B*, 93:140503, Apr 2016.

[19] H. Bruus and K. Flensberg. *Many-Body Quantum Theory in Condensed Matter Physics*. Oxford University Press, 2004.

[20] M. I. Salkola, A. V. Balatsky, and J. R. Schrieffer. Spectral properties of quasiparticle excitations induced by magnetic moments in superconductors. *Phys. Rev. B*, 55:12648–12661, May 1997.

[21] M. M. Salomaa. Schrieffer-wolff transformation for the anderson hamiltonian in a superconductor. *Phys. Rev. B*, 37:9312–9317, Jun 1988.

[22] A. C. Hewson. *The Kondo Problem to Heavy Fermions*. Cambridge University Press, 1993. (cf. Appendix C).

[23] Anders Jellinggaard, Kasper Grove-Rasmussen, Morten Hannibal Madsen, and Jesper Nygård. Tuning yu-shiba-rusinov states in a quantum dot. *Phys. Rev. B*, 94:064520, Aug 2016.

[24] Ivar Martin and Dmitry Mozyrsky. Nonequilibrium theory of tunneling into a localized state in a superconductor. *Phys. Rev. B*, 90:100508, Sep 2014.

[25] H. Haug and A.-P. Jauho. *Quantum Kinetics in Transport and Optics of Superconductors*. Springer, 1996.

[26] Kei Yosida. Bound state due to the s-d exchange interaction. *Phys. Rev.*, 147:223–227, Jul 1966.

[27] W. G. van der Wiel, S. De Franceschi, J. M. Elzerman, T. Fujisawa, S. Tarucha, and L. P. Kouwenhoven. Electron transport through double quantum dots. *Rev. Mod. Phys.*, 75:1–22, Dec 2002.

[28] Rok Žitko. Numerical subgap spectroscopy of double quantum dots coupled to superconductors. *Phys. Rev. B*, 91:165116, Apr 2015.

[29] Anders Jellinggaard. *Quantum Dots Coupled to a Superconductor*. PhD thesis, Niels Bohr Institute, 2016.

[30] S. J. Chorley, M. R. Galpin, F. W. Jayatilaka, C. G. Smith, D. E. Logan, and M. R. Buitelaar. Tunable kondo physics in a carbon nanotube double quantum dot. *Phys. Rev. Lett.*, 109:156804, Oct 2012.

[31] I. Adawi and M. L. Glasser. Evaluation of some transport integrals. *Journal of Applied Physics*, 37(1):364–366, 1966.

[32] Zhaoen Su, Alexandre B. Tacla, Moira Hocevar, Diana Car, Sébastien R. Plissard, Andrew J. Daley, David Pekker, and Sergey M. Frolov. Andreev molecules in semiconductor nanowire double quantum dots. *arXiv*, 2016.

[33] S. B. Kaplan, C. C. Chi, D. N. Langenberg, J. J. Chang, S. Jafarey, and D. J. Scalapino. Quasiparticle and phonon lifetimes in superconductors. *Phys. Rev. B*, 14:4854–4873, Dec 1976.

[34] A. G. Kozorezov, A. A. Golubov, J. K. Wigmore, D. Martin, P. Verhoeve, R. A. Hijmering, and I. Jerjen. Inelastic scattering of quasiparticles in a superconductor with magnetic impurities. *Phys. Rev. B*, 78:174501, Nov 2008.

[35] J.J. Sakurai and J. Napolitano. *Modern Quantum Mechanics*. Addison-Wesley, 2011.

[36] Roland Winkler. *Spin-orbit coupling effects in two-dimensional electron and hole systems*. Springer tracts in modern physics. Springer, Berlin, 2003.